An analytical design tool for a pin fin sorber bed heat/mass exchanger

by

Mohammadjavad Darvish

M.Sc., Sharif University of Technology, 2017

B.Sc., Amirkabir University of Technology (Tehran Polytechnic), 2014

Thesis Submitted in Partial Fulfillment of the

Requirements for the Degree of

Master of Applied Science

in the

School of Mechatronic Systems Engineering

Faculty of Applied Sciences

SIMON FRASER UNIVERSITY

Summer 2021

Declaration of Committee

Name:	**Mohammadjavad Darvish**
Degree:	**Master of Applied Science**
Title:	**An analytical design tool for a pin fin sorber bed heat/mass exchanger**
Committee:	**Chair:** **Ramtin Rakhsha** Lecturer, School of Mechatronics Systems Engineering
	Majid Bahrami Supervisor Professor, School of Mechatronics Systems Engineering
	Mehran Ahmadi Committee Member Lecturer, Sustainable Energy Engineering
	Sami Khan Examiner Assistant Professor, Sustainable Energy Engineering

Abstract

Sorption cooling and heating systems (SCHS) have recently drawn immense attention as an alternative technology that enhances the efficiency of energy systems to reduce reliance on fossil fuels for heating and cooling. However, they have not been widely adopted mainly due to factors such as: i) the sorbents' low thermal conductivity and diffusivity; and ii) low heat and mass transfer due to the inadequacy of existing sorber bed heat exchanger designs. To address these challenges, a pin fin sorber bed design is proposed in this study as a potential alternative to conventional beds, which can provide both high Coefficient of performance (COP) and enhanced heat and mass transfer inside the sorber beds. To assess the performance of the proposed structure, a predictive model is needed to provide accurate and fast evaluation of the SCHS performance as a function of the geometric design and operating parameters. Consequently, a novel closed-form analytical model is used to predict the sorption performance of a pin fin heat/mass exchanger (PF-HMX) prototype, using the Eigenfunction expansion method to solve the governing energy equation. The proposed transient 2-D solution, includes all salient thermophysical and sorption properties, sorbent geometry, operating conditions, and the thermal contact resistance at the interface between the sorber bed heat exchanger and sorption composite. An analysis of variance (ANOVA) method is utilized to understand the percentage contribution of each parameter on the specific cooling power (SCP) and COP. It is shown that the amount of graphite flakes, sorbent thickness and fin radius on one hand and the cycle time and graphite flake content on the other have the highest level of contribution to the COP and SCP, respectively. Moreover, a parametric study found that heat/mass exchanger (HMX) geometry, sorbent properties and cycle time counteract the effects on the COP and SCP, which should be optimized simultaneously to build an optimal design. The analytical model validated successfully using the sorption data from a custom-built gravimetric large temperature jump (G-LTJ) test bed. The experimental results show that the present PF-HMX design with a relatively low mass ratio (MR) can achieve an SCP of 1160 W/kg sorbent, and a COP of 0.68 which are higher than the previously published results in the literature.

Keywords: sorption system; analytical modeling; heat and mass transfer; coefficient of performance; specific cooling power.

Dedication

Lovingly dedicated to
my wonderful wife, Asal,
and to my entire family
for their support and encouragement

In memory of
the 176 beautiful souls of flight PS752
who left us so early

Acknowledgements

My deep gratitude goes first to Professor Majid Bahrami who expertly guided me through my graduate education and supported me in all aspects. I'd like to express my gratitude to my Committee members, Drs. Mehran Ahmadi and Sami Khan, for their discussions and comments on my research project. I am also grateful to Dr. Ramtin Rakhsha for accepting to be the Defense Committee Chairman.

My appreciation also extends to my colleagues and friends at the Laboratory for Alternative Energy Conversion (LAEC). Drs. Hesam Bahrehmand and Mina Rouhani's help and encouragement have been especially valuable, and their insights launched the greater part of this dissertation. I also want to express my gratitude to Dr. Claire McCague, Postdoctoral Fellow at LAEC for her technical support and expert guidance.

I would like to gratefully acknowledge the financial support of the Natural Sciences and Engineering Research Council of Canada (NSERC) through the Advancing Climate Change Science in Canada (ACCSC) Grant No. ACCPJ 536076-18.

Most of all, I am fully indebted to my family and especially to my beautiful wife, Asal, for her support, patience, encouragement and unconditional love.

Table of Contents

List of Tables

List of Figures

Nomenclature

A	heat transfer area, m^2
Bi	heat transfer Biot number
c	specific heat capacity, $Jkg^{-1}K^{-1}$
Fo	Fourier number
H	height, m
h	convective heat transfer coefficient, $Wm^{-2}K^{-1}$
H_{ads}	enthalpy of adsorption, $J\ kg^{-1}$
h_{fg}	enthalpy of evaporation, $J\ kg^{-1}$
k	thermal conductivity, $W\ m^{-1}\ K^{-1}$
L	height of adsorbent, m
m'	slope of uptake versus temperature (-0.0118 for sorption and -0.0123 for desorption) [1]
p	pressure, Pa
p_0	saturation pressure, Pa
R	radius, m
Δ	thickness, m

t	time, s
r	radial coordinate
T	temperature, K
z	coordinate
R	thermal resistance, K m^2 W^{-1}

Greek

λ	eigenvalue in η direction
γ	eigenvalue in ξ direction
η	dimensionless coordinate of r
ξ	dimensionless coordinate of z
τ	cycle time, s
Θ	dimensionless temperature
κ	dimensionless thermal conductivity ratio
α	thermal diffusivity, m^2s^{-1}
μ	dimensionless thermal diffusivity
Λ	dimensionless thermal contact conductance
ω	adsorbate uptake, (kg adsorbate/kg dry adsorbent)

Subscripts

0	initial condition
ads	adsorption
c	channel
cond	condenser
des	desorption
evap	evaporator
eq	equilibrium
f	fin
fs	fin spacing
HTF	heat transfer fluid
s	sorbent

Abbreviations

ANOVA	analysis of variance
COP	coefficient of performance
G-LTJ	gravimetric large temperature jump
GWP	global warming potential

MR	mass ratio
ODP	ozone depletion potential
PF-HMX	pin fin heat and mass exchanger
PVA	polyvinyl alcohol
SCHS	sorption cooling and heating systems
SCP	specific cooling power
TCR	thermal contact resistance
TGA	thermogravimetric sorption analyzer
TPS	transient plane source
VCR	Vapor-compression refrigeration

Executive Summary

Over 60% of residential and 50% of commercial building energy consumption are demanded for heating and cooling [2]. To date, more than 80% of global energy is generated by fossil fuels, showing the significant potential role of thermal uses in our global emissions picture[3]. Fifty-two percent of the global primary energy consumption is dissipated to the ambient air as waste hea, and low-grade energies, temperature sources below 100℃, form 63% of this waste heat [4]. Therefore, utilization of low-grade energies offers substantial environmental benefits amid the world energy crisis. Regarding energy considerations and the reduction of environmental pollutants, a promising alternative to the conventional heating and cooling system is low-grade heat recovery through sorption cooling heating systems (SCHS). Among the different cooling and heating systems, SCHS have recently sparked immense attention as an alternative technology to enhance the efficiency of energy systems and reduce our reliance on fossil fuels for the heating and cooling of buildings and vehicles. However, SCHS are not currently widely adopted mainly due to factors such as: i) the sorbents' low thermal conductivity and diffusivity; ii) low heat and mass transfer due to the inadequacy of existing sorber bed heat exchanger designs; and iii) low operating pressure, all leading to inefficient, large and costly SCHS. To address some of these challenges, sorber bed heat exchangers need to be specifically and carefully designed for SCHS.

Objective

The objective of this study is to establish a systematic approach to propose and develop a novel sorber bed HMX design to address the abovementioned challenges. The systematic approach, includes modeling, assessing, manufacturing and testing a proof-of-concept demonstration for SCHS as a potential alternative to the off-the-shelf sorber bed HMX, which can provide a high SCP and COP with a relatively low mass ratio (MR). Increasing the use of sorption systems would decrease greenhouse gas emissions and reduce Canada's dependence on fossil fuels. The compact and efficient sorber bed would increase the marketability of sorption thermal energy storage, helping to sustainably meet the extra demand on the global energy supply due to the increased utilization of heating and cooling systems.

Research methodology

A systematic approach is adopted to achieve the objectives of this Master's Program, and is summarized in the following milestones which were set and executed:

- Analytically developed a 2-D transient closed-form solution, which includes the geometry of the HMX, salient thermophysical and sorption properties, as well as the operational input parameters. It considers: (i) the transient behavior of the sorber bed; and (ii) the thermal contact resistance at the interface between the sorption material and the HMX;

- Explored the transient effect of adding thermally-conductive additives to sorbent materials and their performance;

- Designed and fabricated a custom-built gravimetric large temperature jump (G-LTJ) test bed in order to validate the analytical model;

- Estimated the effect of key design and operating variables and their level of contribution to the performance of the sorption HMX, namely the COP and SCP; and

- Analytically investigated the performance of the novel design versus the state-of-the-art published research.

Contributions

The main outcomes of this project are highlighted as follows:

1. A novel closed-form analytical solution is developed for determining the conjugated heat and mass transfer and performance of the sorber bed design. The proposed transient 2-D solution for temperature distribution inside the sorbent coating and the heat exchanger (HEX), includes all salient thermophysical and sorption properties, HEX geometry, operating conditions, and the thermal contact resistance at the interface between the sorber bed heat exchanger and the sorption composite. The model successfully predicts temperature variation, uptake, heat transfer, and the geometry effect. Using the present 2-D model, a comprehensive parametric study is performed and it is

found that the sorber bed geometry, heat transfer characteristics, sorbent properties, and cycle time can have counteracting effects on the COP and SCP and should be optimized simultaneously to build an optimal design in future;

2. The ANOVA method was utilized to understand the percentage of contribution of each parameter, as well as to determine the coefficient of a multivariable equation[5]. A Multi-way ANOVA has been done using the n-ANOVA function in MATLAB to find each parameter contribution for the COP and SCP;

3. A gravimetric large temperature jump (G-LTJ) test bed is custom-built to validate the analytical solution; and

4. It was shown that the present PF-HMX design with a relatively low mass ratio (MR) can achieve a SCP of 1160 W/kg sorbent and a COP of 0.68, which is higher than the previously published results in the literature.

Research Roadmap and Contributions

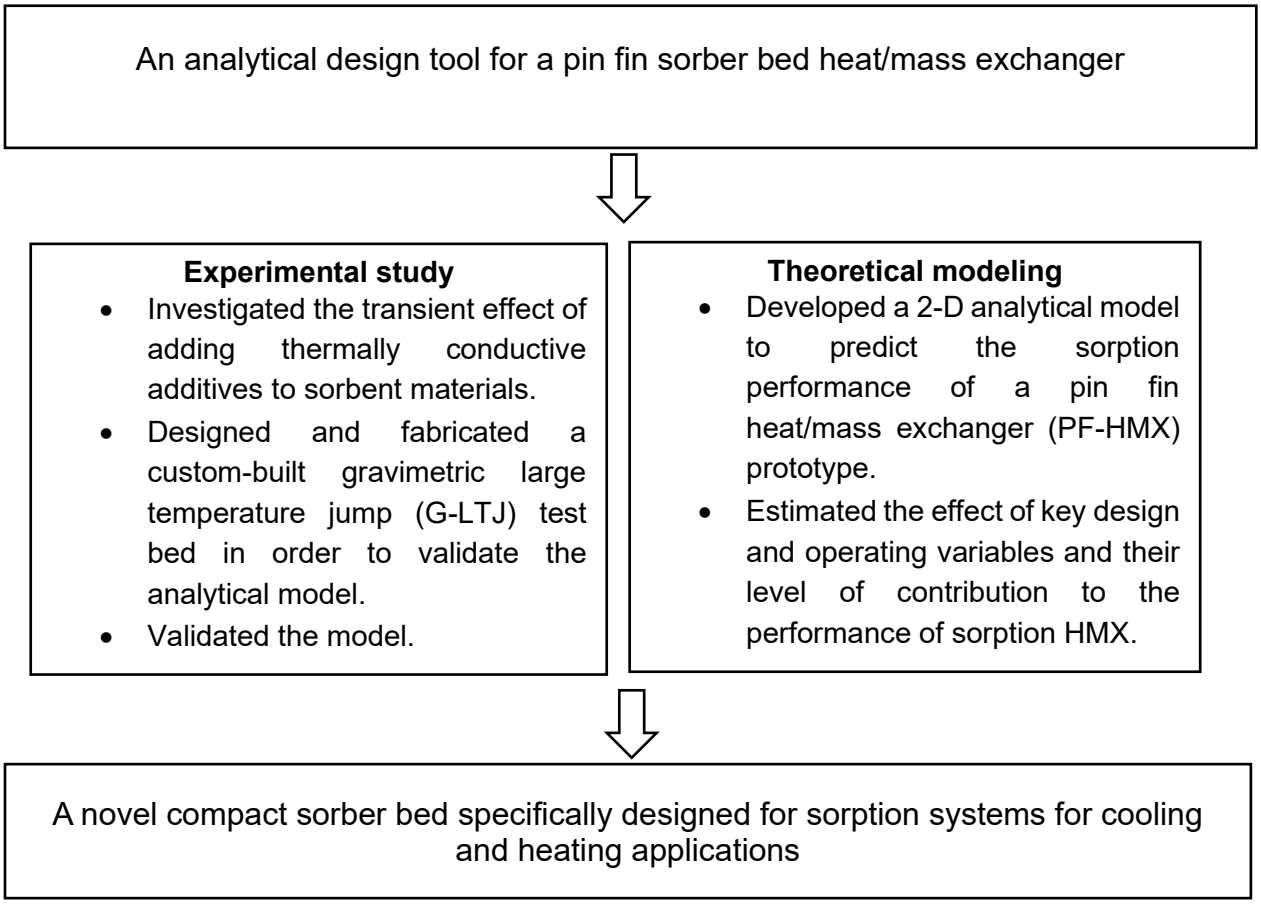

Chapter 1.

Introduction and literature review

Heating and cooling systems consume over 60% of the residential and almost 50% of the commercial building energy [2]. Powered by electricity, vapor-compression systems (VCR) are the most common cooling technologies on the market. And since more than 80% of global energy– including electrical power generation [6], [7]– is generated from fossil fuels, building heating and cooling systems are major greenhouse gas emitters [3], which leads to catastrophic environmental impact, including climate change.

Furthermore, fluorocarbon-type refrigerants used in VCR systems are not only potent greenhouse gases but also implicated in ozone depletion [8], [9].

In the transportation, industrial, and building sectors, low-grade thermal energy is abundant, such as waste heat and solar energy. Hot water, furnaces, boilers, engine exhaust, drier, air compressors are examples of available waste heat [10]. The Canadian energy stream from energy sources to export energy, domestic productive energy, and domestic waste energy is depicted in Figure 1.1. Sixty-seven percent of primary energy is wasted as domestic energy consumption, see Figure 1.1.

The estimated global waste heat distribution for 2016 is shown in Figure 1.2. It can be seen that 52% of the global primary energy is lost as waste heat, with low-grade energies (temperature sources below 100℃) constituting 63% of this untapped energy [11]. Sorption waste heat-driven cooling/heating systems have the potential to offer a solution to world energy needs and reduce environmental pollutants. Sorption cooling and heating systems (SCHS) have recently drawn immense attention as an alternative technology that enhances the efficiency of energy systems to reduce reliance on fossil fuels for heating and cooling. However, they have not been widely adopted due to the following: i) low thermal conductivity and diffusivity of sorbent composites; ii) low heat and mass transfer due to the inefficiency of existing sorber bed heat exchanger designs; and iii) low operating pressure (near vacuum), all of which lead to large, inefficient, and costly SCHS [12]–[15].

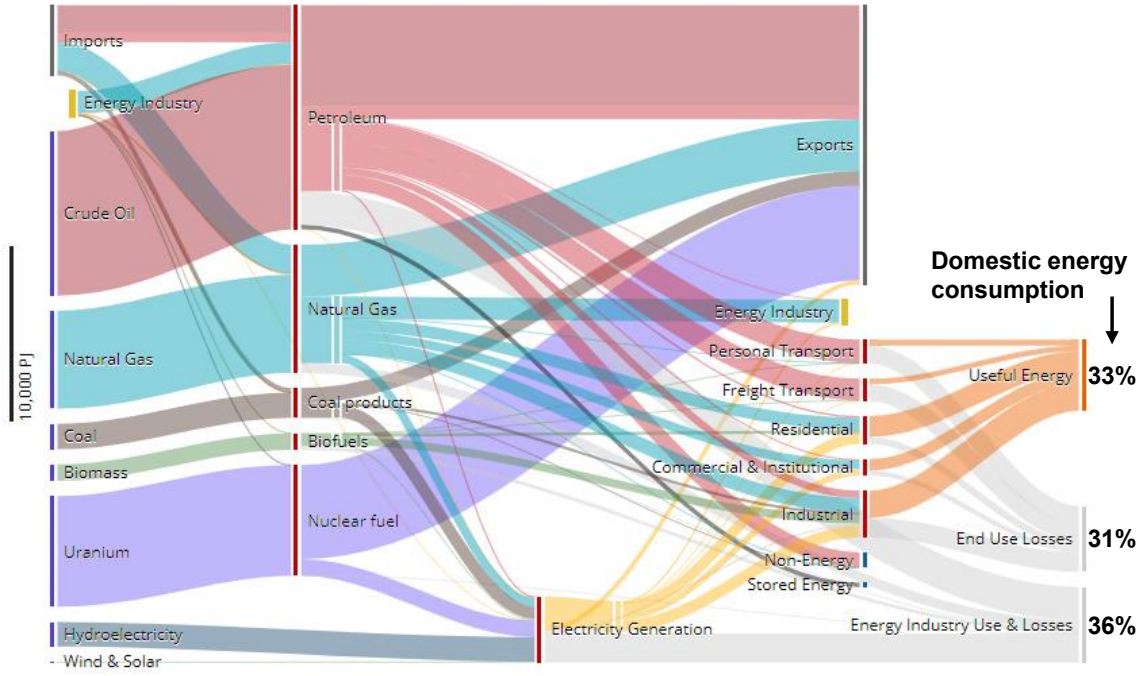

Figure 1.1. **Sankey diagrams associated with fuel and electricity production and use in Canada, data from Canadian Energy Analysis Research (CESAR) [16]**

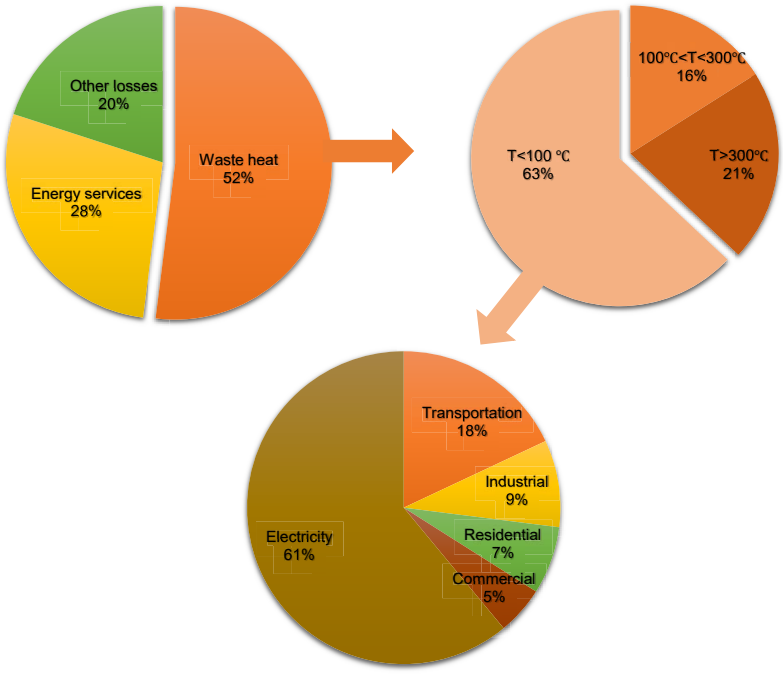

Figure 1.2. **The estimated global waste heat distribution for 2016 with the source temperature [11]**

1.1. Sorption principal

When a porous solid is exposed to a gas or vapor which has affinity, the adsorption of a gas (sorbate) by a solid (sorbent) will be the result of the attraction forces between the individual sorbate molecules and the atoms or ions composing the sorbent [17].

There are two major forces acting between the sorbate and sorbent, the physical and the chemical. If the Van der Waals forces between the sorbate and sorbent create the adsorption, it is called physisorption. If the chemical bonding forces lead to sorption, it is called chemisorption. In general, the sorbate uptake includes a number of physical processes, sorbate transfer from the bulk gas to the sorbent exterior surface, diffusion of the sorbate molecules inside the pores, and the sorption process. When all the pores replete with sorbate, the regeneration process can be done by passing a hot fluid, warmed with waste or solar energy, through the bed to remove the sorbate and make the sorbent ready for the next cycle[18]. A schematic explanation of the Adsorption/Desorption process is given in Figure 1.3.

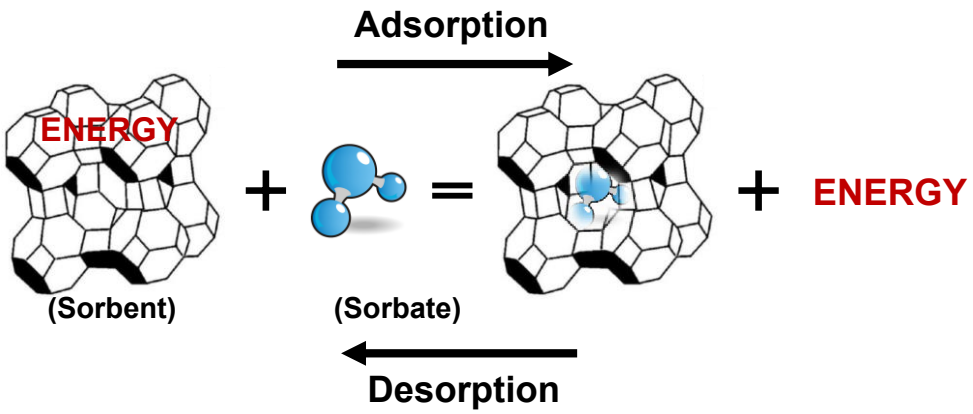

Figure 1.3. A schematic explanation of adsorption and desorption processes

Physisorption is largely controlled by surface properties, such as surface area, micro- and macro-pores, and the size of the grains[19]. Chemical forces between the pairs are much stronger than physical forces[20].

Adsorption is an exothermic process which means energy is liberated during this process which could be understood by considering the Gibbs free energy equation:

$$\Delta G = \Delta H - T\,\Delta S \tag{1}$$

The entropy of adsorbed gas decreases due to relatively low mobility, therefore, the ΔS of adsorption is negative. ΔG must be negative for significant adsorption to take place, which implies that the enthalpy of adsorption (ΔH) will be negative[21]. The enthalpy of adsorption, depending on the magnitude of the van der Waals forces, electrostatic forces, phase change and the presence of any chemical bonds, is usually small in physical adsorption and large in chemical adsorption because the physical forces are weaker than the chemical forces[19]. Almost all industrial projects and research deal with physical sorption due to its reversibility.

The variation in the amount of gas adsorbed by the adsorbent with pressure at constant temperature is expressed as an “adsorption” isotherm. Different theoretical models, such as the Brunauer-Emmett-Teller (BET) model, Freundlich, Langmuir, etc., have been developed to describe the relationship between the mass of sorbate adsorbed by a sorbent and the sorbate’s pressure and temperature, For other excellent reviews on the sorption isotherm subject, the reader is referred to [21]–[23].

1.2. Screening of sorption pairs

1.2.1. Suitable sorbent material properties for a SCHS application

The first phase in developing an effective SCHS is to choose the right sorption working pair for each application. The following properties are used to determine the suitability of a sorption working pair:

- Low-desorption temperature;
- A high coefficient of performance, which requires high water uptake and the heat of sorption;
- A high specific cooling power, which is determined by the sorbent material's uptake rate (sorption kinetics), thermal conductivity, and thermal diffusivity. Both high equilibrium uptake and fast kinetics are needed for a high-performance sorption working pair [24];

- Non-toxic and environmentally friendly;
- Low cost which eases the wide adoption of SCHSs;
- Mechanical strength, cycle-ability, stability, and full reversibility during the adsorption/desorption process under different operating conditions; and
- Non-corrosiveness.

Sorption working pairs are made up of a sorbate fluid (water, ethanol, ammonia, or methanol) and the sorbent. Water was used as the sorbate in this research because of its non-toxicity, high enthalpy of evaporation, non-flammability, metal compatibility, zero ozone depletion potential (ODP), and zero global warming potential (GWP). The low operating pressure, on the other hand, necessitates proper sealing and vacuum chamber construction.

As illustrated in Figure 1.4, the working pair for a SCHS can be classified into three major categories, namely: solid sorption pairs, composite pairs, and chemical sorption pairs. Composite pairs has grown over the past decades in order to improve heat and mass transfer[25]. This type of adsorbent is obtained by an amalgamation of a chemical adsorbent with a porous material[26], [27].

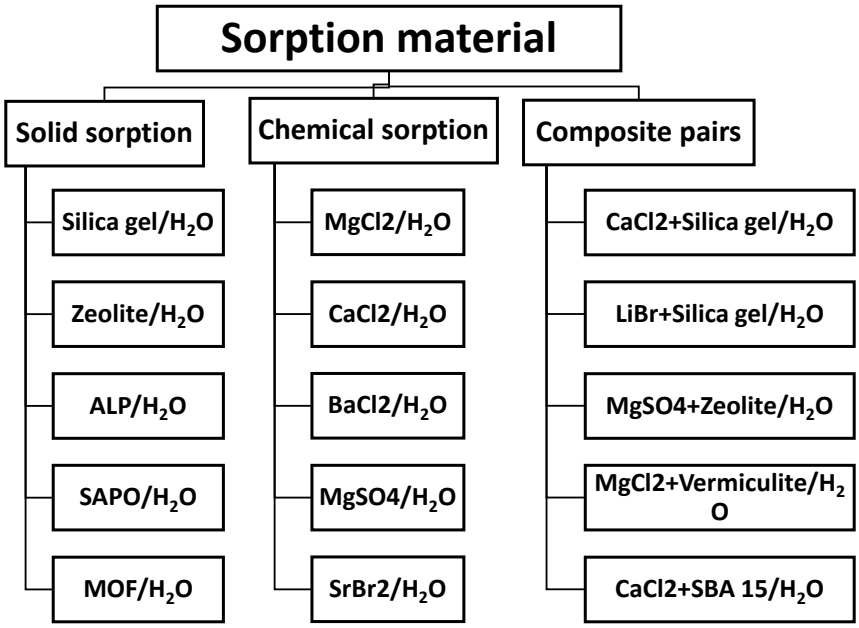

Figure 1.4. The main categories of sorption materials

1.2.2. Solid sorption

The common solid adsorbent materials for SCHS are silica gel, zeolite, aluminophosphates (ALP) and silico-aluminophosphates (SAPO). Metal organic Frameworks (MOFs) adsorbents also started to be studied recently[28].

Silica gel/H_2O is the most well-known solid adsorption material for SCHS application. It has been widely used in a number of other industries, including clothing, pharmaceutical, electronics, computers, paper, and home appliances, due to its hydrophilic properties. The porous structure and the specific surface area depend on the preparation conditions, and for silica gel, this area can be between 250 to 900($\mathrm{m^2/g}$)[24]. Despite its low cost and commercial availability, this type of material suffers from low cycle-ability[29] and low water vapor exchange, which restricts system performance.[30]

Zeolite is a type of aluminasilicate crystal with a wide microporous volume that has been investigated by many research groups. The microporous structure results in a higher connection with water, leading to a higher desorption temperature ($> 150℃$). Moreover, zeolites have a higher long-term durability than silica gel due to their crystalline structure. The most common classical synthetized zeolites are faujasite, A, 13X, and Y.

The high-charging temperature of zeolite sorbents led researchers to develop new classes of zeolite-like micro-porous sorbents with a crystalline structure, namely, aluminophosphates (AlPOs) and silico-aluminophosphates (SAPOs). They require low-grade heat sources, i.e., below 100℃, with a comparable uptake capacity to that of the zeolite. Among the classes of AlPOs and SAPOs, AlPO-18 and SAPO-34 are regarded as the most attractive candidates for storage application under most favorable operating conditions, that is, a low-charging temperature and discharging at water vapor pressure similar to the saturation water vapor pressure at ambient temperature[31]. AQSOA FAMZ02 (commercial SAPO-34), which was developed by the Mitsubishi Plastics Incorporation[32], shows a desirable performance for an adsorption heat pump (AHP) and desiccant air conditioning system driven by heat sources below 90℃ [14], [33], [34].

Recent progress in Materials Science offers a new family of super molecular sorbents called Metal-organic frameworks (MOF). High surface area, crystalline open structures, tunable pore size, and functionality are the properties which make MOF

attractive sorbent candidates[35]. MOF materials present some open issues to be investigated, such as weak cycling stability and the cost. A comparison among the properties of some sorbent materials is reported in Table 1.

Table 1. Thermophysical properties of different sorbent materials

material	Silica gel	Zeolite	AlPOs/SAPOs	Expanded Graphite	MOF	Ref
$k\ \left({}^{W}/_{mK}\right)$	0.15-2	0.15-0.25	0.15-0.25	-	0.1-0.15	[36]
$\rho\ \left({}^{kg}/_{m^3}\right)$	650-700	650-900	800-900	-	1000-2000	[36]
$C_p\ \left({}^{kJ}/_{kg.K}\right)$	0.84-1.13	0.85-1.08	0.85-0.95	0.7	0.8-1.2	[36], [37]
SSA $\left({}^{m^2}/_{g}\right)$	750-850	550-600	-	18-22	1310	[37]
$\omega\ \left({}^{kg}/_{kg}\right)$	0.03-0.23	≤0.3	0.28-0.9	-	0.39	[36], [38]
Ads heat $\left({}^{kJ}/_{kg_{H2O}}\right)$	160-180	50-300	250-300	-	20-200	[36]
T_{des} (°C)	50-150	70-350	80-200	100-200	60-150	[36], [38]
Pore volume $\left({}^{cm^3}/_{kg}\right)$	0.4	-	AlPOs= 0.53 SAPOs= 0.27	-	0.57	[39]–[42]
Cost $\left({}^{\$}/_{kg}\right)$	0.88-0.34	1.65-2.2	-	1.8-2.5	>130	[37]

1.2.3. Composite sorption pairs

Composite sorbents, salt in a porous matrix (CSPM), are developed and proposed to overcome some of the main challenges of previous materials, for instance:

1- Pure salt agglomeration and swelling which leads to a reduction in mass and heat transfer, respectively.

2- Low cycle-ability and thermal conductivity of salt hydrated materials.

3- Low sorption capacity.

Low desorption temperature, improved heat conductivity, higher water uptake, and the possibility of a modification of sorption properties based on the specific storage

application by the variation of the salt and matrix nature are the main benefits of CSPMs. Various salts embedded inside different porous materials, such as silica gel, zeolite, expanded graphite, and activated carbon fiber that have been reported by different researchers, are shown in Table 2.

Table 2. A summary of investigation on composites materials

Ref	Year	Matrixes	Salts	Salt ($wt\%$)	Experimental conditions	
					T (°C)	P_{H2O} (mbar)
[43]	1996	Silica gel (mesoporous)	$CaCl_2$	33.7	20-150	8-133
[44]	2000	Vermiculite	$CaCl_2$	57.3	30-150	8.2-42
[45]	2002	MCM-41	$CaCl_2$	37.7	20-150	8.7-50.3
[46]	2002	carbon Sibunit	$LiBr$	29	30-145	6-81
		Macro-porous expanded graphite		33		
[47]	2004	Silica gel Aluminosilicate	$CaCl_2$& $MgCl_2$	30	-	-
[48]	2005	Attapulgite	$CaCl_2$	30	20-60	-
[49]	2006	Graphite, copper, zeolite A, sand	$MgCl_2$	46-69	35-200	1.18-2.18
[50]	2007	Silica gel	$CaCl_2$	10-40	25-80	-
[51]	2009	Silica gel	$Ca(Cl_3)_2$	45	30-150	9-45
[52]	2010	Attapulgite	$MgCl_2$& $MgSO_4$	19-43	30-130	36
[53]	2010	Silica SBA-15	$CaCl_2$	43	50-100	0-50
[54]	2011	Zeolite 13X & silica gel	$MgSO_4$	15	25-150	21.5
[55]	2011	Vermiculite	$LiNO_3$	63	33-65	12.6-56.2
[56]	2012	FeKIL2	$CaCl_2$	7	40-150	11.8-55.3
[57]	2013	Silica gel, alumina	$CaCl_2$, $MgCl_2$ $LiBr$	30-75	-	-
[58]	2014	Zeolite 13X, Silica gel, Vermiculite	$CaCl_2$, $MgSO_4$ $LiBr$, $LiNO_3$, $Ca(NO_3)_2$	2-65	30-140	-
[59]	2014	Carbon foam, expanded natural graphite	$CaCl_2$, KCl	63-90	25-200	20
[60]	2015	Silica gel- alumina	$CaCl_2$	15	20-150	-

[61]	2015	Activated carbon, silica solution, expanded graphite	$LiCl$	32-45	30-90	25.4
[62]	2015	Wakkanai siliceous shale	$LiCl$, $CaCl_2$	9.6	15-150	22.1
[63]	2016	Activated carbon, expanded graphite	$CaCl_2$, KCl	31-90	25-200	10-20
[64]	2016	Carbon nanotubes	$LiCl$, $CaCl_2$	44-53	35-75	8.7-56
[65]	2016	Vermiculite	$SrBr_2$	10-40	20-300	-
[66]	2017	Vermiculite	$LiCl$	59	35-85	8.7-56

1.2.4. Water sorption isotherm

At 25 °C, the water sorption isotherms of various sorbent materials are shown in Figure 1.5. Using an IGA002 thermo-gravimetric analyzer (TGA), a sorption isotherm of the composite sorbent of microporous silica gel B40, silica gel B60 (siliaFlash, Silicycle, Inc., Quebec, Canada, FAM-Z02(AQSOA Mitsubishi Plastics, Inc.), and silica gel B150/$CaCl_2$ were collected [67]. The water sorption of Sapo-34 can be found in [68]. The water sorption for MOFs (MIL-100(Fe) UoB, Aluminum fumarate, MIL-101 (Cr) UoB, CPO-27 (NI)) can be found in [69].

T_{des}=90 °C, T_{sorp}= T_{cond}=30 °C, T_{evap}=15 °C, which correspond to a p/p_0 of 0.401 and 0.0606 for adsorption and desorption, respectively, are widely used in operating conditions for sorption cooling system applications [70].

The composite sorbents of silica gel B150/$CaCl_2$ is chosen among other candidates in the present study because of the higher water uptake in the operating range, its high market availability and lower cost [71].

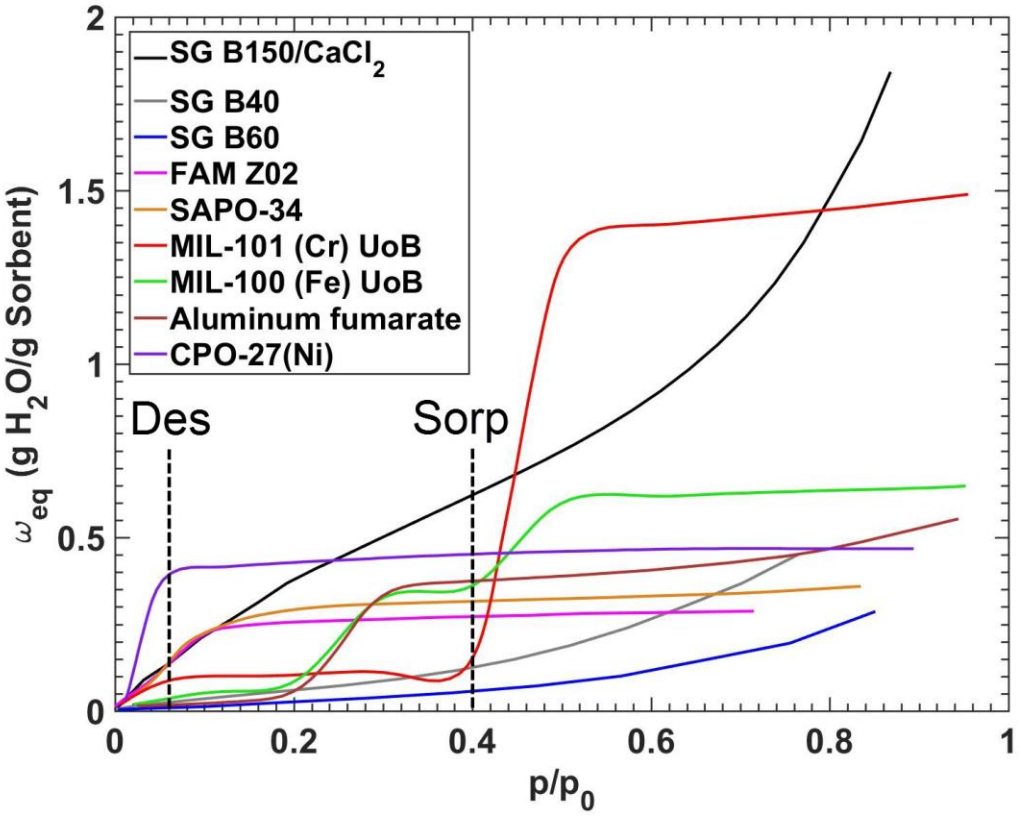

Figure 1.5. The water uptake of the sorbent candidates at 25 ℃ [67].

1.3. Thermodynamic of sorption cycle

Figure 1.6 shows the schematic diagram of a VCR. As can be seen, the refrigerant is evaporated in the evaporator and provides cooling. Afterwards, work is done by the compressor on the refrigerant to increase its pressure. Subsequently, the refrigerant is condensed in the condenser and releases heat. Finally, the refrigerant passes through an expansion valve or a capillary tube to reduce its pressure and become ready for the evaporation process again.

Heating–desorption–condensation and cooling–adsorption–evaporation, on the other hand, are the two major stages in a SCHS. The compressor in the VCR is replaced with sorber beds in the SCHS, as shown in Figure 1.7. Sorber beds are made up of heat exchangers and sorbent materials in the shape of coating, pellets or grains that can desorb the sorbate to the condenser when heated at a higher pressure; and can adsorb the sorbate when connected to the evaporator and cooled down. As a consequence, rather

than using the compressor, the heat will be used to raise the pressure, which is the driving force for refrigeration cycles. As a result, instead of using mechanical work from the engine or electrical energy in VCR, waste heat and solar energy can be used to power the refrigeration cycle.

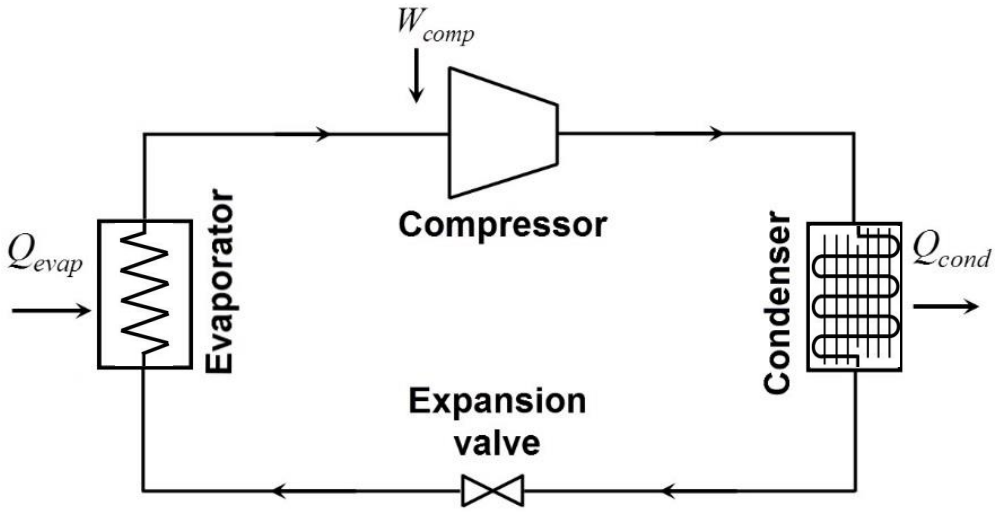

Figure 1.6. A schematic diagram of VCR

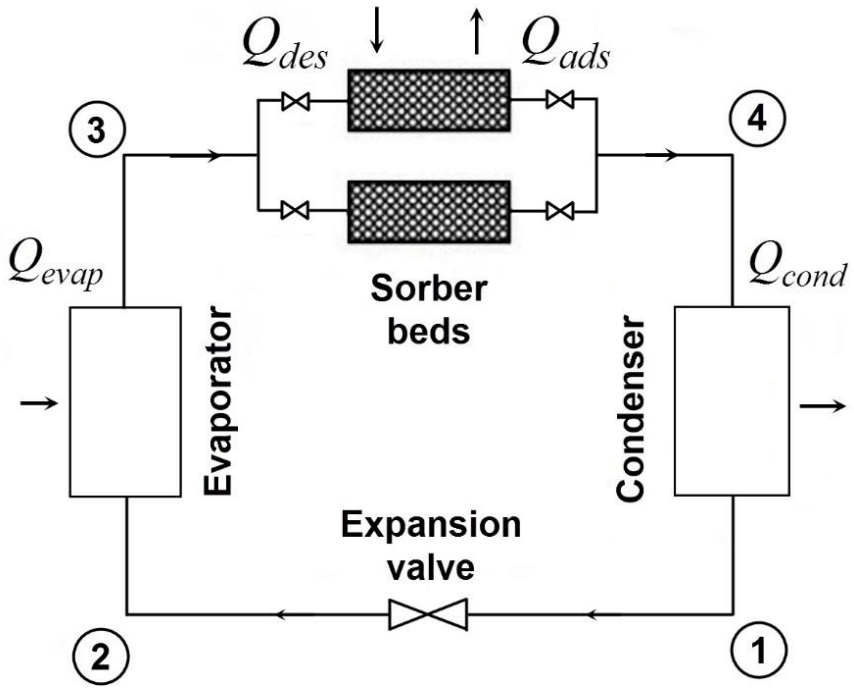

Figure 1.7. A schematic diagram of a SCHS [67]

The thermodynamic cycle of a SCHS, shown in Figure 1.8, includes four processes:

1- *Isosteric cooling:* Both valves between the sorber bed and evaporator and condenser are shut and the sorbent loses its heat during an isosteric cooling process (step 1'-2'). At the same time, the sorbate inside the condenser passes through an expansion valve to reduce its pressure, Step 1-2.

2- *Isobaric adsorption*: During Step 2-3, the valve to the evaporator is opened. The sorbate enters the evaporator, absorbs heat from the environment and evaporates. At the same time, the valve between the sorber bed and evaporator is open and the vapor sorbate is adsorbed at a constant pressure and releases its heat, Step 2-3.

3- *Isosteric heating:* During Step 3-4, the sorbent material absorbs heat from an external heat source through an isosteric process. Both valves are closed at this step to prepare the sorber bed for the desorption process. The heating process at a constant uptake is continued until the sorber bed pressure equals the condenser pressure.

4- *Isobaric desorption:* Finally, the entrance valve to the condenser is opened. In Step 4-1, the external heat source continuously heats the sorber bed because of the endothermic desorption and the sorbate leaves the sorber bed. In Step 4-1, the sorbate is condensed in the condenser.

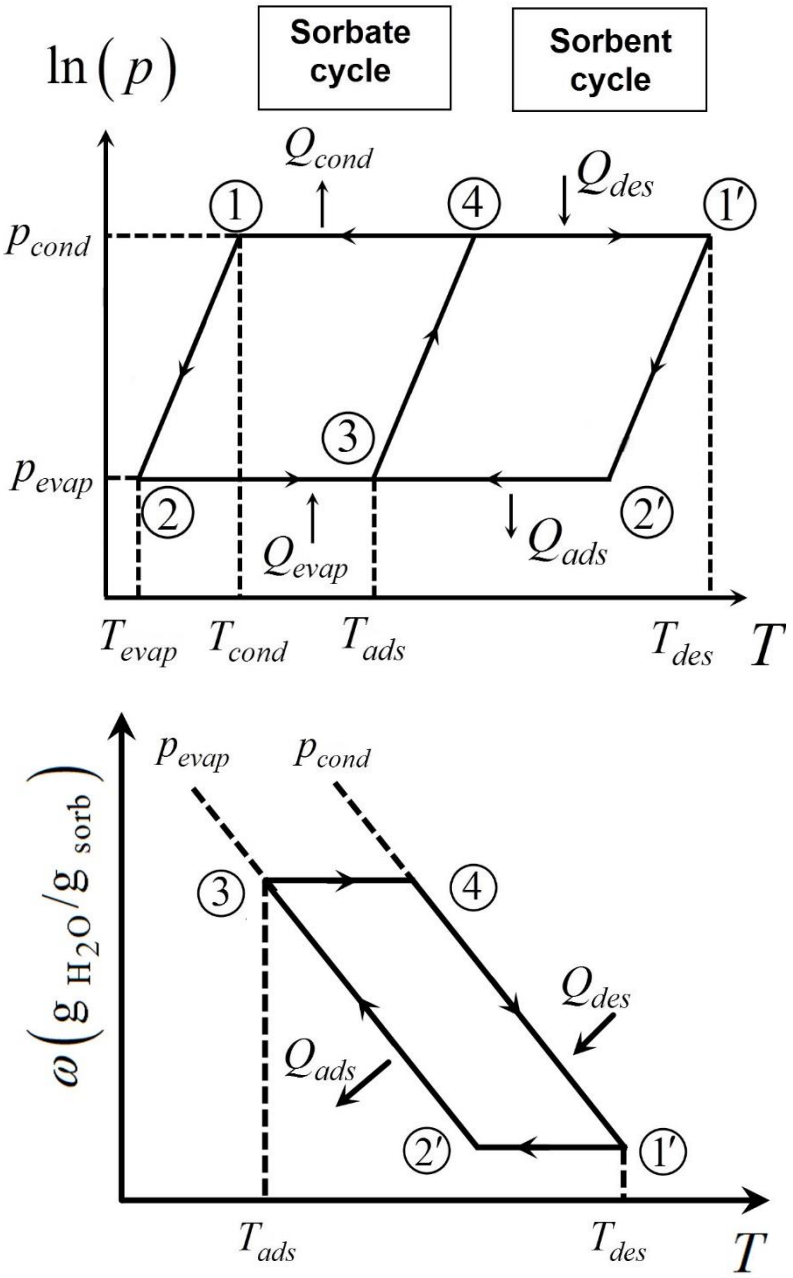

Figure 1.8. A thermodynamic depiction of a sorption cycle [67]

1.4. Absorption cooling systems

Liquid absorbents such as LiCl, LiBr, and $CaCl_2$ absorb the refrigerant such as water in the absorber when the absorbent is cooled with a heat transfer fluid (HTF) through a heat exchanger in absorption cooling systems. Cooling is produced when the refrigerant

is evaporated from the evaporator. After that, the absorbent and refrigerant weak solution is piped to the regenerator, where it is heated with HTF through HEX. The refrigerant is desorbed from the regenerator and condensed in the condenser before passing through an expansion valve to the evaporator. To keep the cycle going, the rich solution is returned to the absorber via an expansion valve [72]. The power consumption of the system is substantially reduced when the compressor in VCR is replaced with a pump in ACS [73]. When low-grade thermal energy, such as heat sources with temperatures less than 100 oC, is utilised, the COP of ACS falls below 0.8 [74]. If higher temperature heat sources and multi-effect ACS are utilised, the COP of ACS can reach 1.8. Despite this, due to the multiple stages of absorption, the system would grow in size and require more heating, such as gas-fired regenerators. Bulkiness, poor COP, corrosive absorbents, limited mass transfer, crystallisation, swelling, and agglomeration of salt are the most significant disadvantages of ACS [63], [72], [73], [75].

1.5. Performance indicators

The SCP is defined as the evaporative cooling rate generated per unit mass of dry sorbent material, and represents how fast the heat and mass transfer processes take place in the sorber bed, Eq. (2).

$$SCP = \frac{Q_{evap}}{m_s \tau} = \frac{m_s \int_{ads} \frac{d\omega}{dt} h_{fg} dt}{m_s \tau} = \frac{\Delta\omega \, h_{fg\,@T_{evap}}}{\tau} \quad (2)$$

where, Q_{evap} is the evaporative cooling energy (J), m_s is the sorbent mass (kg), ω is the sorbate uptake (g sorbate/g sorbent), h_{fg} is the sorbate enthalpy of evaporation (J/kg), and τ is the cycle time (s).

The COP, defined as the ratio of the evaporative cooling energy to the input energy, which is the summation of desorption heat and sensible heat, Eq. (3). The COP can be increased by: (i) enhancing the heat and mass transfer rate in the sorber bed, to increase both the evaporative cooling energy and the desorption heat, which overall increases the COP; and (ii) decreasing the thermal inertia of the HMX, which reduces the (sensible) heat input needed to perform the temperature swing during the adsorption and desorption cycle.

$$COP = \frac{Q_{evap}}{Q_{input}} = \frac{Q_{evap}}{Q_{sens} + Q_{des}} = \frac{m_s \int_{ads} \frac{d\omega}{dt} h_{fg} dt}{\int_{des} \left(\left(m_s \left(c_{p,s} + \omega c_{p,w} \right) + m_{HMX} c_{p,HMX} \right) \frac{dT}{dt} - m_s \frac{d\omega}{dt} H_{ads} \right) dt} \quad (3)$$

where, Q_{evap} is the evaporative cooling energy (J), Q_{input} is the input thermal energy (J), Q_{sens} is the thermal energy required to overcome thermal inertia of the sorber bed HMX (J), Q_{des} is the thermal energy consumed for desorption (J), m_s is the sorbent mass (kg), m_{HMX} is the mass of HMX (kg), ω is the sorbate uptake (g sorbate/g sorbent), h_{fg} is the sorbate enthalpy of evaporation (J/kg), H_{ads} is the enthalpy of adsorption (J/kg), c_p is the specific heat (J/(kg K)), and T is the sorbent temperature (K).

In order to properly evaluate the performance of the sorption cooling system, the MR of the sorber bed masses to the sorbent material is also considered as follows:

$$MR = \frac{m_{HMX} + m_s + m_{HTF}}{m_s} \quad (4)$$

where, m_{HMX} is the mass of HMX (kg), m_s is the sorbent mass (kg), and m_{HTF} is the heat transfer fluid (HTF) mass.

Chapter 2.
Analytical solution of a sorber bed heat/mass exchanger

2.1. Literature review

A number of approaches have been proposed for the modeling of sorption systems in the literature. They can be categorized into three main modeling groups: (i) thermodynamic; (ii) lumped parameter; and (iii) conjugate heat and mass transfer analysis. Thermodynamic analysis [76], [77] is the simplest steady-state simulation in which details of heat and mass transfer are not considered; however, it can reveal the upper limit performance of sorption systems. Lumped models [78]–[81] consists of three governing equations: sorption equilibrium, energy balance, and mass balance. The focus of this modeling approach is on the sorber bed as the geometrical details of the HMX cannot be included in the analysis. Other simplifying assumptions are: (i) a uniform temperature in the sorber bed; (ii) a uniform uptake in the bed; and (iii) a thermodynamic equilibrium for both gas and solid phases. The conjugate heat and mass transfer model considers the variation of temperature and mass content of the HMX in both time and space domains. The governing equations are expressed as the following partial differential equations with initial values and boundary conditions: (i) the conservation of energy; (ii) the conservation of mass; and (iii) the state equation for the sorbent material. Due to the sorption kinetics and thermophysical properties, the aforementioned equations are transient, complex and nonlinear. As such, finding closed-from analytical solutions for such conjugate heat and mass transfer are extremely challenging. Therefore, numerical methods are commonly used, examples include: i) the finite difference method [82]–[90]; ii) the finite volume method [91]–[95]; and iii) the finite element method [96]–[103]; the key issue with numerical modeling is the high computation time that makes optimization and control of the operational parameters in real-time application. There are a few analytical closed-form models in the literature that provide low computation time and high accuracy [1], [104]–[106].

There are several studies in the literature with the focus of developing sorber beds. The specification and performance of these SCHS are summarized in Table 3 which includes working pairs, sorber bed HMX design, and reported SCP, COP, and MR.

However, one can conclude that the literature lacks a closed-form solution, which includes the geometry of the HMX, salient thermophysical and sorption properties, as well as operational input parameters and considers: (i) the transient behavior of sorber bed; and (ii) the thermal contact resistance at the interface between the sorption material and the HMX.

Table 3. A summary of the specifications and performance of available studies with a reasonable compromise between the SCP, COP and MR. * The HTF data was not available in the publication.

Ref	Sorption pair	S-HMX	t_{cycle} (min)	SCP (W/kg)	COP	MR
[107]	Coating silica gel + $CaCl_2$(SWS-1I)/ water	Aluminum finned tube	10	137	0.15	4.47 *
[108]	Coating AQSOA-FAMZ02/ water	Extruded aluminum finned-tube heat exchanger		295	0.21	5.37 *
[109]	Loose grain AQSOA-FAM Z02/water	Round tube-fin packed	20	120	0.3	7.86
[109]	Loose grain AQSOA-FAM Z02/water	Round tube-fin packed	20	70	0.45	3.29
[110]	Loose grain $LiNO_3$–Silica KSK/water (SWS-9I)	Aluminum finned flat tube	6.4	318	0.176	2.82 *
[111]	Loose grain AQSOA-FAM Z02/water	Aluminum finned flat tube	7	394	0.6	3.61
[112]	Coating zeolite, SAPO-34/water	Aluminum finned flat tube	5	675	0.24	10
[112]	Loose grain zeolite, SAPO-34/water	Aluminum finned flat tube	5	498	0.4	4.11
[113]	Coating SAPO- 34/water	Aluminum sintered metal fiber structures soldered on flat fluid channels	10	852	0.4	4.15
[104]	Coating silica gel + $CaCl_2$/water	Aluminum plate-finned HMX	10	1005	0.6	4.7
[106]	Coating silica gel + CaCl2/water	Aluminum finned-tube HMX	10	766	0.55	4

2.2. Model development

Based on the general approach reported in our research group previous publications [1], [104], [106], a new 2-D analytical solution is proposed to determine the parameters inside the in-line arrangement of a pin fin heat/mass exchanger. These include: the transient temperature distribution, heat transfer rate, uptake and the sorption performance. Figure 2.1 shows the solution domain schematically, which includes the PF-HMX, HTF, and the sorbent material. The assumptions used to develop the model include:

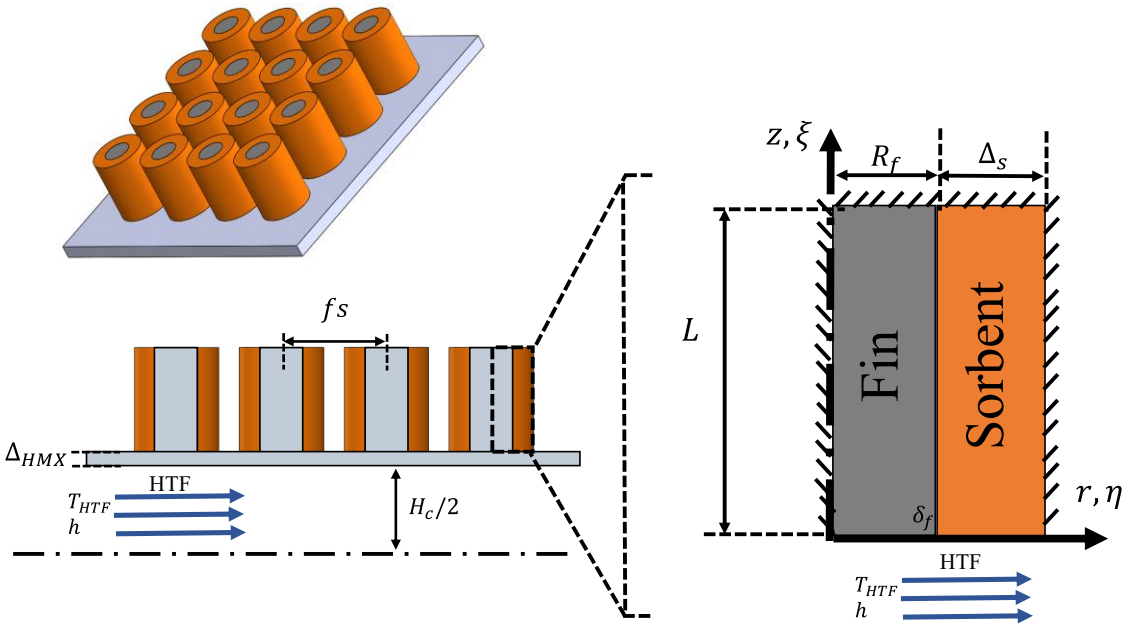

Figure 2.1. A schematic of the solution domain consisting of a sorbent coating and pin fin heat and mass exchanger. The in-line arrangement is shown. For dimensions of the PF-HMX, see Table 5.

- Two-dimensional, transient heat and mass transfer with constant thermo-physical properties;
- Constant temperature for the HTF, due to the relatively higher heat capacity of the heat transfer fluid [114];
- The radiative heat transfer is neglected the because of low temperature difference between the sorbent and surrounding (10-20 K); and

- The boundaries of the sorbent and the fin that are in contact with low pressure refrigerant vapor are assumed to be adiabatic, i.e., due to the low Biot number [115][12].

$$
\begin{aligned}
h(T_{vapor}-T_s)=k_s\frac{\partial T_s}{\partial r}\Rightarrow \mathrm{O}\left(Bi_r\right)=\mathrm{O}\left(\frac{h\Delta_s}{k_s}\right)=\frac{0.5\times 0.005}{0.3}=0.0083\\
h(T_{vapor}-T_s)=k_s\frac{\partial T_s}{\partial z}\Rightarrow \mathrm{O}\left(Bi_z\right)=\mathrm{O}\left(\frac{hL}{k_s}\right)=\frac{0.5\times 0.015}{0.3}=0.025\\
h(T_{vapor}-T_f)=k_s\frac{\partial T_f}{\partial z}\Rightarrow \mathrm{O}\left(Bi_{z,f}\right)=\mathrm{O}\left(\frac{hL}{k_f}\right)=\frac{0.5\times 0.015}{236.5}=3.17e^{-5}
\end{aligned}
\tag{5}
$$

where, T is the temperature (K), k is the thermal conductivity (W/(m K)), Bi is the Biot number (-), h is the convective heat transfer coefficient (W/(m^2 K)), r and z are the coordinates, L is the fin height (m), Δ_s is the sorbent thickness (m), and s and f represent the sorbent and HMX domains, respectively.

It should be noted that low Biot number results in low temperature gradient in fin but the temperature gradient in sorbent is significant due to the heat generation inside sorbent. Therefore, the lumped model is not applicable for these systems.

Fin efficiency is also calculated as follows:

$$
\begin{aligned}
m&=\sqrt{\frac{2h}{kR_f}}=\sqrt{\frac{2\times 0.5}{236.5\times 0.002}}=0.02181\\
\eta_f&=\frac{\tanh(mL)}{mL}=99.9\%
\end{aligned}
\tag{6}
$$

where, h is the convective heat transfer coefficient (W/(m^2 K)), k is the thermal conductivity of fin (W/(m K)), R_f is the fin radius (m), and L is the fin height (m).

From these assumptions, the energy equation can be written as follows for both the sorbent and the HMX fin:

$$
\frac{\partial T_i}{\partial t}=\alpha_{i,r}\left(\frac{\partial^2 T_i}{\partial r^2}+\frac{1}{r}\frac{\partial T_i}{\partial r}\right)+\alpha_{i,z}\frac{\partial^2 T_i}{\partial z^2}+\frac{1}{\left(\rho c_p\right)_i}G_i(t),\ T_i\left(r,z,t\right),\ i=s,f
\tag{7}
$$

$$G_i(t)=\begin{cases}\rho_s H_{ads}\dfrac{d\omega}{dt}, & i=s\\ 0, & i=f\end{cases} \tag{8}$$

where, T_i is the temperature of the ith layer (K), α is the thermal diffusivity for the ith layer (m^2/s), ρ is the density for the ith layer (kg/m^3), c_p is the specific heat (J/(kg K)), r and z are the coordinates, t is time (s), H_{ads} is the enthalpy of adsorption (J/kg), and G_i is the heat generation inside the ith layer and i=s and i=f represent the sorbent and HMX domains, respectively. The boundary conditions are:

$$\frac{\partial T_i(0,z,t)}{\partial r}=0 \tag{9}$$

$$\frac{\partial T_s(\Delta_s+R_f,z,t)}{\partial r}=0 \tag{10}$$

$$\frac{\partial T_i(r,L,t)}{\partial z}=0 \tag{11}$$

$$R=\frac{\Delta_{HMX}}{k_{f,z}}+\frac{1}{h}+TCR\cdot A \quad \left(\frac{K\ m^2}{W}\right)$$

$$\frac{1}{R}\left(T_s(r,0,t)-T_{HTF}\right)=k_s\frac{\partial T_s(r,0,t)}{\partial z} \tag{12}$$

$$\frac{1}{R}\left(T_f(r,0,t)-T_{HTF}\right)=k_{f,z}\frac{\partial T_f(r,0,t)}{\partial z}$$

$$k_{f,r}\frac{\partial T_f(R_f,z,t)}{\partial r}=k_s\frac{\partial T_s(R_f,z,t)}{\partial r}$$

$$-k_{f,r}\frac{\partial T_f(R_f,z,t)}{\partial r}=\frac{1}{TCR\cdot A}\left(T_f(R_f,z,t)-T_s(R_f,z,t)\right) \tag{13}$$

where, T_i is the temperature of the ith layer (K), Δ_s is the sorbent thickness (m), Δ_{HMX} is the HMX thickness (m), R_f is the fin radius (m), L is the fin height (m), A is the heat transfer area (m^2), k is the thermal conductivity for the ith layer (W/(m K)), h is the convective heat transfer coefficient ($W/(m^2 K)$), r and z are the coordinates, t is time (s), and the TCR is the thermal contact resistance between the fin and the sorbet.

The initial condition for temperature is

$$T_i(r,z,0)=T_0 \tag{14}$$

Non-dimensional variables were defined:

$$\eta=\frac{r}{R_f+\Delta_s} \qquad \xi=\frac{z}{L} \qquad Fo=\frac{t\alpha_z}{L^2} \qquad \theta_i=\frac{T_i-T_{HTF}}{T_0-T_{HTF}}$$

$$\delta=\frac{L}{\Delta_s+R_f} \qquad \delta_f=\frac{R_f}{R_f+\Delta_s} \qquad \mu_r{}^2=\frac{\alpha_r}{\alpha_z} \qquad \mu_s{}^2=\frac{\alpha_s}{\alpha_z}$$

$$\kappa=\frac{k_s}{k_{f,\mathrm{r}}} \qquad \Lambda=\frac{R_s+R_f}{k_{f,r}TCR\ A} \qquad Bi_S=\frac{L}{Rk_S} \qquad Bi_f=\frac{L}{Rk_{f,z}}$$

$$g_i(Fo)=\begin{cases}\dfrac{H_{ads}}{c_{p,s}(T_0-T_{fluid})}\dfrac{d\omega}{dFo}, & i=s\\ 0, & i=f\end{cases}$$

where, θ_i is the dimensionless temperature of the ith layer, Fo (Fourier number) is the dimensionless time, η and ξ are the dimensionless coordinates, and g_i is the dimensionless heat generation inside the ith layer. Using the aforementioned dimensionless variables, the dimensionless energy equation as well as the boundary and initial conditions can be obtained:

$$\frac{\partial\theta_i}{\partial Fo}=(\mu_{i,\eta}\delta)^2\left(\frac{\partial^2\theta_i}{\partial\eta^2}+\frac{1}{\eta}\frac{\partial\theta_i}{\partial\eta}\right)+\mu_{i,\xi}{}^2\frac{\partial^2\theta_i}{\partial\xi^2}+g_i(Fo) \tag{15}$$

$$\frac{\partial\theta_i(\eta,1,Fo)}{\partial\xi}=0 \tag{16}$$

$$\frac{\partial\theta_f(0,\xi,Fo)}{\partial\eta}=0 \tag{17}$$

$$\frac{\partial\theta_s(1,\xi,Fo)}{\partial\eta}=0 \tag{18}$$

$$\begin{aligned}&\frac{\partial\theta_s(\eta,0,Fo)}{\partial\xi}-Bi_s\theta_s(\eta,0,\mathrm{Fo})=0\\ &\frac{\partial\theta_f(\eta,0,Fo)}{\partial\xi}-Bi_f\theta_f(\eta,0,\mathrm{Fo})=0\end{aligned} \tag{19}$$

$$\frac{\partial \theta_f(\delta_f,\xi,Fo)}{\partial \eta} = \kappa \frac{\partial \theta_s(\delta_f,\xi,Fo)}{\partial \eta}$$
$$-\frac{\partial \theta_f(\delta_f,\xi,Fo)}{\partial \eta} = \Lambda\left(\theta_f(\delta_f,\xi,Fo) - \theta_s(\delta_f,\xi,Fo)\right) \quad (20)$$

The Eigenfunction expansion method is utilized to solve the dimensionless energy equations, Eqs. (15)-(20). The closed-form relationship to find the transient temperature distribution in both sorbent and HMX is as follows:

$$\theta(\eta,\xi,Fo) = \sum_{n=1}^{\infty}\sum_{m=1}^{\infty} \psi_n(\xi)\, \mathrm{X}_{nm}(\eta)\, \Gamma_{nm}(Fo) \quad (21)$$

where Γ is the temporal Eigenfunction whereas ψ and X are spatial Eigenfunction in ξ and η directions, respectively.

The dimensionless energy equation obtained as Eq. (15) where

$$\mu_{i,\eta} = \begin{cases} \mu_r, & i = f \\ \mu_s, & i = s \end{cases} \quad (22)$$

$$\mu_{i,\xi} = \begin{cases} 1, & i = f \\ \mu_s, & i = s \end{cases} \quad (23)$$

Based on Eqs. (15)-(20), the following eigenvalue problem can be derived in the ξ direction [116], [117].

$$\psi'' + \gamma^2 \psi = 0 \quad (24)$$

$$\psi' - Bi\,\psi = 0 \ \text{ at } \xi=0 \quad (25)$$

$$\psi = 0 \ \text{ at } \xi=0 \quad (26)$$

The following transcendental equation is achieved to calculate the eigenvalues:

$$\gamma \tan(\gamma) = Bi \tag{27}$$

where Bi is the Biot number and γ is the eigenvalue.

The Eigenfunction related to each eigenvalue are given as follows:

$$\psi = \cos(\gamma\xi) + \tan(\gamma)\sin(\gamma\xi) \tag{28}$$

Furthermore, the following eigenvalue problem can be established in η direction.

$$\frac{d^2\mathrm{X}}{d\eta^2} + \frac{1}{\eta}\frac{d\mathrm{X}}{d\eta} + \omega_k^2\mathrm{X} = 0 \tag{29}$$

$$\left.\frac{d\mathrm{X}}{d\eta}\right|_{\eta=0,1} = 0 \tag{30}$$

where,

$$\omega_k{}^2 = \frac{\lambda r_k - q_k}{p_k},\ k = s,f \tag{31}$$

$$r_s = \frac{\left(\left(\rho c_p\right)_s - \left(\rho H_{ads} a\right)_s\right)k_z}{\left(\rho c_p\right)_f \delta^2} \tag{32}$$

$$r_f = \frac{k_{f,z}}{\delta^2} \tag{33}$$

$$q_k = \left(\mu_{k,\eta}\gamma\right)^2 r_k \tag{34}$$

$$q_k = \left(\mu_{k,\eta}\gamma\right)^2 r_k \tag{35}$$

$$p_f = k_{f,r} \tag{36}$$

$$\dot{m} = \frac{d\,\omega}{dT_s} \tag{37}$$

where, ρ is the density (kg/m^3), c_p is the specific heat (J/(kg K)), H_{ads} is the enthalpy of adsorption (J/kg), and m$'$ is the slope between the temperature and water uptake. Water uptake can be simulated as a function of operating conditions, such as the pressure and the temperature of the sorber bed. A linear relationship between water uptake and sorbent temperature is achieved by [1], [118] for each pressure during the isobaric desorption and adsorption processes, Eqs. (38)-(39).

$$\omega_{des} = -0.0123T + 4.0106 \tag{38}$$

$$\omega_{ads} = -0.0118T + 3.9852 \tag{39}$$

This is a singular eigenvalue problem because of non-continuous p, r and q. Further, ω^2_k, depending upon the thermophysical properties and geometrical characteristics of the sorbent and the fin, can be positive, negative or zero. Therefore, there is no simple solution with the Eigenfunction and transcendental equation for the eigenvalue problem. The approximated solution proposed by [116], [119] is followed in the present paper. The eigenvalue problem is approximated by identically dividing the cylinder (sorbent and fin) into n-1 intervals. The finer the division, the better the approximation. The following equations represent the new eigenvalue problem with boundary conditions.

$$\frac{d^2\mathrm{X}}{d\eta^2} + \frac{1}{\eta}\frac{d\mathrm{X}}{d\eta} + \omega_k^2\mathrm{X} = 0 \tag{40}$$

$$\left.\frac{d\mathrm{X}}{d\eta}\right|_{\eta=0} = 0 \tag{41}$$

$$\mathrm{X}_k = \mathrm{X}_{k+1}\,,\ k = 2,3,..,\mathrm{n}\text{-}1 \tag{42}$$

$$p_k \frac{d\mathrm{X}_k}{d\eta} = p_{k+1} \frac{d\mathrm{X}_{k+1}}{d\eta} \ , k = 2,3,..,\text{n-1} \tag{43}$$

$$\left.\frac{d\mathrm{X}}{d\eta}\right|_{\eta=1} = 0 \tag{44}$$

The following equations are also established to consider the TCR as an imaginary layer at the interface between sorbent and the fin.

$$\frac{d^2\mathrm{X}}{d\eta^2} + \frac{1}{\eta}\frac{d\mathrm{X}}{d\eta} + \omega_k^2 \mathrm{X} = 0 \tag{45}$$

$$\omega_k = 0 \tag{46}$$

$$p_k \frac{d\mathrm{X}}{d\eta} = \frac{R_f + \Delta_s}{TCR.A}(\mathrm{X}_{k+1} - \mathrm{X}_k) \tag{47}$$

where, Δ_s is the sorbent thickness (m), R_f is the fin radius (m), TCR is the thermal contact resistance between the sorbent and the heat exchanger (K/W), and A is the surface area of the TCR interface (m^2), respectively. The following eigenfunction can be achieved for each interval ($\eta_{k-1}<\eta<\eta_k$):

$$\begin{aligned}\mathrm{X}_k(\eta) = \mathrm{X}_k(\eta_{k-1})\frac{J_0(\omega_k\eta)Y_0(\omega_k\eta_k) - J_0(\omega_k\eta_k)Y_0(\omega_k\eta)}{J_0(\omega_k\eta_{k-1})Y_0(\omega_k\eta_k) - J_0(\omega_k\eta_k)Y_0(\omega_k\eta_{k-1})} \\ +\mathrm{X}_k(\eta_k)\frac{J_0(\omega_k\eta_{k-1})Y_0(\omega_k\eta) - J_0(\omega_k\eta)Y_0(\omega_k\eta_{k-1})}{J_0(\omega_k\eta_{k-1})Y_0(\omega_k\eta_k) - J_0(\omega_k\eta_k)Y_0(\omega_k\eta_{k-1})},\ \omega_k{}^2 > 0\end{aligned} \tag{48}$$

$$\mathrm{X}_k(\eta) = \mathrm{X}_k(\eta_{k-1}) Log\frac{\frac{\eta}{\eta_k}}{\frac{\eta_{k-1}}{\eta_k}} + \mathrm{X}_k(\eta_k) Log\frac{\frac{\eta_{k-1}}{\eta}}{\frac{\eta_{k-1}}{\eta_k}},\ \omega_k{}^2 = 0 \tag{49}$$

$$\mathrm{X}_k(\eta)=\mathrm{X}_k(\eta_{k-1})\frac{I_0(\omega_k^*\eta)\mathrm{K}_0(\omega_k^*\eta_k)-I_0(\omega_k^*\eta_k)\mathrm{K}_0(\omega_k^*\eta)}{I_0(\omega_k^*\eta_{k-1})\mathrm{K}_0(\omega_k^*\eta_k)-I_0(\omega_k^*\eta_k)\mathrm{K}_0(\omega_k^*\eta_{k-1})}$$
$$+\mathrm{X}_k(\eta_k)\frac{I_0(\omega_k^*\eta_{k-1})\mathrm{K}_0(\omega_k^*\eta)-I_0(\omega_k^*\eta)\mathrm{K}_0(\omega_k^*\eta_{k-1})}{I_0(\omega_k^*\eta_{k-1})\mathrm{K}_0(\omega_k^*\eta_k)-I_0(\omega_k^*\eta_k)\mathrm{K}_0(\omega_k^*\eta_{k-1})},\ {\omega_k}^2<0 \tag{50}$$

$$\omega_k^*=\sqrt{\mathrm{abs}\left({\omega_k}^2\right)} \tag{51}$$

The Eigenfunctions for each interval can be calculated as follows by substituting the abovementioned Eigenfunctions into boundary conditions ((41)-(44))

$$A_1\mathrm{X}_0-B_1\mathrm{X}_1=0 \tag{52}$$

$$B_k\mathrm{X}_{k-1}+(A_k+A_{k+1})\mathrm{X}_k-B_{k+1}\mathrm{X}_{k+1}=0,\ k=2,...,n-1 \tag{53}$$

$$-B_n\mathrm{X}_{n-1}+A_n\mathrm{X}_n=0 \tag{54}$$

where,

$$A_k=p_k\omega_k\left(\frac{J_0(\omega_k\eta_k)Y_1(\omega_k\eta_{k-1})-Y_0(\omega_k\eta_k)J_1(\omega_k\eta_{k-1})}{J_0(\omega_k\eta_{k-1})Y_0(\omega_k\eta_k)-J_0(\omega_k\eta_k)Y_0(\omega_k\eta_{k-1})}\right),\ {\omega_k}^2>0 \tag{55}$$

$$A_k=1,\ {\omega_k}^2=0 \tag{56}$$

$$A_k=p_k\omega_k\left(\frac{I_0(\omega_k^*\eta_k)K_1(\omega_k^*\eta_{k-1})+K_0(\omega_k^*\eta_k)\mathrm{I}_1(\omega_k^*\eta_{k-1})}{I_0(\omega_k^*\eta_{k-1})K_0(\omega_k^*\eta_k)-I_0(\omega_k^*\eta_k)K_0(\omega_k^*\eta_{k-1})}\right),\ \omega_k^2<0 \tag{57}$$

$$B_k=p_k\omega_k\left(\frac{J_0(\omega_k\eta_{k-1})Y_1(\omega_k\eta_{k-1})-Y_0(\omega_k\eta_{k-1})J_1(\omega_k\eta_{k-1})}{J_0(\omega_k\eta_{k-1})Y_0(\omega_k\eta_k)-J_0(\omega_k\eta_k)Y_0(\omega_k\eta_{k-1})}\right),\ {\omega_k}^2>0 \tag{58}$$

$$B_k=1,\ {\omega_k}^2=0 \tag{59}$$

$$B_k = p_k \omega_{k+1} \left(\frac{I_0(\omega_k^* \eta_{k-1}) K_1(\omega_k^* \eta_{k-1}) - I_1(\omega_k^* \eta_{k-1}) K_0(\omega_k^* \eta_{k-1})}{I_0(\omega_k^* \eta_{k-1}) K_0(\omega_k^* \eta_k) - I_0(\omega_k^* \eta_k) K_0(\omega_k^* \eta_{k-1})} \right), \ \omega_k^2 < 0 \tag{60}$$

A linear system of homogenous equation is formed based on Eqs. (52)-(54) is derived as follows in order to calculate the Eigenfunctions.

$$[K]\{X\} = 0 \tag{61}$$

The transcendental equation is obtained to calculate the eigenvalues by equating the determinant of coefficient matrix $[K]$ to zero.

$$\det([K]) = 0 \tag{62}$$

The sign-count method, developed by Mikhailov and Vulchanov, is utilized to solve the transcendental equation [116].

The number of positive eigenvalues between zero and some prescribed positive value, $\tilde{\lambda}$, can be evaluated as follows:

$$N(\tilde{\lambda}) = N_0(\tilde{\lambda}) + s\left(\left[K(\tilde{\lambda}) \right] \right) \tag{63}$$

$$N_0(\tilde{\lambda}) = \sum_{k=1}^{n} N_{0,k}(\tilde{\lambda}) \tag{64}$$

$$\tilde{\omega}_k{}^2 = \frac{\tilde{\lambda} r_k - q_k}{p_k} \tag{65}$$

where, the number of negative elements along the main diagonal of the triangulated form of $K(\tilde{\lambda})$ is considered as $s([K(\tilde{\lambda})])$, Eq. (66),and the eigencondition equation to find the positive eigenvalues at each layer is calculated based on Eq.(67).

$$\frac{D_1}{D_0},\frac{D_2}{D_1},\ldots,\frac{D_n}{D_{n-1}} \tag{66}$$

$$J_0(\omega_k\eta_{k-1})\mathrm{Y}_0(\omega_k\eta_k)=J_0(\omega_k\eta_k)\mathrm{Y}_0(\omega_k\eta_{k-1}) \tag{67}$$

where,

$$\begin{aligned} &D_0=1, D_1=A_1,\\ &D_k=D_{k-1}\left(A_k+A_{k-1}\right)-D_{k-2}B_{k-1}{}^2, k=2,\ldots,n-1\\ &D_n=D_{n-1}\left(A_n\right)-D_{n-2}B_{n-1}{}^2 \end{aligned} \tag{68}$$

The flowchart utilized to calculate the eigenvalues is shown in Figure 2.2. The order of the eigenvalue, i, precision, ε_i, lower bound, λ_l, upper bound, λ_u, and the increment, $\tilde{\delta}$, are set and the iterations are performed until the accuracy is met. The accuracy in obtaining the eigenvalues is set to 0.001.

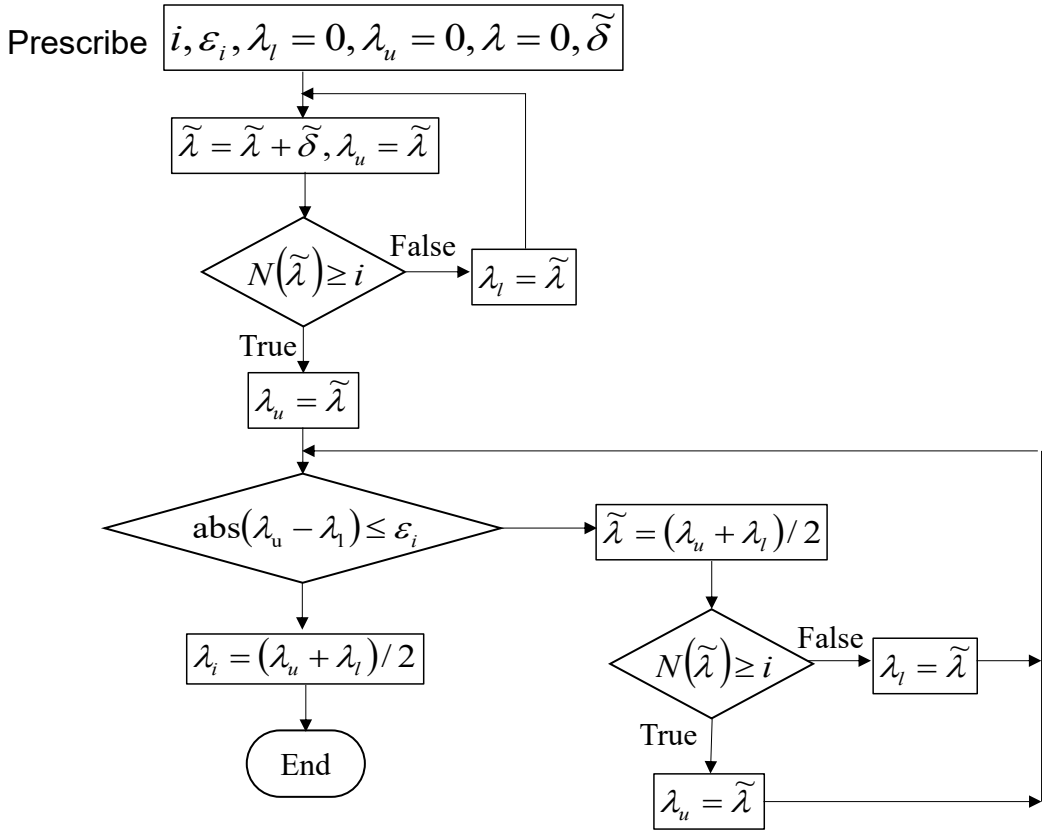

Figure 2.2. The iterative algorithm used to acquire the eigenvalues

Eventually, the Eigenfunction is evaluated as follows:

$$\mathrm{X}_0 = -1 \tag{69}$$

$$\mathrm{X}_1 = -A_1 / B_1 \tag{70}$$

$$\mathrm{X}_{k+1} = \left(\left(A_k + A_{k+1} \right) \mathrm{X}_k - B_k \mathrm{X}_{k-1} \right) / B_{k+1}, k = 1,2,...,n-1 \tag{71}$$

Subsequently, the accuracy of the Eigenfunction is evaluated for the last interval. If the required accuracy, 1e-8 for this study, is not satisfied, then the finer intervals will be chosen based on the algorithm proposed by [119] until it is satisfied, Figure 2.3.

$$\left| -B_n X_{n-1} + A_n X_n \right| \le \varepsilon_{global}, \ \varepsilon_{global} \cong \varepsilon_{\max}.n \tag{72}$$

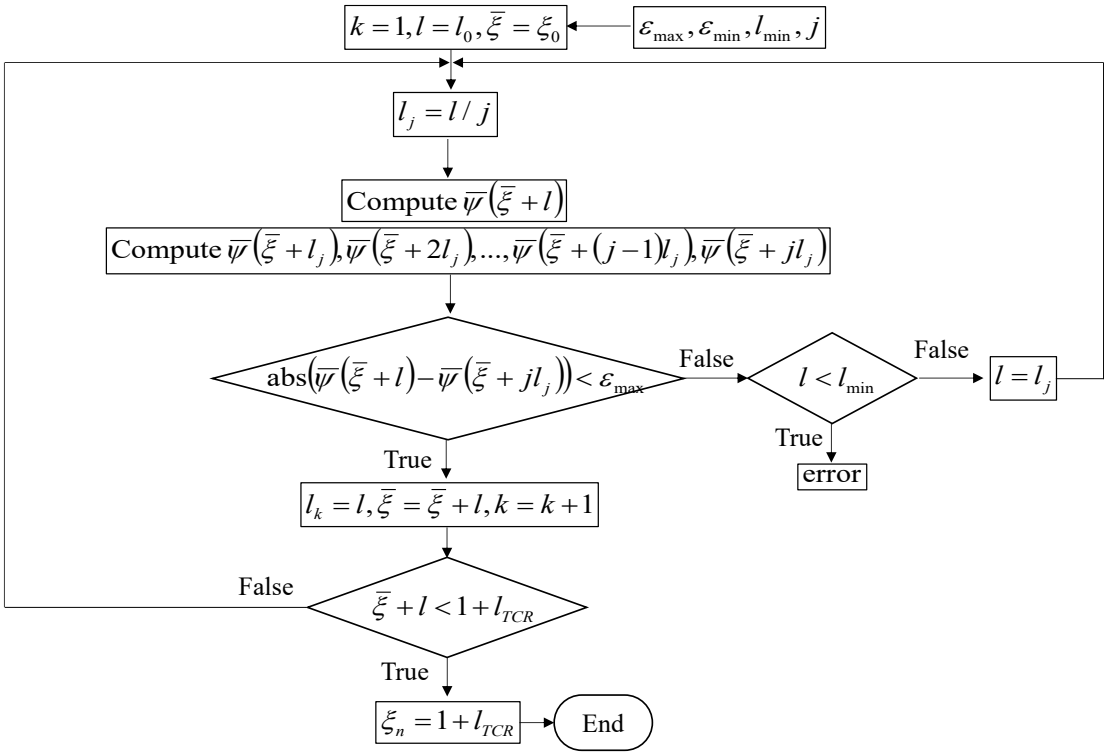

Figure 2.3. The algorithm to refine the division of the interval

To this end, the Eigenfunctions in ξ and η directions are evaluated. The last step is to acquire the Gamma function. The Gamma function, which shows the time variation

of θ, can be expanded in the form of infinite series of products of Eigenfunctions in ξ and η directions as follows:

$$g_i(Fo) = \sum_{n=1}^{\infty}\sum_{m=1}^{\infty} g^*_{nm}(Fo)\ \psi_n(\xi)\ \mathrm{X}_{nm}(\eta) \tag{73}$$

where, g^*_{nm} can be calculated based on orthogonal property of the Eigenfunctions as follows.

$$g^*_{nm}(Fo) = \frac{g_i(Fo)\int_0^1 \psi d\xi \left(\sum_{k=1}^{n} r_k \int_{\eta_k}^{\eta_{k+1}} \mathrm{X}_k d\eta\right)}{\int_0^1 \psi^2 d\xi \left(\sum_{k=1}^{n} r_k \int_{\eta_k}^{\eta_{k+1}} \mathrm{X}_k^2 d\eta\right)} \tag{74}$$

By substituting Eqs. (73) and (21) into Eq.(15), the following ordinary differential equation can be obtained for Gamma function.

$$\frac{d\Gamma}{dFo} = g^*_{nm}(Fo) - \lambda\Gamma \tag{75}$$

Finally, the Gamma function is evaluated as follows.

$$\Gamma = e^{-\lambda Fo}\left(C_{nm} + \int_{Fo'=0}^{Fo} g^*_{nm}(Fo')e^{\lambda Fo'}dFo'\right) \tag{76}$$

where,

$$C_{nm} = \frac{\int_0^1 \psi d\xi \left(\sum_{k=1}^{n} r_k \int_{\eta_k}^{\eta_{k+1}} \mathrm{X}_k d\eta\right)}{\int_0^1 \psi^2 d\xi \left(\sum_{k=1}^{n} r_k \int_{\eta_k}^{\eta_{k+1}} \mathrm{X}_k^2 d\eta\right)} \tag{77}$$

A MATLAB code, can be found in the Appendix B, is developed to calculate the Eigenfunctions and eigenvalues in both spatial coordinates along with the Gamma function as a function of the Fourier number (dimensionless time). After solving the equations, the dimensionless closed-form relationship to find the transient temperature distribution in both the sorbent and HMX is as follows:

$$\theta(\eta,\xi,Fo)=\sum_{n=1}^{\infty}\sum_{m=1}^{\infty}\psi_n(\xi)\ \mathrm{X}_{nm}(\eta)\ \Gamma_{nm}(Fo) \tag{78}$$

Chapter 3. Performance evaluation of PF-HMX

3.1. Experimental study

3.1.1. Sample preparation

To enhance the thermal diffusivity of the sorbent material, a consolidated composite, consisting of $CaCl_2$, silica gel B150, with added natural graphite flakes is prepared. The thermally-conductive additive, natural graphite flake, reduces the active sorbent fraction in the composite creating a need for establishing an optimum composition for the specific application, more details can be found in our previous study [118].

A number of $CaCl_2$-silica gel composite sorbents with 0-20 wt.% graphite flake contents are prepared, Table 4. Polyvinyl alcohol (PVA) binder (40,000 MW, Amresco Inc.) is dissolved in water. Following this, $CaCl_2$ and silica gel (SiliaFlash® B150, Silicycle, Inc., Quebec, Canada) and graphite flakes (consisting of both 150 μm fine particles and thin flakes up to 1.3 mm long, Sigma-Aldrich) are added to the aqueous solution. The slurry composites are filled into the small aluminum dishes and oven-dried at 70 °C then cured at 140 °C, each for 4 hours, Figure 3.1.

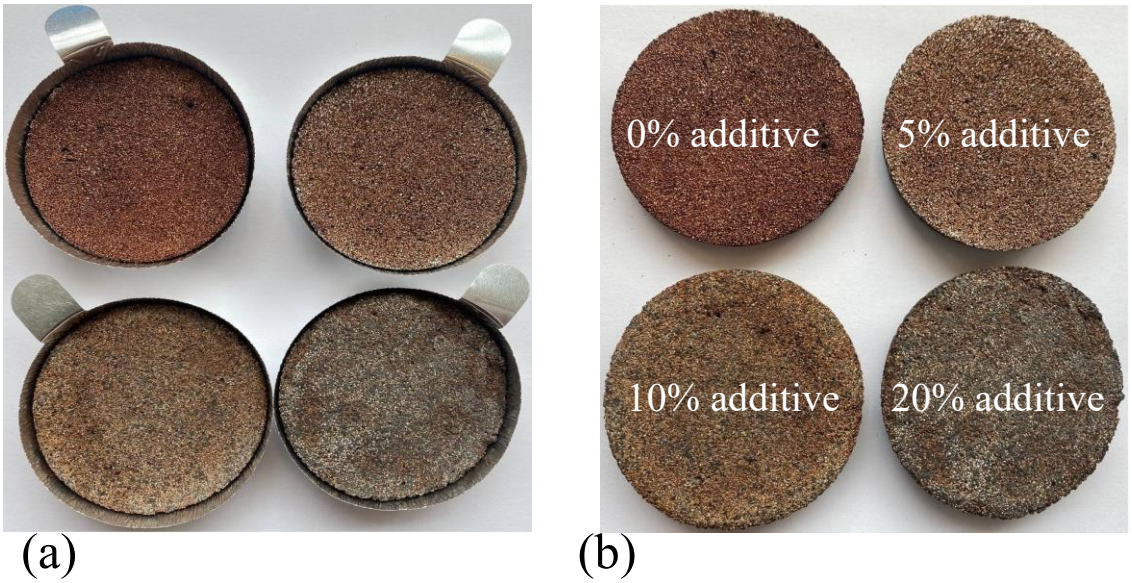

Figure 3.1. (a) Sorbent samples within the aluminum dishes; (b) Disc shape sorbents with different amount of additives (Graphite flake).

Table 4. Compositions and dry mass of the sorbent composite samples, shown in Figure 3.1.

#	Silica gel (wt%)	$CaCl_2$ (wt%)	PVA (wt%)	Graphite Flake (wt%)	Dry mass (g)
1	45	45	10	0	7.54
2	42.5	42.5	10	5	8.65
3	40	40	10	10	8.60
4	35	35	10	15	9.00

3.1.2. Thermal conductivity and thermal diffusivity measurement

Thermophysical characteristics of the heat exchanger and sorbent materials with different amount of additives were measured using a transient plane source (TPS), hot disk thermal constants analyzer, as per ISO 22007- 2 (ISO220 07-2, 20 08) (TPS 250 0S, ThermTest Inc., Frederiction, Canada) [120], [121]. TPS is shown in Figure 3.2 with an image and diagram taken from Ref. [122]. TPS testing information can be found elsewhere [122].

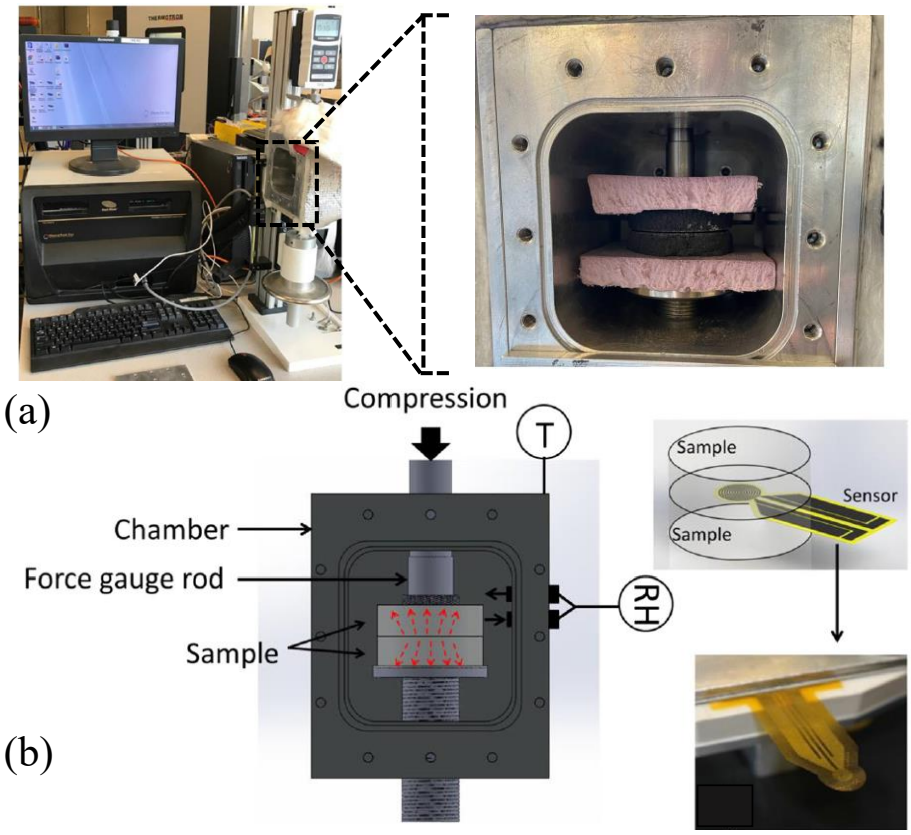

Figure 3.2. (a) Image; and b) Schematic of TPS [122]

Figure 3.3 shows the average values of thermal diffusivity and thermal conductivity versus graphite flake content. As can be seen in Figure 3.3, by adding graphite flake, the sorbent thermal diffusivity improves by up to 470%, which enhances the heat transfer from the HMX to the sorbent. The experiment data can be found in Table 8 in the Appendix A.

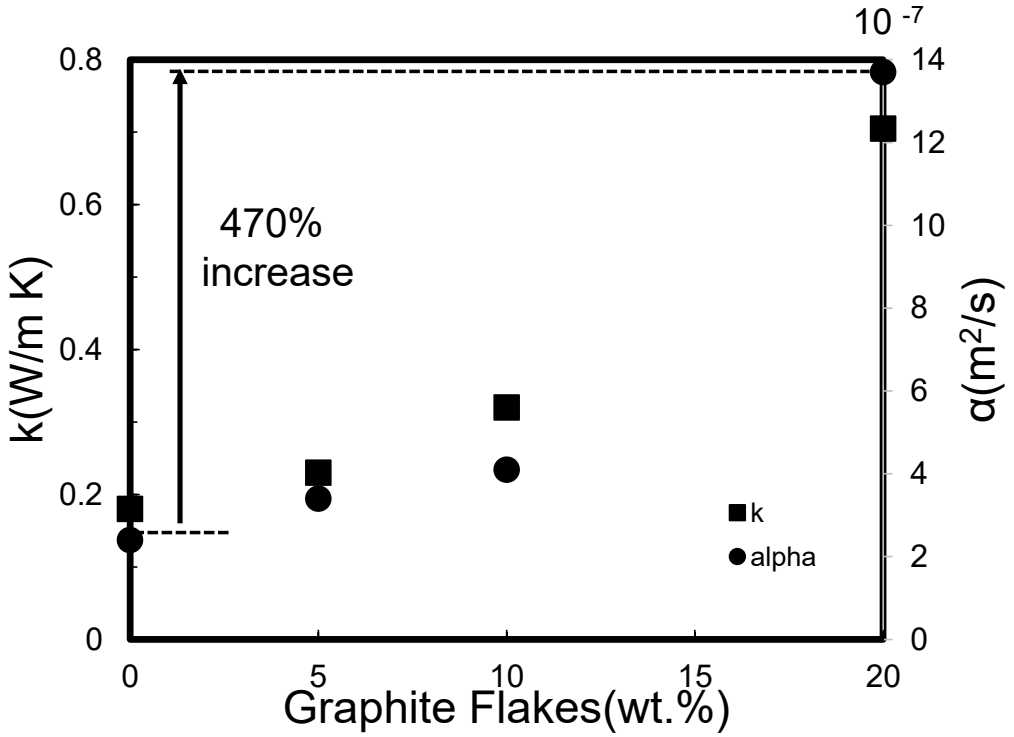

Figure 3.3. Thermal diffusivity and thermal conductivity of the composite sorbents in Table 4

3.1.3. G-LTJ test bed

A number of $CaCl_2$-silica gel composite sorbents with 0-20 wt.% graphite flake content is prepared. The slurry composites were coated on the designed PF-HMX and oven-dried at 70 °C then cured at 140 °C, each for 4 hours, see Figure 3.4 for more details. The sorbent thickness around each fin and fin diameters are measured as 5 mm and 4 mm, respectively. Thermophysical characteristics of the heat exchanger and sorbent materials with different amount of additives were measured using a transient plane source (TPS), hot disk thermal constants analyzer, as per ISO 22007- 2 (ISO220 07-2, 20 08) (TPS 250 0S, ThermTest Inc., Frederiction, Canada) and described in Table 5 [120], [121]. The sorbent thickness around each fin and fin diameters are measured as 5 mm and 4

mm, respectively. Figure 3.5 shows the gravimetric large temperature jump (G-LTJ) test bed custom-built in our lab used to validate the developed analytical solution.

Table 5. Graphite flake content in the sorbent, thermophysical properties, geometrical specifications, and SCHS cycle parameters used for the baseline case and model validation.

	Baseline case			**Validation with a G-LTJ test bed**		
	Sorbent	**Al fin**	**Al tube**	**Sorbent**	**Al fin**	**Copper tube**
φ (wt%)	10	-	-	0-20		
ρ (kg/m^3)	665	2699	2699		2699	8932
c (J/kgK)	1082	909	909		909	386
α (m^2/s)	4.1e-7	9.6e-5	9.6e-5		9.6e-5	1.1e-4
h_{ads} (J/kg)	2.77e6	-	-	2.77e6		1.5
R_f, Δ_s, Δ_{HMX} (mm)	Δ_s = 2	R_f = 2		Δ_s = 5	R_f = 2	
L, H_c, W_c (cm)	L=2	L=2	H_c=0.6, W_c=1.3	L=1.5	L=1.5	H_c=0.5, W_c=4
t (min)	15			In Figure 3.9		
$TCR.A$(K m^2/W)	0.0019([1])					

To simulate the operation of a SCHS, HTF was pumped through the PF-HMX and the temperature was cycled between 30°C and 67°C for sorption and desorption, respectively. Two four-way valves were used to switch the HTF between the sorber bed and the buffer for the desorption and sorption processes. The buffer was used for a heat recovery purpose. The sorber bed and the copper PF-HMX were placed inside a vacuum chamber, which was connected to the evaporator/condenser that was maintained at 15 °C. The whole test bed was degassed for five hours using a vacuum pump to dry the sorbent material before the tests. The vacuum chamber was placed on a precision balance (ML4002E, Mettler Toledo) with an accuracy of 0.01 g to measure the mass change due to the sorbate uptake. Five K-type thermocouples with an accuracy of 1.1 °C were passed using a feed-through in the vacuum chamber to measure the sorbent temperature. The instruments were connected to a PC through a data acquisition system and an in-house software written in the LabVIEW environment. The maximum uncertainties of the measured COP and SCP were estimated to be 8% and 5.7%, respectively.

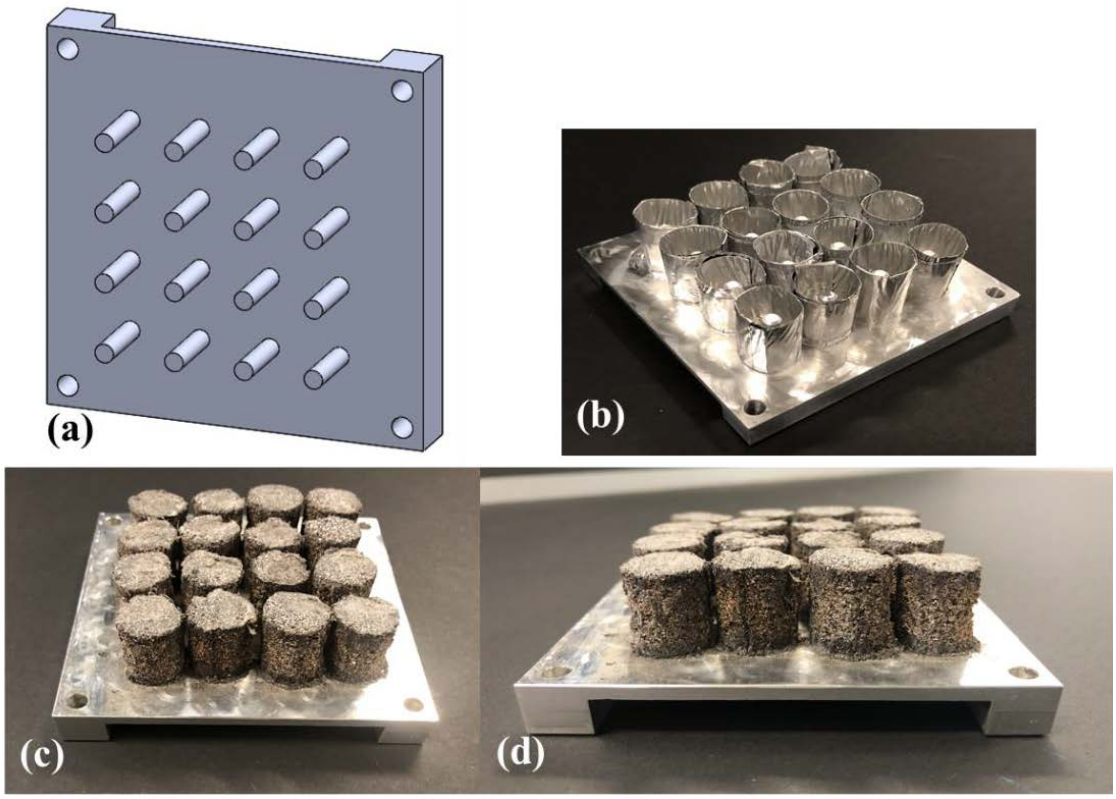

Figure 3.4. **(a) A pin fin structure designed in SolidWorks to be bolted on top of a copper heat exchanger in the GLTJ test bed; (b) building cylinders around the pin fins and fill them with sorbent material; and (c, d) the PF-HMX coated with the composite sorbent, silica gel, CaCl2, PVA and graphite flakes.**

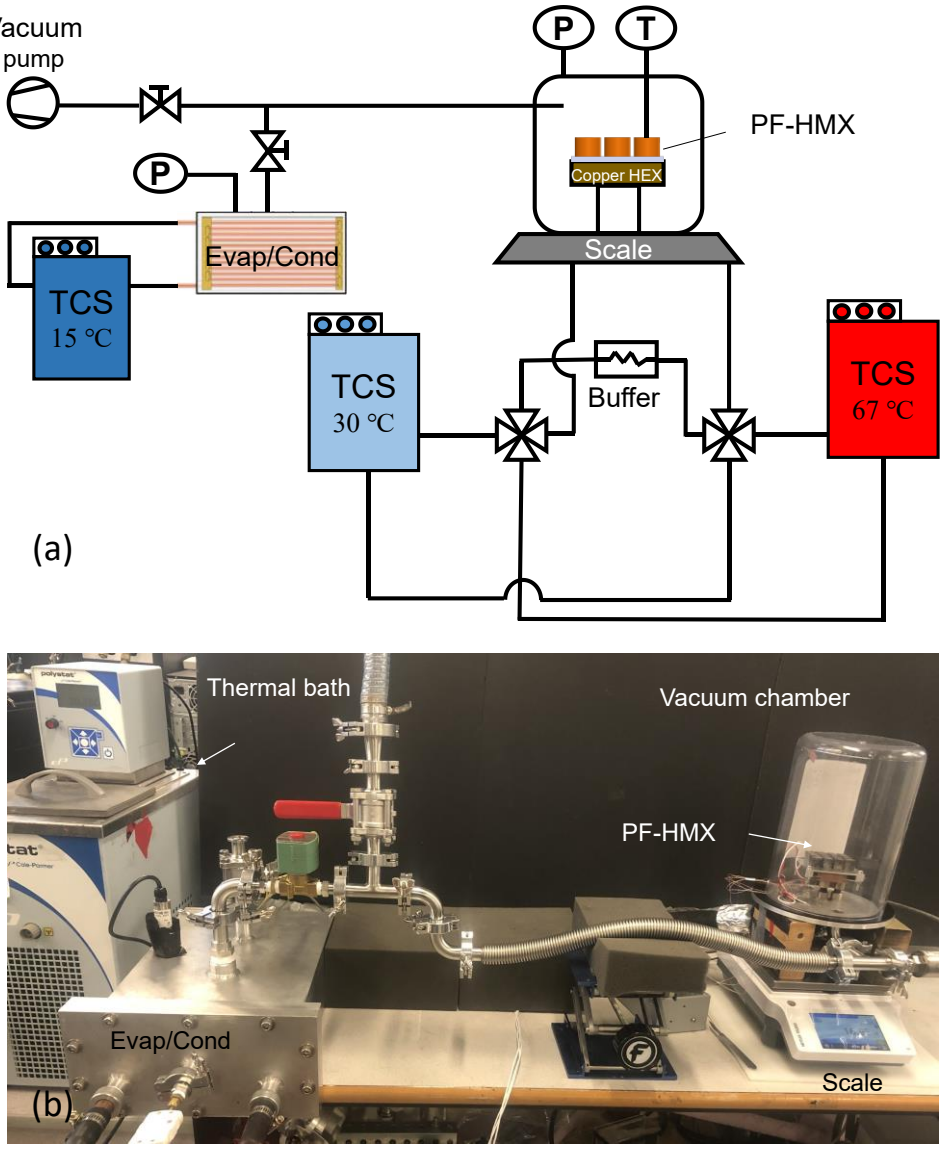

Figure 3.5. (a) A schematic diagram; and (b) a picture of the G-LTJ test bed.

3.2. Uncertainty analysis

The SCP is defined as the evaporative cooling rate generated per mass of dry sorbent material, Eq. (79).

$$SCP = \frac{Q_{evap}}{m_s \tau} = \frac{m_s \int_{ads} \frac{d\omega}{dt} h_{fg} dt}{m_s \tau} = \frac{\Delta\omega h_{fg\,@T_{evap}}}{\tau} \tag{79}$$

Based on the method developed by Moffat [123], the uncertainty of the SCP can be estimated as follows.

$$\frac{\delta SCP}{SCP} = \frac{\delta \Delta\omega}{\Delta\omega} = \frac{\sqrt{2}\delta\omega}{\Delta\omega} \tag{80}$$

$$\omega = \frac{m_{sorbate}}{m_{sorbent}} \tag{81}$$

$$\frac{\delta\omega}{\omega} = \sqrt{\left(\frac{\delta m_{sorbate}}{m_{sorbate}}\right)^2 + \left(\frac{\delta m_{sorbent}}{m_{sorbent}}\right)^2} \cong \left(\frac{\delta m_{sorbate}}{m_{sorbate}}\right) = \frac{0.01g}{m_{sorbate}} \tag{82}$$

The sorbate mass change was measured by a precision balance (ML4002E, Mettler Toledo) with the accuracy of 0.01 g, whereas the sorbent mass was measured using an analytical balance (OHAUS AX124) with a precision of 0.0001 g. Accordingly, the sorbent mass uncertainty was negligible compared to that of the sorbate.

Finally, the uncertainty in the SCP calculation is obtained using Eq. (84). Substituting the sorbent mass and differential sorbate uptake in Eq. (84), the maximum SCP uncertainty is calculated to be 5.7% for different samples and cycle times.

$$\delta\omega = \frac{0.01g}{m_{sorbent}} \tag{83}$$

$$\frac{\delta SCP}{SCP} = \frac{0.01\sqrt{2}}{m_{sorbent}\,\Delta\omega} \tag{84}$$

The COP is defined as the ratio of the evaporative cooling energy to the input energy, Eq. (85)

$$COP = \frac{Q_{evap}}{Q_{input}} = \frac{Q_{evap}}{Q_{sens} + Q_{des}} = \frac{m_s \int_{ads} \frac{d\omega}{dt} h_{fg} dt}{\int_{des} \left(\left(m_s \left(c_{p,s} + \omega c_{p,w} \right) + m_{HMX} c_{p,HMX} \right) \frac{dT}{dt} - m_s \frac{d\omega}{dt} H_{ads} \right) dt} \quad (85)$$

The uptake measurement is the main uncertainty in the COP estimation and can be calculated using Eq. ((86). The maximum uncertainty of the COP is calculated to be 8% for different samples and cycle times.

$$\frac{\delta COP}{COP} = \frac{\sqrt{2}\delta\Delta\omega}{\Delta\omega} = \frac{2\delta\omega}{\Delta\omega} \quad (86)$$

3.3. Model validation

Figure 3.6 shows the mass change of the sorber bed for the sample with a 0 % amount of graphite flakes. The measured mass change of the sorber bed is due to: (i) the water uptake by sorbent material; (ii) fluctuations such as thermal expansion, contraction, and vibration of the flexible hoses; and (iii) density changes of the heat transfer fluid (HTF) due to the temperature swings between the adsorption and desorption processes. In order to deconvolute the mass change caused by the water uptake from other fluctuations, a number of the baseline experiments were run under the same operating conditions but with the valve between the sorber bed and the evaporator/condenser kept shut. Consequently, the baseline did not include the effect of water uptake. After measuring the baseline signal, the valve was opened and the experiment was repeated; the blue line shows the total mass change of the sorber bed, including water uptake. Subtracting the total mass from the baseline represents the actual water uptake changes. The experiment data can be found in Table 10 in the Appendix A.

Figure 3.7 shows variation of the average sorbent temperature versus time for varying amounts of graphite flakes. By adding graphite flake, the sorbent thermal diffusivity improves, which enhances the heat transfer from the HMX to the sorbent. For samples

with higher amounts of graphite flake and lower amounts of active material, the heat of sorption decreases. The experiment data can be found in Table 11 in the Appendix A.

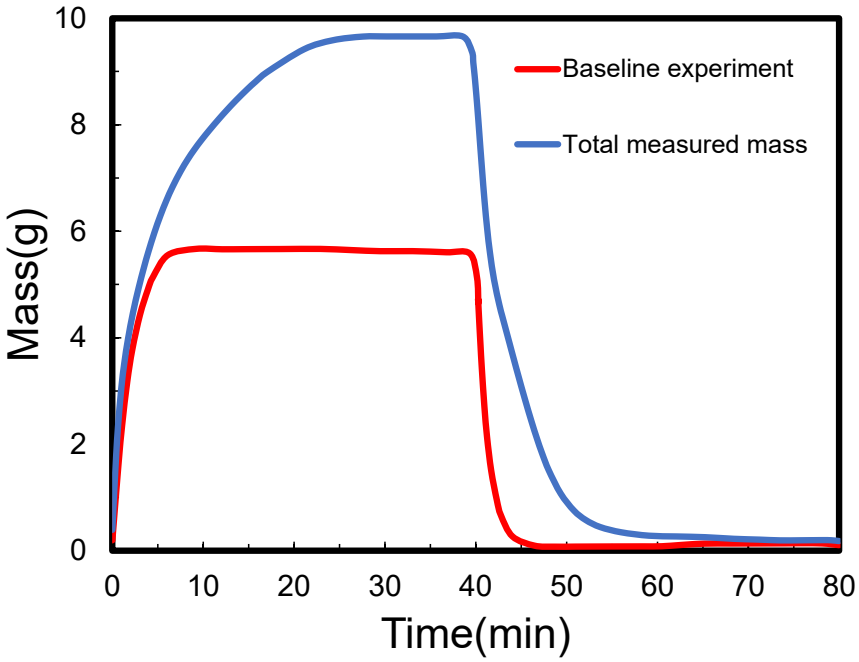

Figure 3.6. Mass changes of the sorber bed with 0% graphite flake content in the G-LTJ test bed due to the variations in water density and fluctuations during sorption (30 ℃) and desorption (67 ℃).

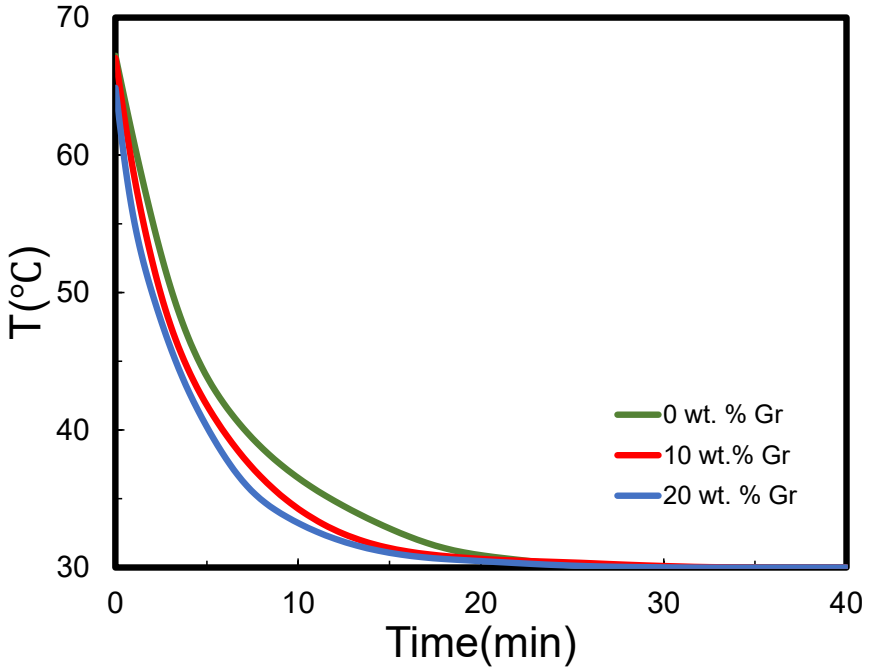

Figure 3.7. Variation of the average sorbent temperature through time for different amounts of graphite flake.

Figure 3.8 shows the variation of water uptake versus time for varying amounts of graphite flake in the sorbent. In the early stage of sorption (the first 10 to 15 minutes), adding graphite flake enhances water uptake. As the sorbent approaches saturation, the heat generation rate reduces and the trend starts to reverse. Moreover, a greater amount of graphite flake reduces the amount of active material leading to lower uptake and performance as the sorbent reaches equilibrium. The equilibrium uptakes measured with the G-LTJ test bed are in good agreement with the thermogravimetric sorption analyzer (TGA) equilibrium data. For more information, see [121]. The experiment data can be found in Table 12 in the Appendix A.

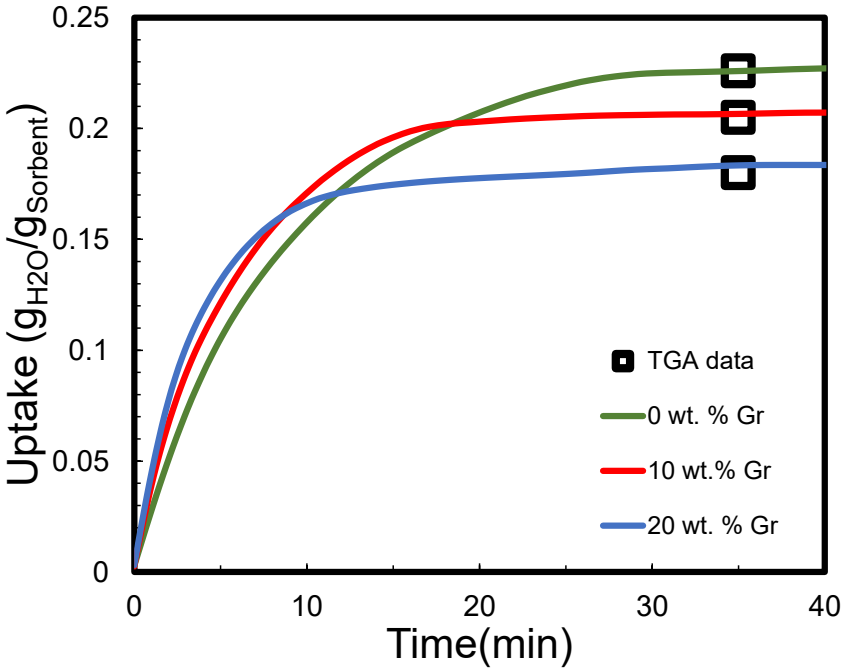

Figure 3.8. The effect of graphite flake content on water uptake

Figure 3.9 shows the effect of graphite flakes on the SCP and COP based on Eqs. (2) and (3). It can be seen that the present analytical model is in a good agreement with the experimental results. Moreover, for small sorption times (the first 10 to 15 minutes), the SCP increases 10 to 30% by adding graphite flakes. Thus, during the early stages of sorption, the sorption rate and heat generation is high, resulting in a need for higher thermal diffusivity, which in turn, causes higher uptake. However, over longer periods of time, such as when the sorbent approaches saturation, the need for higher thermal diffusivity reduces as the sorption rate decreases. The trend starts to reverse and the sorbent with higher active material has higher uptake and of course higher SCP.

Additionally, for the small sorption time, the sample with larger amount of graphite flake has a higher uptake and thus, a higher COP. As we approach the saturation phase, the sample with a smaller amount of additives and a greater amount of active material has the highest uptake and COP.

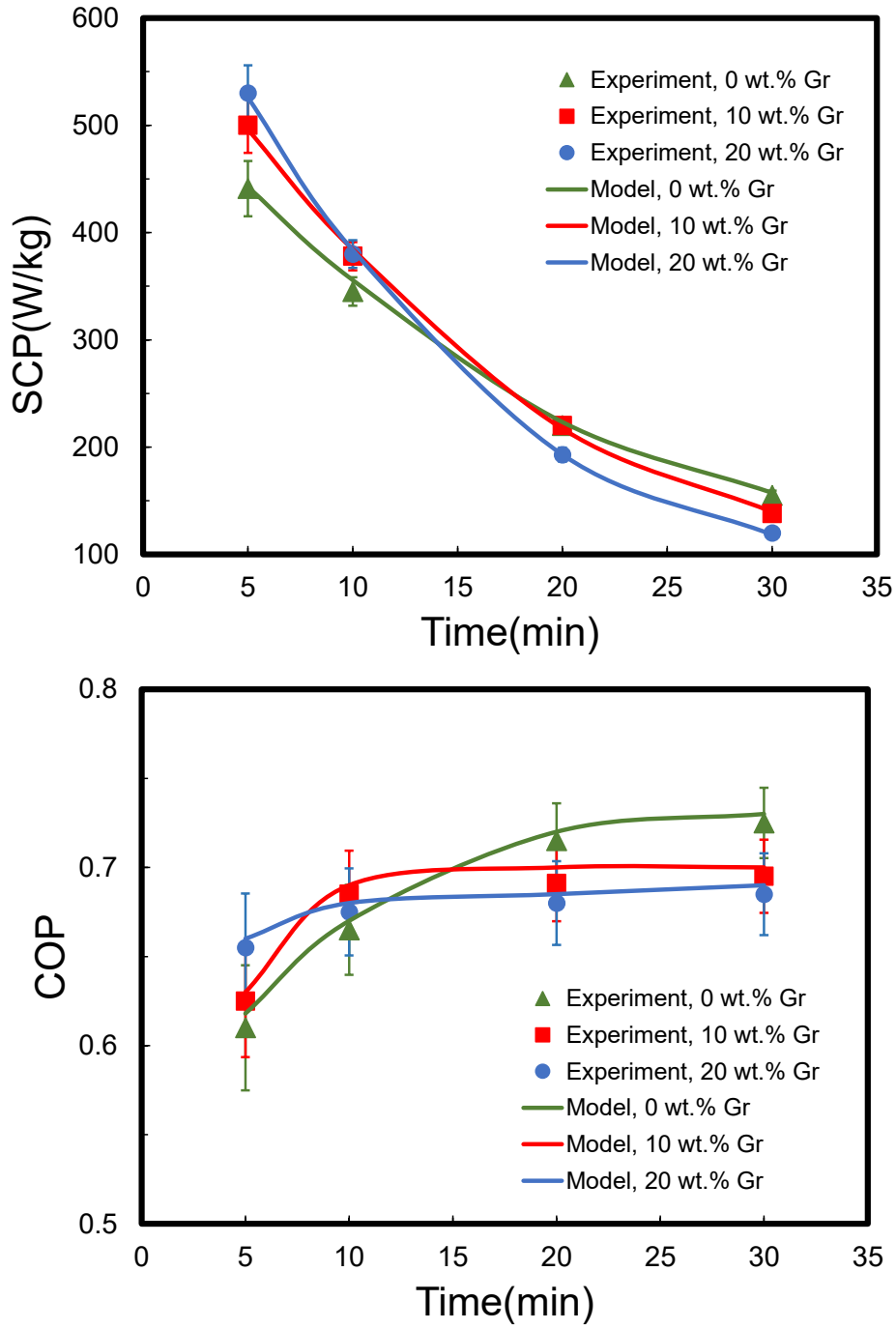

Figure 3.9. **A comparison between the present analytical model and the experimental data collected from our G-LTJ test bed for 0 and 20 wt% graphite flake content in the sorbent composite.**

3.4. Parametric study

A comprehensive parametric study is carried out to examine the effect of key design and operating variables on the COP and SCP, namely, the fin radius, sorbent thickness, fin height, fluid channel height, graphite flake content in the sorbent, and the cycle time. Sorber bed characteristic parameters are considered as a baseline in which each parameter is changed over an arbitrarily chosen range while other parameters are kept constant. It should be noted that the results are particular to the values and conditions described in Table 5 and might be different for other input parameters. The SCP and COP for the baseline condition listed in Table 2 are 737 W/kg K and 0.66, respectively.

The following conclusions can be made from Figure 3.10 (a-e):

- The SCP reduces by the fin height increment because the heat transfer resistance along the fin increases; also the extra fin materials add to the thermal inertia which reduces the SCP. However, COP is almost constant by increasing the fin height. As can be seen, there is a slight increase up to a value and then a decrease as both numerator and denominator in the COP, Eq. (2), are increasing and they can have different rate with respect to the geometry;

- The SCP increases by increasing the fin radius as the heat transfer along the fin enhances due to the larger cross-sectional area. Nonetheless, the COP decreases by increasing the fin radius because the dead weight mass (thermal inertia) is increases;

- The SCP decreases by the sorbent thickness increment because the sorbent heat transfer resistance enhances. However, the COP increases by the sorbent thickness increment as the amount of active material increases;

- The SCP increases by reducing the cycle time as the sorption rate is higher at the beginning of sorption and drops as the sorbent approaches saturation. Nevertheless, the COP decreases slightly by reducing the cycle time as more energy needs to be provided for the sensible heat of the sorber bed HMX thermal inertia with respect to the desorption heat; and

- Thermal diffusivity can be enhanced by additive material. Previous studies showed that thermal diffusivity of the sorbent can be increased up to 500% by adding graphite flakes as an additive, although it will reduce the amount of active material [121]. Therefore, it is important to select an optimum amount of additive, which depends on the geometry and heat transfer characteristics of a sorber bed. The SCP and COP both increase by the graphite flake content increment to the point until it keeps up with heat transfer resistance in the fin. After the climax, the SCP starts to decrease by increasing the graphite flake content as the active sorbent material decreases.

It is evident that geometry, sorbent properties and cycle time can have counteracting effects on the COP and SCP and should be optimized simultaneously to build an optimal design to be investigated in future studies. The next section is focused on an analysis of variance of the proposed PF-HMX to address the need for this simultaneous optimization.

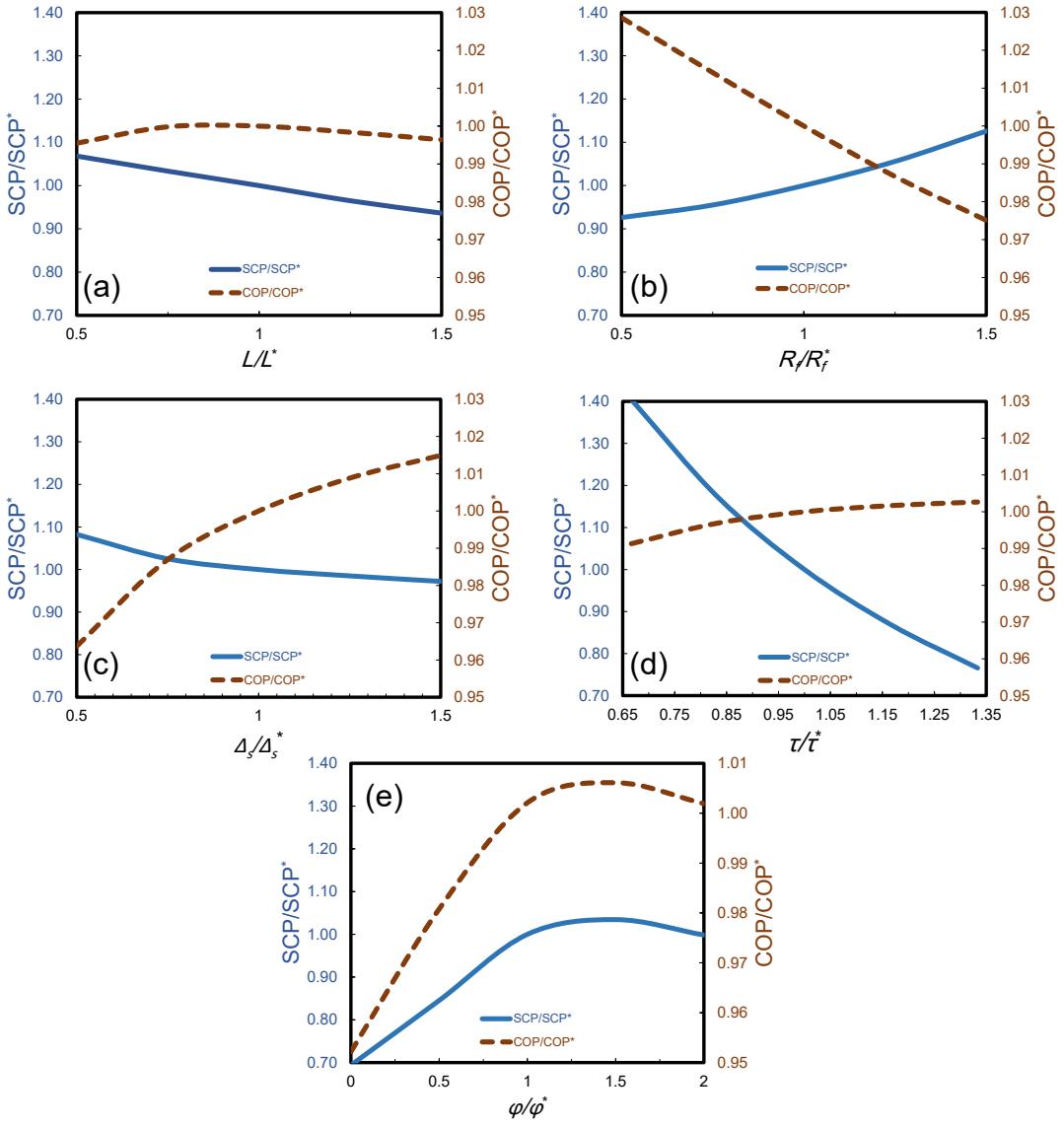

Figure 3.10. A parametric study: the COP and SCP Variation with the sorber bed's geometry, heat transfer characteristics and cycle time (a) fin height, (b) fin radius, (c) sorbent thickness, (d) cycle time, and (e) graphite flake content in the sorbent. The SCP* and COP* are the baseline values shown in Table 5.

3.5. Analysis of variance (ANOVA)

An ANOVA is a statistically decision-making tool to detect differences in the average performance. It helps testing the significance of all main factors by calculating the sums of square, level of contribution, F-statistic ratio and p-value, see Ref [124][125]. The ANOVA method is utilized to understand the percentage contribution of each

parameter on the SCP and COP [5]. A Multi-way ANOVA analysis is performed using the N-ANOVA function in MATLAB. Table 6 shows the sample points of variables generated using the Box-Behnken design [126] with three levels of design parameters.

Table 6. Three levels of the PF-HMX design parameters

	Level 1	**Level 2 (baseline case)**	**Level 3**
Fin height (L (cm))	1	2	3
Fin radius (R_f (mm))	1	2	3
Sorbent thickness (Δ_s (mm))	1	2	3
Graphite flake content (φ (wt.%))	0	10	20
Fluid channel height (Hc (mm))	4	6	8
Cycle time (τ (min))	10	15	20

The null hypothesis is used to see whether a variable has a substantial effect on the objective function. When α is greater than the p-value, then the null hypothesis is rejected. α is the significance level and it is usually equal to 0.05 which means there is a 5% probability that null hypothesis was incorrect and the parameter has a significant effect. The p-value also can be estimated by MATLAB as a function of the F-static ratio, α, and degree of freedoms.

We found that all p-values, shown in Table 7, are less than α except the p-value for the heat transfer fluid channel height which is greater than α, therefore, all factors are affecting the responses except the heat transfer fluid channel height that should be considered as a parameter as its share in the objective functions is negligible.

Table 7. The calculated p-value of all design parameters by MATLAB for the SCP and COP

Parameters	**COP**	**SCP**
Fin height (L (cm))	4.78e-12	7.04e-8
Fin radius (R_f (mm))	5.73e-25	4.41e-16
Sorbent thickness (Δ_s (mm))	9.76e-28	6.66e-8
Graphite flake content (φ (wt. %))	8.11e-32	2.57e-28
Fluid channel height (Hc (mm))	5.14e-2	6.34e-2
Cycle time (τ (min))	3.72e-16	6.64e-36

The results of this analysis for both the COP and SCP are shown in Figure 3.11 and represent how all these parameters affect the COP and SCP of the system. The conclusion will be as follows:

- The amount of graphite flake, sorbent thickness and fin radius have the highest level of contribution to the COP;
- The fin height and cycle time have the second largest impact on the COP;
- The cycle time and graphite flake content have the largest impact on the SCP;
- The sorbent thickness and fin height have the second largest impact on the SCP; and
- The HTF channel height has the lowest level of contribution to both the SCP and COP.

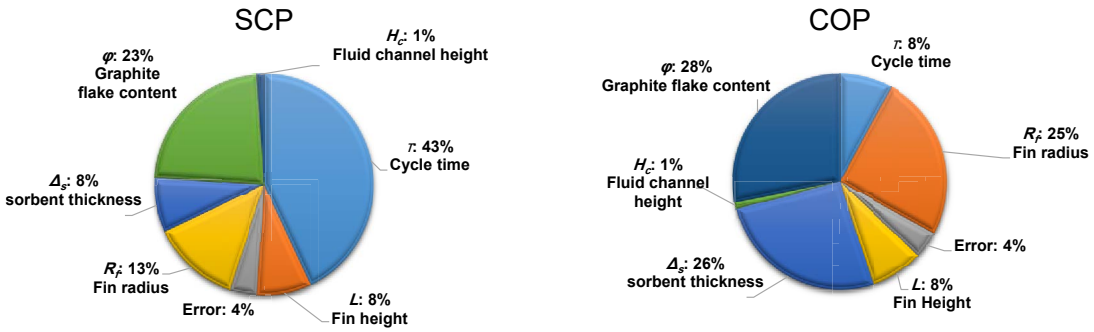

Figure 3.11. The level of contribution of the design parameters to the SCP and COP, L: fin height, R_f: fin radius, Δ_s: sorbent thickness, φ: graphite flake content in sorbent, t: cycle time, and H_C: fluid channel height.

3.6. Performance evaluation

The baseline case is investigated for the operating conditions of the sorption chiller: T_{des}=90 °C, T_{ads}=T_{cond}=30 °C and T_{evap}=15 °C. The SCP, COP, and MR are calculated as the performance metrics based on Eqs. (2), (3), and (4). Note that the mass of heat transfer fluid was not available for some studies. The PF-HMX with relatively low MR reaches a SCP of 1160 W/kg and COP of 0.68. Figure 3.12 displays the performance of the PF-HMX versus the state-of-the-art published research. Note that the composite

silica gel/$CaCl_2$ sorbent used in the PF-HMX, [104] and [106] provides higher SCP and COP. Silica gel/$CaCl_2$ sorption kinematic occurs over the entire range of relative pressure $0.06<P/P_0<0.4$ which makes it a good candidate for AC applications [121]. Conversely, the sorption for zeolite-based materials, such as SAPO-34 and FAM Z02, utilized in [107]–[113] occurs in a narrow range of relative pressure which limits the application to specific operational temperatures.

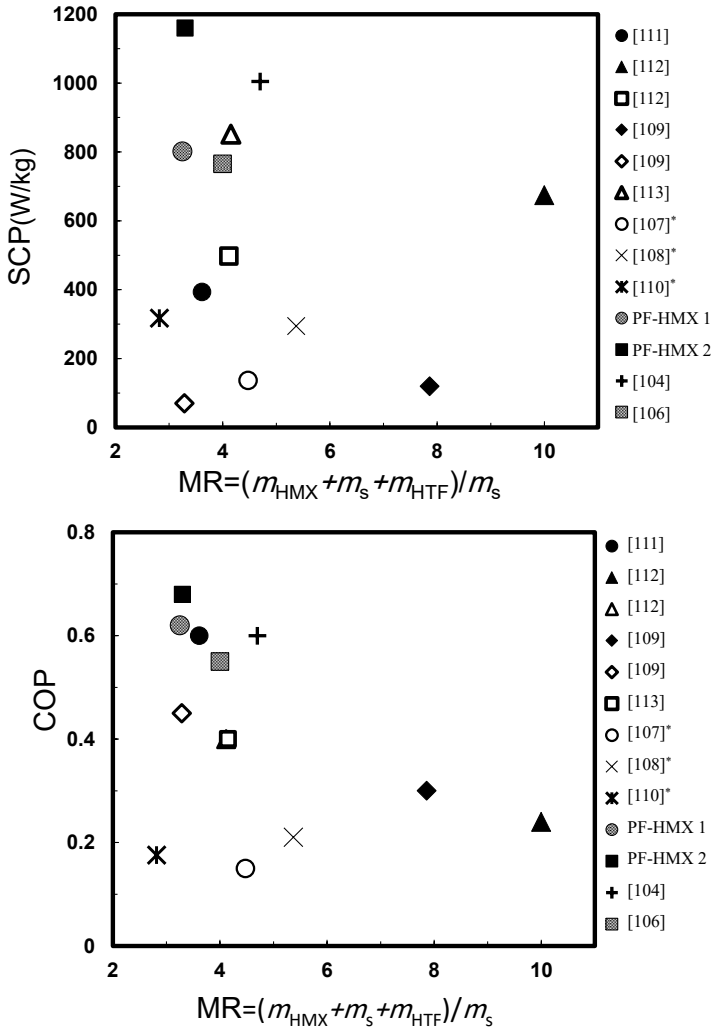

Figure 3.12. A PF-HMX comparison in terms of the MR, SCP and COP versus the available studies. The fin radius and sorbent thickness of the PF-HMX 1 are 2 mm and 5 mm, respectively, while the fin radius and sorbent thickness for the PF-HMX 2 are 1mm and 2 mm, respectively. * HTF data not provided.

Chapter 4. Conclusions, limitations and future work

4.1. Conclusion

The aim of this Master's project was to develop a sorber bed heat and mass exchanger for use in sorption systems. The application of sorption cooling and heating was the focus of this research. However, the modeling, ANOVA, design, manufacturing and testing methodology can be extended to other sorption applications such as energy storage, dehumidification, with heat transformer, gas separation and desalination.

A novel closed-form 2-D analytical model was developed to determine the conjugate heat and mass transfer and performance of the PF-HMX. Developed analytical model take into account the spatial and temporal variation of temperature and water uptake and have a short computation tie, which is beneficial for real-time control and the optimization of a PF-HMX design. The analytical solution included material properties, operating conditions and all design parameters such as sorbent geometry, HMX geometry, and fluid channel height. The current 2-D model was successfully validated based on experimental results collected from the custom-built G-LTJ test bed.

The effect of the HMX geometry, heat transfer characteristics, and cycle time on sorption efficiency, i.e., the SCP and COP, was investigated using a parametric study. it was shown that the heat transfer and geometrical characteristics of the sorber bed, such as the sorbent thickness, fin radius, fin height, amount of graphite flakes, cycle time, and fluid channel height, have conflicting effects on the COP and SCP.

An analysis of variance (ANOVA) method is utilized to understand the percentage contribution of each parameter on the specific cooling power (SCP) and coefficient of performance (COP). It is shown that the amount of graphite flake, sorbent thickness and fin radius on one hand and the cycle time and graphite flake content on the other have the highest level of contribution to the COP and SCP, respectively. Thus, a multi-objective optimization procedure should be conducted to find an optimal design of sorber bed for future studies based on geometrical and heat transfer characteristics of the sorber bed.

To this end, we compared two arbitrary geometries of the PF-HMX with other studies and found that PF-HMXs with a relatively low MR could provide a high SCP and COP. The PF-HMX was found to have the highest SCP of 1160 W/kg and the highest COP of 0.68 with a relatively low mass ration of 3.3 compared to the state of the- rt.

4.2. Limitations

The following are the limitations, potential for further progress and application of this thesis to other sorption applications:

- If the assumptions in Section 2.2 are met, the analytical model can be used. Otherwise, significant changes to the model will be needed, such as the inclusion of mass transfer equations and convection terms.

  Furthermore, an analytical model was developed for closed sorption cooling heating systems. Other closed sorption systems like thermal energy storage, desalination and heat transformers can also benefit from it. The open sorption systems, such as dehumidification and gas separation applications, would necessitate major changes to the model. The solution domain and governing equations should be modified to include additional layers of the flow stream and convection terms.

- Other thermally conductive additives can also be used to improve the sorbent thermal diffusivity. Furthermore, sorbents other than silica gel/$CaCl_2$ can be used as the sorbent. For the new composite, equilibrium adsorption and thermo-physical properties should be measured and incorporated into the model as inputs. The sorbent assumptions mentioned in Section 2.2 should be double-checked.

- For various sorption applications, ANOVA and parametric studies should be conducted using modified analytical models as the performance parameters change.

4.3. Future work

The following are some examples of potential future research directions for this study:

- Investigation of other thermally-conductive material other that graphite flakes, such as Expanded Natural Graphite (ENG);
- Optimization of the PF-HMX using a multi-objective genetic algorithm to optimize the SCHS's performance;
- Design and construction of an optimized PF-HMX for a SCHS application;
- Investigation of other HMX designs, such as nature-inspired and radial fin HMXs;
- The proposed methodology in this Master's project can be applied to other sorption applications; and
- Use of a quadratic function to approximate the water uptake relationship with sorbent temperature and solve the governing equations semi-analytically.

References

[1] H. Bahrehmand, M. Ahmadi, and M. Bahrami, “Analytical modeling of oscillatory heat transfer in coated sorption beds,” *Int. J. Heat Mass Transf.*, vol. 121, pp. 1–9, 2018.

[2] D. Ürge-Vorsatz, L. F. Cabeza, S. Serrano, C. Barreneche, and K. Petrichenko, “Heating and cooling energy trends and drivers in buildings,” *Renew. Sustain. Energy Rev.*, vol. 41, pp. 85–98, 2015.

[3] J. M. Cullen and J. M. A. Ã, “The efficient use of energy : Tracing the global flow of energy from fuel to service,” *Energy Policy*, vol. 38, no. 1, pp. 75–81, 2010.

[4] C. Forman, I. K. Muritala, R. Pardemann, and B. Meyer, “Estimating the global waste heat potential,” *Renew. Sustain. Energy Rev.*, vol. 57, pp. 1568–1579, 2016.

[5] A. Asghar, A. Aziz, A. Raman, W. Mohd, and A. Wan, “A Comparison of Central Composite Design and Taguchi Method for Optimizing Fenton Process,” vol. 2014, 2014.

[6] A. A. Askalany, M. Salem, I. M. Ismael, A. H. H. Ali, M. G. Morsy, and B. B. Saha, “An overview on adsorption pairs for cooling,” *Renew. Sustain. Energy Rev.*, vol. 19, pp. 565–572, 2013.

[7] W. Pridasawas, *Solar-driven refrigeration systems with focus on the ejector cycle*, no. 06/55. Department of Energy Technology, Royal Institute of Technology, 2006, 2006.

[8] J. M. Pinheiro, S. Salústio, J. Rocha, A. A. Valente, and C. M. Silva, “Analysis of equilibrium and kinetic parameters of water adsorption heating systems for different porous metal/metalloid oxide adsorbents,” *Appl. Therm. Eng.*, vol. 100, pp. 215–226, 2016.

[9] H. Demir, M. Mobedi, and S. Ülkü, “A review on adsorption heat pump: Problems and solutions,” *Renew. Sustain. Energy Rev.*, vol. 12, no. 9, pp. 2381–2403, 2008.

[10] J. L. Chin and others, “State-of-the-Art Technologies on Low-Grade Heat Recovery and Utilization in Industry,” *Chapters*, 2019.

[11] C. Forman, I. K. Muritala, R. Pardemann, and B. Meyer, “Estimating the global waste heat potential,” *Renew. Sustain. Energy Rev.*, vol. 57, pp. 1568–1579, 2016.

[12] Y. Zhao, E. Hu, and A. Blazewicz, “Dynamic modelling of an activated carbon–methanol adsorption refrigeration tube with considerations of interfacial

convection and transient pressure process," *Appl. Energy*, vol. 95, pp. 276–284, 2012.

[13] W. D. Wu, H. Zhang, and D. W. Sun, "Mathematical simulation and experimental study of a modified zeolite 13X-water adsorption refrigeration module," *Appl. Therm. Eng.*, vol. 29, no. 4, pp. 645–651, 2009.

[14] A. Sharafian, S. M. N. Mehr, P. C. Thimmaiah, W. Huttema, and M. %J E. Bahrami, "Effects of adsorbent mass and number of adsorber beds on the performance of a waste heat-driven adsorption cooling system for vehicle air conditioning applications," vol. 112, pp. 481–493, 2016.

[15] E. J. Hu, D. Zhu, X. Sang, L. Wang, and Y. Tan, "Enhancement of Thermal Conductivity by Using Polymer- Zeolite in Solid Adsorption Heat Pumps," *J. Heat Transfer*, vol. 1, no. August, pp. 1991–1993, 1997.

[16] Canadian Energy Systems Analysis Research (CESAR), "No Title," *Canadian Energy Flows*, 2013. [Online]. Available: https://www.cesarnet.ca/visualization/sankey-diagrams-canadas-energy-systems.

[17] D. J. Close and R. V. %J S. E. Dunkle, "Use of adsorbent beds for energy storage in drying of heating systems," vol. 19, no. 3, pp. 233–238, 1977.

[18] C. J. Geankoplis, *Transport processes and separation process principles:(includes unit operations)*. Prentice Hall Professional Technical Reference, 2003.

[19] N. C. Srivastava and I. W. %J A. thermal engineering Eames, "A review of adsorbents and adsorbates in solid–vapour adsorption heat pump systems," vol. 18, no. 9–10, pp. 707–714, 1998.

[20] A. S. Ülkü and M. Mobedi, "Adsorption in energy storage," in *Energy Storage Systems*, Springer, 1989, pp. 487–507.

[21] D. M. Ruthven, *Principles of adsorption and adsorption processes*. John Wiley & Sons, 1984.

[22] M. M. %J J. of colloid Dubinin and interface science, "Adsorption in micropores," vol. 23, no. 4, pp. 487–499, 1967.

[23] S. J. Gregg, K. S. W. %J A. Sing surface area, and L. porosity. Academic Press, "The physical adsorption of gases by nonporous solids: The type II isotherm," pp. 41–110, 1982.

[24] D. D. Do, *Adsorption analysis: equilibria and kinetics*, vol. 2. Imperial college press London, 1998.

[25] L. W. Wang, R. Z. Wang, J. Y. Wu, K. Wang, S. G. %J E. C. Wang, and

Management, “Adsorption ice makers for fishing boats driven by the exhaust heat from diesel engine: choice of adsorption pair,” vol. 45, no. 13–14, pp. 2043–2057, 2004.

[26] Z. Aidoun and M. %J A. thermal engineering Ternan, “Salt impregnated carbon fibres as the reactive medium in a chemical heat pump: the NH3–CoCl2 system,” vol. 22, no. 10, pp. 1163–1173, 2002.

[27] K. Wang, J. Y. Wu, R. Z. Wang, L. W. %J E. C. Wang, and Management, “Effective thermal conductivity of expanded graphite–CaCl2 composite adsorbent for chemical adsorption chillers,” vol. 47, no. 13–14, pp. 1902–1912, 2006.

[28] L. G. Gordeeva, M. V Solovyeva, and Y. I. %J E. Aristov, “NH2-MIL-125 as a promising material for adsorptive heat transformation and storage,” vol. 100, pp. 18–24, 2016.

[29] N. Yu, R. Z. Wang, Z. S. Lu, L. W. %J I. journal of heat Wang, and mass transfer, “Study on consolidated composite sorbents impregnated with LiCl for thermal energy storage,” vol. 84, pp. 660–670, 2015.

[30] C. Bales *et al.*, “Laboratory tests of chemical reactions and prototype sorption storage units,” vol. 32, 2008.

[31] L. Scapino, H. A. Zondag, J. Van Bael, J. Diriken, and C. C. M. %J A. E. Rindt, “Sorption heat storage for long-term low-temperature applications: A review on the advancements at material and prototype scale,” vol. 190, pp. 920–948, 2017.

[32] H. Kakiuchi, M. Iwade, S. Shimooka, K. Ooshima, M. Yamazaki, and T. %J I.-A. Takewaki, “Novel zeolite adsorbents and their application for AHP and Desiccant system,” vol. 17, 2005.

[33] B. %J J. of C. E. of J. Dawoud, “On the effect of grain size on the kinetics of water vapor adsorption and desorption into/from loose pellets of FAM-Z02 under a typical operating condition of adsorption heat pumps,” vol. 40, no. 13, pp. 1298–1306, 2007.

[34] S. Santamaria, A. Sapienza, A. Frazzica, A. Freni, I. S. Girnik, and Y. I. %J A. energy Aristov, “Water adsorption dynamics on representative pieces of real adsorbers for adsorptive chillers,” vol. 134, pp. 11–19, 2014.

[35] Y. I. %J A. T. E. Aristov, “Challenging offers of material science for adsorption heat transformation: a review,” vol. 50, no. 2, pp. 1610–1618, 2013.

[36] A. Frazzica, V. Brancato, V. Palomba, and S. Vasta, “Sorption Thermal Energy Storage,” in *Recent Advancements in Materials and Systems for Thermal Energy Storage*, Springer, 2019, pp. 33–54.

[37] D. Aydin, S. P. Casey, S. %J R. Riffat, and S. E. Reviews, “The latest

advancements on thermochemical heat storage systems," vol. 41, pp. 356–367, 2015.

[38] H. Jarimi, D. Aydin, Z. Yanan, G. Ozankaya, X. Chen, and S. %J I. J. of L.-C. T. Riffat, "Review on the recent progress of thermochemical materials and processes for solar thermal energy storage and industrial waste heat recovery," vol. 14, no. 1, pp. 44–69, 2018.

[39] V. Brancato, A. %J S. E. M. Frazzica, and S. Cells, "Characterisation and comparative analysis of zeotype water adsorbents for heat transformation applications," vol. 180, pp. 91–102, 2018.

[40] H. T. Chua, K. C. Ng, A. Chakraborty, N. M. Oo, M. A. %J J. of C. Othman, and E. Data, "Adsorption characteristics of silica gel+ water systems," vol. 47, no. 5, pp. 1177–1181, 2002.

[41] L. Calabrese *et al.*, "Development and characterization of silane-zeolite adsorbent coatings for adsorption heat pump applications," vol. 116, pp. 364–371, 2017.

[42] M. V Solovyeva, Y. I. Aristov, and L. G. %J A. T. E. Gordeeva, "NH2-MIL-125 as promising adsorbent for adsorptive cooling: Water adsorption dynamics," vol. 116, pp. 541–548, 2017.

[43] E. S. B. V, "Received April 30, 1996 Accepted June 12, 1996," vol. 59, no. 2, pp. 325–333, 1996.

[44] S. Solar and E. Gmbh, "SELECTIVE WATER SORBENTS FOR MULTIPLE APPLICATIONS. 11. CaCl 2 CONFINED TO EXPANDED VERMICULITE Yu.I. Aristov," vol. 71, no. 2, pp. 377–384, 2000.

[45] M. Tokarev, L. Gordeeva, V. Romannikov, I. Glaznev, and Y. Aristov, "New composite sorbent CaCl2 in mesopores for sorption cooling/heating," *Int. J. Therm. Sci.*, vol. 41, no. 5, pp. 470–474, 2002.

[46] L. G. Gordeeva, G. Restuccia, A. Freni, and Y. I. Aristov, "Water sorption on composites 'LiBr in a porous carbon,'" *Fuel Process. Technol.*, vol. 79, no. 3, pp. 225–231, 2002.

[47] J. Jänchen, D. Ackermann, H. Stach, and W. Brösicke, "Studies of the water adsorption on Zeolites and modified mesoporous materials for seasonal storage of solar heat," *Sol. Energy*, vol. 76, no. 1–3, pp. 339–344, 2004.

[48] J. Jänchen, D. Ackermann, E. Weiler, H. Stach, and W. Brösicke, "Calorimetric investigation on zeolites, AlPO4's and CaCl 2 impregnated attapulgite for thermochemical storage of heat," *Thermochim. Acta*, vol. 434, no. 1–2, pp. 37–41, 2005.

[49] O. Opel, H. . Rammelburg, M. Gerard, and W. Ruck, "Thermochemical Storage

Materials Research - Tga / Dsc-Hydration Studies," *1st Int. Conf. Sustain. Energy Storage, Vol. 1st*, 2011.

[50] H. Wu, S. Wang, and D. Zhu, "Effects of impregnating variables on dynamic sorption characteristics and storage properties of composite sorbent for solar heat storage," *Sol. Energy*, vol. 81, no. 7, pp. 864–871, 2007.

[51] I. A. Simonova, A. Freni, G. Restuccia, and Y. I. Aristov, "Water sorption on composite 'silica modified by calcium nitrate,'" *Microporous Mesoporous Mater.*, vol. 122, no. 1–3, pp. 223–228, 2009.

[52] K. Posern and C. Kaps, "Calorimetric studies of thermochemical heat storage materials based on mixtures of MgSO4 and MgCl2," *Thermochim. Acta*, 2010.

[53] I. V. Ponomarenko, I. S. Glaznev, A. V. Gubar, Y. I. Aristov, and S. D. Kirik, "Synthesis and water sorption properties of a new composite 'CaCl 2 confined into SBA-15 pores,'" *Microporous Mesoporous Mater.*, 2010.

[54] S. Hongois, F. Kuznik, P. Stevens, and J. J. Roux, "Development and characterisation of a new MgSO4-zeolite composite for long-term thermal energy storage," *Sol. Energy Mater. Sol. Cells*, 2011.

[55] A. Sapienza, I. S. Glaznev, S. Santamaria, A. Freni, and Y. I. Aristov, "Adsorption chilling driven by low temperature heat: New adsorbent and cycle optimization," *Appl. Therm. Eng.*, vol. 32, no. 1, pp. 141–146, 2012.

[56] A. Ristić, D. Maučec, S. K. Henninger, and V. Kaučič, "New two-component water sorbent CaCl 2 -FeKIL2 for solar thermal energy storage," *Microporous Mesoporous Mater.*, 2012.

[57] Y. Y. Tanashev, A. V. Krainov, and Y. I. Aristov, "Thermal conductivity of composite sorbents 'salt in porous matrix' for heat storage and transformation," *Appl. Therm. Eng.*, 2013.

[58] S. P. Casey, J. Elvins, S. Riffat, and A. Robinson, "Salt impregnated desiccant matrices for 'open' thermochemical energy storage - Selection, synthesis and characterisation of candidate materials," *Energy Build.*, vol. 84, pp. 412–425, 2014.

[59] M. M. Druske *et al.*, "Developed materials for thermal energy storage: Synthesis and characterization," in *Energy Procedia*, 2014.

[60] A. Jabbari-Hichri, S. Bennici, and A. Auroux, "Enhancing the heat storage density of silica–alumina by addition of hygroscopic salts (CaCl 2 , Ba(OH) 2 , and LiNO 3)," *Sol. Energy Mater. Sol. Cells*, 2015.

[61] N. Yu, R. Z. Wang, Z. S. Lu, and L. W. Wang, "Study on consolidated composite sorbents impregnated with LiCl for thermal energy storage," *Int. J. Heat Mass*

Transf., 2015.

[62] H. Liu, K. Nagano, and J. Togawa, “A composite material made of mesoporous siliceous shale impregnated with lithium chloride for an open sorption thermal energy storage system,” *Sol. Energy*, 2015.

[63] K. Korhammer *et al.*, “Sorption and thermal characterization of composite materials based on chlorides for thermal energy storage,” *Appl. Energy*, 2016.

[64] A. Grekova, L. Gordeeva, and Y. Aristov, “Composite sorbents ‘li/Ca halogenides inside Multi-wall Carbon Nano-tubes’ for Thermal Energy Storage,” *Sol. Energy Mater. Sol. Cells*, 2016.

[65] Y. N. Zhang, R. Z. Wang, Y. J. Zhao, T. X. Li, S. B. Riffat, and N. M. Wajid, “Development and thermochemical characterizations of vermiculite/SrBr2 composite sorbents for low-temperature heat storage,” *Energy*, 2016.

[66] A. D. Grekova, L. G. Gordeeva, and Y. I. Aristov, “Composite ‘LiCl/vermiculite’ as advanced water sorbent for thermal energy storage,” *Appl. Therm. Eng.*, 2017.

[67] H. Bahrehmand and M. Bahrami, “Development of novel sorber bed heat exchangers for sorption cooling systems,” *PhD thesis*, 2020.

[68] Y. Luo, H. H. Funke, J. L. Falconer, and R. D. Noble, “Adsorption of CO2, CH4, C3H8, and H2O in SSZ-13, SAPO-34, and T-type zeolites,” *Ind. Eng. Chem. Res.*, vol. 55, no. 36, pp. 9749–9757, 2016.

[69] A.-D. Raya, S. Mahmoud, E. Elsayed, P. Youssef, and F. Al-Mousawi, “Metal-organic framework materials for adsorption heat pumps,” *Energy*, vol. 190, p. 116356, 2020.

[70] A. Sharafian and M. Bahrami, “Assessment of adsorber bed designs in waste-heat driven adsorption cooling systems for vehicle air conditioning and refrigeration,” *Renew. Sustain. Energy Rev.*, vol. 30, pp. 440–451, 2014.

[71] A. Freni *et al.*, *Characterization of Zeolite-Based Coatings for Adsorption Heat Pumps*. SPRINGER BRIEFS IN APPLIED SCIENCES AND TECHNOLOGY, 2015.

[72] R. Nikbakhti, X. Wang, A. K. Hussein, and A. Iranmanesh, “Absorption cooling systems – Review of various techniques for energy performance enhancement,” *Alexandria Eng. J.*, vol. 59, no. 2, pp. 707–738, 2020.

[73] A. Sharafianardakani, “Waste heat-driven adsorption cooling systems for vehicle air conditioning applications,” p. 231, 2015.

[74] R. Gomri, “Investigation of the potential of application of single effect and multiple effect absorption cooling systems,” *Energy Convers. Manag.*, vol. 51, no. 8, pp.

1629–1636, 2010.

[75] L. F. Cabeza, A. Sole, and C. Barreneche, “Review on sorption materials and technologies for heat pumps and thermal energy storage,” *Renew. Energy*, vol. 110, pp. 3–39, 2017.

[76] S. Henninger, M. Schicktanz, P. Hugenell, S. H, and H. Henning, “Evaluation of methanol adsorption on activated carbons for thermally driven chillers, part I: thermophysical characterisation.,” *Int J Refrig*, vol. 35, pp. 543–553, 2012.

[77] Z. Tamainot-Telto, S. J. Metcalf, R. E. Critoph, Y. Zhong, and R. Thorpe, “Carbon – ammonia pairs for adsorption refrigeration applications : ice making , air conditioning and heat pumping Les couples charbon actif-ammoniac pour les applications ` adsorption : fabrication de glace , frigorifiques a ` chaleur conditionnement d ’,” *Int. J. Refrig.*, vol. 32, no. 6, pp. 1212–1229, 2009.

[78] B. Saha, I. El-Sharkawy, A. Chakraborty, and S. Koyama, “Study on an activated carbon fiber-ethanol adsorption chiller: part I – system description and modelling.,” *Int J Refrig*, vol. 30, pp. 86–95, 2007.

[79] Q. W. Pan, R. Z. Wang, L. W. Wang, and D. Liu, “Design and experimental study of a silica gel-water adsorption chiller with modular adsorbers,” *Int. J. Refrig.*, vol. 67, pp. 336–344, 2016.

[80] R. Ahmed and R. Al-Dadah, “Physical and operating conditions effects on silica gel/water adsorption chiller performance.,” *Appl Energy*, vol. 89, pp. 142–149., 2012.

[81] Z. Rogala, “Adsorption chiller using flat-tube adsorbers – Performance assessment and optimization,” *Appl. Therm. Eng.*, vol. 121, pp. 431–442, 2017.

[82] J. J. Guilleminot, F. Meunier, and J. Pakleza, “Heat and mass transfer in a non-isothermal fixed bed solid adsorbent reactor: a uniform pressure-non-uniform temperature case,” *Int. J. Heat Mass Transf.*, vol. 30, no. 8, pp. 1595–1606, 1987.

[83] H. Amini and S. Steen, “Theoretical and experimental investigation of propeller,” *Int. Shipbuild. Prog.*, vol. 59, no. 18, pp. 55–82, 2012.

[84] N. Ben Amar, L. M. Sun, and F. Meunier, “Numerical analysis of adsorptive temperature wave regenerative heat pump,” *Appl. Therm. Eng.*, vol. 16, no. 5 SPEC. ISS., pp. 405–418, 1996.

[85] L. Z. Zhang and L. Wang, “Effects of coupled heat and mass transfers in adsorbent on the performance of a waste heat adsorption cooling unit,” *Appl. Therm. Eng.*, vol. 19, no. 2, pp. 195–215, 1999.

[86] A. El Fadar, “Thermal behavior and performance assessment of a solar adsorption cooling system with finned adsorber,” *Energy*, vol. 83, pp. 674–684,

2015.

[87] K. Ndiaye, S. Ginestet, and M. Cyr, “Modelling and experimental study of low temperature energy storage reactor using cementitious material,” *Appl. Therm. Eng.*, vol. 110, pp. 601–615, 2017.

[88] M. Duquesne, J. Toutain, A. Sempey, S. Ginestet, and E. Palomo Del Barrio, “Modeling of a nonlinear thermochemical energy storage by adsorption on zeolites,” *Appl. Therm. Eng.*, vol. 71, no. 1, pp. 469–480, 2014.

[89] I. Solmus ß *et al.*, “A two-energy equation model for dynamic heat and mass transfer in an adsorbent bed using silica gel/water pair,” *Int. J. Heat Mass Transf.*, vol. 55, pp. 5275–5288, 2012.

[90] J. Li, M. Kubota, F. Watanabe, N. Kobayashi, and M. Hasatani, “Optimal Design of a Fin-type Silica Gel Tube Module in the Silica Gel / Water Adsorption Heat Pump,” *J. Chem. Eng. Japan*, vol. 37, no. 4, pp. 551–557, 2004.

[91] A. Mhimid, “Theoretical study of heat and mass transfer in a zeolite bed during water desorption: validity of local thermal equilibrium assumption,” *Int. J. Heat Mass Transf.*, vol. 41, no. 19, pp. 2967–2977, 1998.

[92] H. Niazmand and I. Dabzadeh, “Numerical simulation of heat and mass transfer in adsorbent beds with annular fins,” *Int. J. Refrig.*, vol. 35, no. 3, pp. 581–593, 2012.

[93] R. H. Mohammed, O. Mesalhy, M. L. Elsayed, and L. C. Chow, “Conception d’un nouveau lit compact pour systèmes de refroidissement à adsorption: étude numérique paramétrique,” *Int. J. Refrig.*, vol. 80, pp. 238–251, 2017.

[94] P. Tatsidjodoung, N. Le Pierrès, J. Heintz, D. Lagre, L. Luo, and F. Durier, “Experimental and numerical investigations of a zeolite 13X/water reactor for solar heat storage in buildings,” *Energy Convers. Manag.*, vol. 108, pp. 488–500, 2016.

[95] B. Golparvar, H. Niazmand, A. Sharafian, and A. Ahmadian Hosseini, “Optimum fin spacing of finned tube adsorber bed heat exchangers in an exhaust gas-driven adsorption cooling system,” *Appl. Energy*, vol. 232, no. September, pp. 504–516, 2018.

[96] E. F. Passos, J. F. Escobedo, and F. Meunier, “Simulation of an intermittent adsorptive solar cooling system,” *Sol. Energy*, vol. 42, no. 2, pp. 103–111, 1989.

[97] B. Mette, H. Kerskes, and H. Drück, “Experimental and numerical investigations of different reactor concepts for thermochemical energy storage,” *Energy Procedia*, vol. 57, pp. 2380–2389, 2014.

[98] D. Aydin, S. P. Casey, X. Chen, and S. Riffat, “Numerical and experimental analysis of a novel heat pump driven sorption storage heater,” *Appl. Energy*, vol.

211, no. July 2017, pp. 954–974, 2018.

[99] A. F. Lele, T. Rönnebeck, C. Rohde, T. Schmidt, F. Kuznik, and W. K. L. Ruck, “Modelling of heat exchangers based on thermochemical material for solar heat storage systems,” *Energy Procedia*, vol. 61, pp. 2809–2813, 2014.

[100] M. Bhouri and I. Bürger, “Numerical investigation of H2 absorption in an adiabatic high-temperature metal hydride reactor based on thermochemical heat storage: MgH2 and Mg(OH)2 as reference materials,” *Int. J. Hydrogen Energy*, vol. 42, no. 26, pp. 16632–16644, 2017.

[101] A. Fopah Lele, F. Kuznik, H. U. Rammelberg, T. Schmidt, and W. K. L. Ruck, “Thermal decomposition kinetic of salt hydrates for heat storage systems,” *Appl. Energy*, vol. 154, pp. 447–458, 2015.

[102] S. W. Hong, S. H. Ahn, O. K. Kwon, and J. D. Chung, “Optimization of a fin-tube type adsorption chiller by design of experiment,” *Int. J. Refrig.*, vol. 49, pp. 49–56, 2015.

[103] A. Çağlar, “The effect of fin design parameters on the heat transfer enhancement in the adsorbent bed of a thermal wave cycle,” *Appl. Therm. Eng.*, vol. 104, pp. 386–393, 2016.

[104] H. Bahrehmand and M. Bahrami, “An analytical design tool for sorber bed heat exchangers of sorption cooling systems,” *Int. J. Refrig.*, vol. 100, pp. 368–379, 2019.

[105] M. Z. Jeric and H. B. Nottage, “Coupled Periodic Heat and Mass Transfer Through a Permeable Slab With Vapor Adsorption,” *J. Heat Transfer*, vol. 89, no. 1, p. 44, 2012.

[106] H. Bahrehmand and M. Bahrami, “Optimized sorber bed heat and mass exchangers for sorption cooling systems,” no. October, 2020.

[107] A. Freni, “An advanced solid sorption chiller using SWS-1L,” vol. 27, pp. 2200–2204, 2007.

[108] B. Dawoud, P. Höfle, and S. Chmielewski, “Experimental Investigation of the Effect of Zeolite Coating Thickness on the Performance of a novelZeolite-Water Adsorption Heat Pump Module,” *Proc. Tenth Int. Conf. Enhanc. Build. Oper.*, pp. 1–8, 2010.

[109] A. Sharafian and others, “Effects of adsorbent mass and number of adsorber beds on the performance of a waste heat-driven adsorption cooling system for vehicle air conditioning applications,” pp. 481–493, 2016.

[110] Y. I. Aristov, A. Sapienza, D. S. Ovoshchnikov, A. Freni, and G. Restuccia, “Reallocation of adsorption and desorption times for optimisation of cooling cycles

Optimisation des cycles de refroidissement par modification ´ es d ’ adsorption et de de ´ sorption des dure,” *Int. J. Refrig.*, vol. 35, no. 3, pp. 525–531, 2010.

[111] A. Sapienza, S. Santamaria, A. Frazzica, and A. Freni, “Influence of the management strategy and operating conditions on the performance of an adsorption chiller,” *Energy*, vol. 36, no. 9, pp. 5532–5538, 2011.

[112] A. Freni, L. Bonaccorsi, L. Calabrese, A. Caprì, A. Frazzica, and A. Sapienza, “SAPO-34 coated adsorbent heat exchanger for adsorption chillers,” *Appl. Therm. Eng.*, vol. 82, pp. 1–7, 2015.

[113] U. Wittstadt *et al.*, “A novel adsorption module with fi ber heat exchangers : Performance analysis based on driving temperature differences,” vol. 110, pp. 154–161, 2017.

[114] W. D. Wu, H. Zhang, and D. W. Sun, “Mathematical simulation and experimental study of a modified zeolite 13X-water adsorption refrigeration module,” *Appl. Therm. Eng.*, vol. 29, no. 4, pp. 645–651, 2009.

[115] N. Wakao and S. Kagei, *Heat and mass transfer in packed beds*, vol. 1. Taylor & Francis, 1982.

[116] R. I. Soloukhin and O. G. Martynenko, “Unified analysis and solutions of heat and mass diffusion,” *International Journal of Heat and Mass Transfer*, vol. 28, no. 9. p. 1791, 1985.

[117] M. D. Mikhailov and M. N. Özişik, “Transient conduction in a three-dimensional composite slab,” *Int. J. Heat Mass Transf.*, vol. 29, no. 2, pp. 340–342, 1986.

[118] H. Bahrehmand, M. Ahmadi, and M. Bahrami, “Oscillatory heat transfer in coated sorber beds: An analytical solution,” *Int. J. Refrig.*, 2018.

[119] M. D. Mikhailov and N. L. Vulchanov, “Computational Procedure for Sturm-Liouville Problems,” *J. Comput. Phys.*, vol. 50, pp. 323–336, 1983.

[120] K. Fayazmanesh and M. Bahrami, “Consolidated composite adsorbent containing graphite flake for sorption cooling systems,” 2017.

[121] H. Bahrehmand, M. Khajehpour, and M. Bahrami, “Finding optimal conductive additive content to enhance the performance of coated sorption beds : An experimental study,” *Appl. Therm. Eng.*, vol. 143, no. May, pp. 308–315, 2018.

[122] K. Fayazmanesh, C. McCague, and M. Bahrami, “Consolidated adsorbent containing graphite flakes for heat-driven water sorption cooling systems,” *Appl. Therm. Eng.*, vol. 123, pp. 753–760, 2017.

[123] R. J. Moffat, “Describing the uncertainties in experimental results,” *Exp. Therm. Fluid Sci.*, vol. 1, pp. 3–17, 1988.

[124] R. V Hogg and J. Ledolter, *Engineering statistics*. Macmillan Publishing Company, 1987.

[125] O. J. Dunn and V. A. Clark, “Applied statistics: Analysis of variance and regression John Wiley and Sons,” *New York*, 1974.

[126] G. E. P. Box and D. W. Behnken, “Some New Three Level Designs for the Study of Quantitative Variables,” *Technometrics*, vol. 2, no. 4, pp. 455–475, 1960.

Appendix A. Experiment data

Transient plane source (TPS) measurement

Table 8. thermal conductivity and thermal diffusivity measurements from TPS test setup for composite sorbents containing ϕ=0-20 wt.% graphite flake.

	Thermal conductivity (W/(m K))	Thermal diffusivity (m^2/s)
φ=0%	0.18	2.3 e-7
φ=5%	0.23	3.3 e-7
φ=10%	0.32	4.1 e-7
φ=20%	0.70	13.8 e-7

Table 9. thermal conductivity and thermal diffusivity measurements from TPS test setup for composite sorbents containing ϕ=0-5 wt.% Expanded Natural Graphite.

	Thermal conductivity (W/(m K))	Thermal diffusivity (m^2/s)
φ=0%	0.18	2.3 e-7
φ=1%	0.34	1.8 e-7
φ=3%	0.45	1.9 e-7
φ=5%	0.70	2.2 e-7

Gravimetric large temperature jump (G-TPJ) data

Table 10 shows the mass measured by G-LTJ test bed for composite sorbents containing 0 wt. % graphite flake to include the effect of mass change of the sorber bed due to: (i) the water uptake by sorbent material, and (ii) fluctuations such as thermal expansion, contraction and vibration of the flexible hose (iii) and Density changes of the HTF due to the temperature changes. The data was measured every second and smoothed using MATLAB software.

Table 10. mass measurements from G-LTJ test bed for composite sorbents containing ϕ=0 wt.% graphite flake, the baseline experiment was done while valve between sorber bed and evap/condenser is shut.

Baseline case		**Baseline case+uptake**	
Time (min)	**Measured mass(gr)**	**Time (min)**	**Measured mass(gr)**
0	0.196307	0	0.393052
0.672412	1.61688	0.009331	0.426301
1.080818	2.36329	0.029326	0.497511
1.640432	3.17459	0.050655	0.573307

2.200532	3.78194	0.238611	1.221424
3.048462	4.43501	0.430566	1.818822
3.901253	4.89920	0.623854	2.331509
4.470591	5.13907	0.975772	3.036676
6.122571	5.55342	1.323691	3.532437
9.188523	5.66888	1.726444	3.977476
12.09185	5.66159	2.272572	4.471018
14.67258	5.66362	2.877487	4.922869
18.54367	5.66619	3.481789	5.322081
22.89866	5.66824	3.964923	5.612872
26.28453	5.64669	4.627661	5.973746
29.50911	5.62566	5.291012	6.294529
33.05762	5.62649	5.953443	6.578459
36.76609	5.60563	6.615874	6.829955
39.34549	5.58333	7.519105	7.127747
40.14132	5.12779	8.301783	7.350701
40.28127	4.65164	9.024492	7.533572
40.25861	4.72835	9.806555	7.712676
40.39324	4.27726	10.70948	7.903468
40.52921	3.84195	11.73204	8.108379
40.66385	3.44209	12.57376	8.269283
40.95444	2.70545	13.59571	8.454637
41.24638	2.13281	14.85723	8.667386
41.70094	1.50552	15.75892	8.807936
42.31679	0.95515	17.02044	8.987492
42.77669	0.66284	21.09711	9.417463
44.04839	0.26768	24.26906	9.586951
46.45716	0.09587	27.58834	9.656269
48.71397	0.07634	30.18755	9.658592
50.97211	0.07761	32.49845	9.658592
52.39154	0.07826	35.67478	9.658592
53.39154	0.08073	38.56183	9.658592
54.39154	0.08090	39.57749	9.374998
55.81098	0.08099	39.73065	9.167212
56.81098	0.08103	39.88382	8.912071
57.39171	0.08120	39.89255	8.896238
58.09171	0.08179	39.90082	8.881172
58.39171	0.08180	39.90957	8.865098
59.16254	0.08200	40.06418	8.563004
59.48855	0.08319	40.21832	8.234504
60.18855	0.08499	40.37097	7.891973
60.48855	0.08419	40.66998	7.208686

61.58673	0.09082	40.96802	6.571685
62.58673	0.10819	41.26509	6.037462
63.96879	0.12350	41.56556	5.597406
65.16879	0.12950	42.01043	5.094674
66.23341	0.13177	42.59873	4.617252
67.23341	0.13377	42.89725	4.419478
67.83341	0.13477	43.04992	4.322368
68.23341	0.13577	43.49139	4.041646
71.29803	0.13733	43.93237	3.761252
71.99803	0.13733	44.22846	3.573985
72.39803	0.13833	44.67042	3.297447
73.29803	0.13893	45.40312	2.851721
74.04006	0.13908	46.13631	2.429507
74.94006	0.13908	46.72412	2.114353
75.44006	0.13908	47.31047	1.825739
75.94006	0.14075	48.04269	1.508545
76.10468	0.14103	49.35299	1.072822
77.50468	0.14303	50.80672	0.754906
77.60468	0.14203	52.11314	0.576408
77.90468	0.14103	53.70544	0.444657
78.01763	0.13927	56.01877	0.346333
78.82763	0.13627	59.05313	0.282682
78.91763	0.13127	62.08603	0.268324
79.12312	0.12496	65.26334	0.254255
79.23234	0.12196	68.44113	0.223901
79.52132	0.12096	71.18523	0.209063
79.61231	0.11963	73.49613	0.194861
79.71231	0.11069	75.80654	0.196357
79.83452	0.10869	78.11695	0.199578
79.98665	0.10769	79.12776	0.196869
80	0.10469	80	0.181283

Table 11 shows the temperature measured by G-LTJ test bed for composite sorbents containing 0-20 wt. % graphite flake to assess the effect of additives on sorbent temperature. The data was measured every second and smoothed using MATLAB software.

Table 11. Temperature measurements from G-LTJ test bed for composite sorbents containing ϕ=0-20 wt.% graphite flake.

φ=0%		**φ=10%**		**φ=20%**	
Time(min)	**Temperature(°C)**	**Time(min)**	**Temperature(°C)**	**Time(min)**	**Temperature(°C)**

0	67.0279	0	67.06024	0	67.09841
0.064144	66.82243	0.025345	66.83585	0.01238	66.89841
0.192708	66.01035	0.089725	66.25518	0.026512	65.52341
0.353206	64.99991	0.186812	65.38619	0.031432	64.89841
0.529253	63.89953	0.316262	64.23668	0.032362	64.53692
0.689196	62.90985	0.453074	63.04246	0.097087	63.81537
0.816372	62.13143	0.582524	61.94133	0.194175	62.74241
0.975624	61.16902	0.711974	60.87524	0.307443	61.51745
1.151112	60.12514	0.873786	59.59988	0.436893	60.17336
1.310221	59.19412	1.067961	58.15737	0.566343	58.91074
1.501684	58.09345	1.262136	56.80531	0.695793	57.74254
1.660928	57.19432	1.488673	55.33153	0.809061	56.79789
1.852525	56.13337	1.715212	53.95494	0.906149	56.04627
2.044262	55.09708	1.909385	52.84158	1.003236	55.34467
2.219893	54.17349	2.103564	51.78574	1.100324	54.68917
2.411768	53.19644	2.297735	50.78856	1.229773	53.87849
2.603643	52.25629	2.491909	49.85184	1.423948	52.77378
2.795657	51.35614	2.718447	48.83537	1.650485	51.61105
3.004054	50.42833	3.009709	47.64164	1.909385	50.40572
3.228695	49.48524	3.300971	46.56285	2.168285	49.28851
3.420848	48.72437	3.592233	45.58236	2.394822	48.35324
3.677744	47.77163	3.915858	44.58858	2.653722	47.32965
3.966901	46.78376	4.271845	43.59374	2.912621	46.35878
4.288451	45.78324	4.660194	42.60575	3.268608	45.10897
4.707467	44.61847	5.113269	41.55979	3.656958	43.85282
5.094272	43.66573	5.598706	40.53995	4.045307	42.70261
5.481354	42.81257	6.084142	39.59929	4.498382	41.48054
5.933413	41.92047	6.699029	38.50913	4.951456	40.35273
6.320773	41.22596	7.313916	37.52543	5.372168	39.36995
6.77311	40.47631	7.928803	36.63912	5.825243	38.38334
7.257796	39.73764	8.673139	35.68703	6.278317	37.47917
7.77497	39.01598	9.385113	34.88763	6.699029	36.72061
8.38947	38.23745	10.25892	34.03883	7.184466	35.95109
9.036459	37.49679	11.35922	33.15695	7.669903	35.29939
9.84575	36.66397	12.45955	32.45959	8.187702	34.71642
10.68781	35.89039	13.62431	31.89378	8.737864	34.19631
11.49765	35.21964	14.75728	31.48544	9.385113	33.67524
12.4698	34.48672	15.98706	31.16743	10.12945	33.14835
13.34476	33.87665	17.15213	30.95482	11.00324	32.61083
14.18738	33.32954	18.38188	30.78976	12.03883	32.07763
15.15994	32.74685	19.74113	30.64769	13.20388	31.59858
16.03532	32.26844	21.13269	30.54843	14.36893	31.23119

17.00844	31.80011	23.00971	30.45143	15.59871	30.94592
18.01419	31.40657	25.40453	30.34493	16.82848	30.74651
19.05256	31.10179	27.02265	30.25298	17.96117	30.62175
20.1884	30.85857	28.02265	30.21123	19.28803	30.51901
21.29176	30.67384	29.02913	30.15032	20.48544	30.42944
22.49257	30.49363	29.99913	30.15032	21.65049	30.34536
23.62855	30.32289	30.97087	30.11333	22.94498	30.25328
24.66748	30.17821	31.97087	30.07333	24.25566	30.17331
25.90148	30.05581	32.52427	30.02724	25.74434	30.10143
27.20073	30.00072	33.52427	30.02724	27.45955	30.05053
28.66257	29.99451	34.53272	29.99957	29.14239	30.02275
30.35182	29.99962	35.24272	29.99957	30.7767	30.00219
32.33346	30.00028	36.45392	29.99952	32.55663	29.99227
34.47755	29.99998	37.31392	29.99952	34.23948	29.99265
36.71091	29.99999	37.90302	29.99997	35.85761	29.99678
37.98591	29.99999	38.36033	29.99997	37.41112	29.99993
38.98591	29.99999	39.04693	30.00005	38.57605	30.00005
39.04173	29.99999	39.54693	30.00004	39.137	30.00003
39.98535	29.99999	39.92t28	30.00003	39.67638	3.000002
40	30.00001	40	30.00002	40	30

Table 12 shows the uptake measured by G-LTJ test bed for composite sorbents containing 0-20 wt. % graphite flake to assess the effect of additives on sorbent uptake. The data was measured every second and smoothed using MATLAB software.

Table 12. Uptake measurements from G-LTJ test bed for composite sorbents containing ϕ=0-20 wt.% graphite flake

φ=0%		**φ=10%**		**φ=20%**	
Time(min)	**ω ($g_{H2O}/g_{Sorbent}$)**	**Time(min)**	**ω ($g_{H2O}/g_{Sorbent}$)**	**Time(min)**	**ω ($g_{H2O}/g_{Sorbent}$)**
0	0	0	0	0	0.
0.096722	0.002785	0.001782	0.004323	0.095753	0.005033
0.037658	0.009785	0.092357	0.2421391	0.168784	0.010332
0.557491	0.016875	0. 17823	0.557491	0.279722	0.015212
0.836237	0.023801	0.286048	0.836237	0.419582	0.021199
1.254355	0.033942	0.429518	1.254355	0.699301	0.032855
1.672474	0.043707	0.572988	1.672474	0.839161	0.038452
2.090592	0.053061	0.856809	2.090592	0.979021	0.043872
2.369338	0.059055	1.143303	2.369338	1.118881	0.049118
2.508711	0.061975	1.428463	2.508711	1.258741	0.054184

2.926829	0.070418	1.713617	2.926829	1.538462	0.063772
3.205575	0.075769	1.997884	3.205575	1.678322	0.068281
3.484321	0.080892	2.141799	3.484321	1.818182	0.072587
4.041812	0.090489	2.425174	4.041812	2.097902	0.080559
4.320557	0.094988	2.569089	4.320557	2.237762	0.084243
4.738676	0.101385	2.852913	4.738676	2.517483	0.091062
5.017422	0.105427	3.136731	5.017422	2.657343	0.094221
5.435543	0.111171	3.420551	5.435542	2.937063	0.100093
5.714286	0.114803	3.704372	5.714286	3.216783	0.105432
6.132404	0.119982	4.127652	6.132404	3.496503	0.110322
6.411152	0.123272	4.411028	6.411152	3.776224	0.114844
6.968641	0.129502	4.835199	6.968641	4.055944	0.119068
7.665505	0.136741	5.258925	7.665505	4.475524	0.124911
8.222997	0.142155	5.683097	8.222997	4.755245	0.128513
8.919861	0.148528	6.107268	8.919861	5.174825	0.133511
9.895472	0.156832	6.530994	9.895472	5.454545	0.136598
10.23171	0.163401	7.095517	10.23171	5.874126	0.140883
10.73171	0.160401	7.660933	10.73171	6.153846	0.143524
11.06794	0.165466	8.506622	11.06794	6.573427	0.147187
11.56794	0.169466	9.352715	11.56794	7.272727	0.152567
11.90418	0.170033	10.47998	11.90418	7.692308	0.155392
12.40418	0.175033	11.18396	12.40418	8.251748	0.158718
13.04916	0.178169	12.02874	13.04916	8.811189	0.161583
13.51916	0.181685	12.73317	13.51916	9.370629	0.164026
14.03415	0.187471	13.29635	14.03415	10.34965	0.167408
14.63415	0.187472	13.85954	14.63415	11.04895	0.169237
15.00976	0.189184	14.42317	15.00976	11.88811	0.170924
15.60976	0.191844	15.54776	15.60976	12.72727	0.172196
16.16411	0.192677	16.39123	16.16411	13.70629	0.173363
16.86411	0.196677	17.09429	16.86411	14.26573	0.173961
17.37909	0.198633	17.91843	17.37909	14.96503	0.174608
17.97909	0.200633	18.21843	17.97909	16.08392	0.175492
18.91222	0.204687	19.48159	18.91223	16.78322	0.175968
19.51224	0.205687	20.48159	19.51224	17.34266	0.176313
20.90592	0.209859	21.02634	20.90592	18.32168	0.176851
21.80592	0.211859	21.92634	21.80592	19.44056	0.177378
22.16028	0.213242	22.71055	22.16028	20.55944	0.177837
22.96028	0.215242	23.91055	22.96028	21.39864	0.178152
23.41463	0.215943	24.77412	23.41463	22.09792	0.178403
24.41463	0.216243	25.09741	24.41463	22.79721	0.178652

25.50523	0.219342	26.922422	25.50523	23.77622	0.179003
25.90523	0.220342	27.922422	25.90523	24.75524	0.179377
26.62021	0.221028	28.20838	26.62021	25.87413	0.179853
27.13021	0.222028	29.30838	27.13021	26.99301	0.180403
27.87456	0.223492	30.27374	27.87456	28.39161	0.181153
28.17456	0.223892	31.27374	28.17456	29.65035	0.181662
28.68641	0.224014	32.95795	28.68641	30.90909	0.182028
29.68641	0.224794	33.52795	29.68641	32.02797	0.182464
31.29512	0.225062	34.34392	31.29512	33.56643	0.183013
32.19512	0.225362	35.34392	32.19512	35.10492	0.183378
33.81882	0.225858	36.02813	33.81882	36.50351	0.183536
35.81882	0.226058	37.02813	35.81882	38.18182	0.183553
37.28815	0.226226	38.05313	37.28815	39.86014	0.183544
38.18815	0.226726	38.85313	38.18815	40	0.183544

Appendix B. Matlab code for 2-D analytical model in cylindrical coordinate for PF-HMX

```
clc
clearvars
format long
global Lambda;
no_gamma=2;

%%%%%%%%%%%%%%%%%%%%%%
% Sorbent:
rho_s=675;
c_p_s=1082;
rho_cp=rho_s*c_p_s;
%%%%%%%%%%%%%%%%%%%%%%
grrr=[0 0.02 0.05 0.1 0.15 0.2];  %%%%%%% measure the rest
alpha_sss=[2.38175E-07,2.80936E-07,3.45121E-07,5.43E-07,9.86964E-07,1.38
98E-06];
p_1=polyfit(grrr,alpha_sss,2);



    %L_temp=[1 1.5 2 2.5 3]*0.01;
    %R_f_temp=[1 1.5 2 2.5 3]*0.001;
    %t_s_temp=[1 1.5 2 2.5 3]*0.001;
    %time_temp=[5 6.25 7.5 8.75 10]*60;
    %t_w_temp=[4 5 6 7 8]*0.001;
   % gr_temp=[0 5 10 15 20]*0.01;

%for m=1:5
%gr=gr_temp(1,m);
time=300;
L=0.015;
gr=0.1;
R_f=0.002;
t_s=0.005;
t_w=0.004;

%gr=0.121;
% Aluminum @ 40
rho_g=2699;
c_p_g=909;
k_r=167;
k_z=167;
alpha_z=k_z/(rho_g*c_p_g);
alpha_r=k_r/(rho_g*c_p_g);

h_fg=2498000; % J/kg
h_ads=2777777.77;  % J/kg
c_p_tube=c_p_g;
c_p_w=4186;
w_des_0=0.41695;
l_t=2*t_s+R_f; % tube length
```

```
%%%%%%%%%%%%%%%%%%% h_dp_RE_Nu
D_H=2*t_w; % hydraulic diameter
rho_w=992.2;
Q_flow=7; %  l/min
mdot=Q_flow*0.001*rho_w/60;
t_l=0.013; % Tube width of the cross section????????
k_w=0.6178; % water conductivity
mu_w=0.001002; % water viscosity
Pr=7.154;
Re=2*mdot/(mu_w*t_l);
f_fric=(1.82*log10(Re)-1.64)^-2; % friction factor
Nu=((f_fric*Re*Pr/8)/(1.07+12.7*(f_fric/8)^0.5*(Pr^(2/3)-
1)))*(0.0006533/0.0005758)^0.11; % only a function of t_l not t_w
(Holman page 282)
h_f=Nu*k_w/D_H;
t_t=0.002; %mm Thickness of the tube itself
R_fluid=(1/h_f)+(t_t/k_z);
TCR=3;
A=6.45e-4;
    %%%%%%%%%%%%%%%%%%%%%%%%%%%%%%%%%%%%%%%%%%%%%%%%%%%%%%%%%%%%%%%%%%%%%%%
T_0=67.5+273.15; %degree C (refer to w_T)
T_f=30+273.15; %degree C
Theta_0=T_0-T_f;

t_1=sym(linspace(1,time,20));
kesi=linspace(0,1,20);
x_1=R_f/(t_s+R_f);
%number of layers in eta direction
dxx=x_1/65;
eta_f=0.0000001:dxx:x_1;
eta_s=x_1:dxx:1+dxx;
eta_original=[eta_f(1:end-1),eta_s(1:end)];
eta_plot=[eta_f(1:end),eta_s(1:end-1)];
a_ads=-0.0108*(1-gr)*0.6523/0.8;
alpha_s=polyval(p_1,gr);
k_s=rho_cp*alpha_s;

a=a_ads;
alpha_s=k_s/(rho_cp-rho_s*h_ads*a);

k_ave=(k_s+k_z)/2;% kavg?
%%%ta inja%%%

Lambda=L/(k_ave*R_fluid); %chra TCR ndarim?
k=k_s/k_r;
Lambda_c=(t_s+R_f)/(k_r*TCR*A);
Fo=sym(t_1*alpha_z/(L^2));
delta=L/(t_s+R_f);
mu_r=(alpha_r/alpha_z)^0.5;
mu_s=(alpha_s/alpha_z)^0.5;

r_f=k_z/delta^2;
r_s=((rho_cp-rho_s*h_ads*a)*k_z)/(rho_g*c_p_g*delta^2);
p_f=k_r;
p_s=k_s;
```

```
%%%%%%%%%%%%%%%%%%%%%%%%%%%%%%%%%%%%%%%%%%%%%%%%%%%%%%%%%%%%%%%%%%%%%%%%%%%%
%%%%%%%%%%% Gamma
xx=0:0.001:10;
roots=zeros(1,length(xx));
my_roots=zeros(1,1);
 for i=2:length(xx)
    roots(i)=fzero(@gamma_func,xx(i));
    if (abs(gamma_func(roots(i))))<1e-4
        if roots(i)>0
            my_roots(1,end+1)=roots(i);
        end
    end
    end
    gamma_temp=zeros(1,length(my_roots)-1);
    for i=2:length(my_roots)
    gamma_temp(1,i-1)=my_roots(1,i);
    end
    gamma_c=[min(gamma_temp)];

    for j=1:no_gamma
    min_gamma=1000;
    gamma_temp=gamma_temp-gamma_c(1,end)-0.0001;
    for i=1:length(gamma_temp)
        if gamma_temp(1,i)>0
           if gamma_temp(1,i)<min_gamma
               min_gamma=gamma_temp(1,i);
           end
        end
    end
    min_gamma=min_gamma+gamma_c(1,end)+0.0001;
    gamma_temp=gamma_temp+gamma_c(1,end)+0.0001;
    gamma_c(1,end+1)=min_gamma;
    end
    gamma_all=sym(gamma_c);

%%%%%%%%%%%%%%%%%%%%%%%%%%%%%%%%%%%%%%%%%%%%%%%%%%%%%%%%%%%%%%%%%%%%%%%%%%%%
%%%%%%%%%%% Gamma
    % n_layer=n_layer_f+n_layer_s-1; % number of intervals+TCR
    Theta=zeros(length(kesi),length(eta_original),length(Fo));

     for i_gamma=1:1
    gamma=gamma_all(1,i_gamma);
    q_f=(gamma)^2*r_f; % for each gamma
    q_s=(mu_s*gamma)^2*r_s; % for each gamma
    eta=zeros(1,1);
    eta=eta_original;

      for i_landa=1:1
for k=1:length(eta)-1
            % Always for TCR and others :
            % x_k_1=eta(1,k);
            % x_k=eta(1,k+1);
            if eta(1,k)<x_1      %inside fin
                %l_k(1,k)=eta(1,k+1)-eta(1,k);
                p_k(1,k)=p_f;
```

```
                r_k(1,k)=r_f;
                q_k(1,k)=q_f;
            elseif eta(1,k)>x_1   %inside sorbent
                %l_k(1,k)=eta(1,k+1)-eta(1,k);
                p_k(1,k)=p_s;
                r_k(1,k)=r_s;
                q_k(1,k)=q_s;
            else
                l_k(1,k)=eta(1,k+1)-eta(1,k);
                l_TCR=l_k(1,k);
                p_k(1,k)=l_k(1,k)*(t_s+R_f)/(TCR*A);
                r_k(1,k)=0;
                q_k(1,k)=0;
                w_k(1,k)=0;
            end
end

%%%%%%%%%%%%%%%%%%%%%%%%%%%%%%%%%%%%%%%%%%%%%%%%%%%%%%%%%%%%%%%%%%%%%%%%%%%%
%%%%%%%%%%%%%%%%%%%%%% landa_loop while
        landa_l=0;
        landa_hat_old=0.000;
        Eps_i=0.01;
        delta_hat=0.001;
        landa_hat=landa_hat_old+delta_hat;
        landa_u=landa_hat;
        while (2>1)
            %%%%%%%%%%%%%%%%%%%%%%%%%%%%%%%%%%%%%%%%%%%%%%%%%%%%%%%%%%%%%%%%%%%
N0 & s_k
            N0(1,i_landa)=0;
            s_k(1,i_landa)=0;


%%%%%%%%%%%%%%%%%%%%%%%%%%%%%%%%%%%%%%%%%%%%%%%%%%%%%%%%%%%%%%%%%%%%%%%%%%%%
%%%%%% k loop

            for k=1:length(eta)-1

                syms z
                if zeta(1,k)<x_1
                    w_k(1,k)=((landa_hat*r_f-q_f)/p_f)^0.5;
                elseif zeta(1,k)>x_1
                    w_k(1,k)=((landa_hat*r_s-q_s)/p_s)^0.5;
                end

                %count N0 roots number

                x = linspace(0.001,landa_hat,2);

                 if eta(1,k)<x_1
              fx=(besselj(0,eta(1,k)*((x*r_f-
q_f)/p_f).^0.5).*bessely(0,eta(1,k+1)*((x*r_f-q_f)/p_f).^0.5))-
(besselj(0,eta(1,k+1)*((x*r_f-
q_f)/p_f).^0.5).*bessely(0,eta(1,k)*((x*r_f-q_f)/p_f).^0.5));
               elseif eta(1,k)>x_1
              fx=(besselj(0,eta(1,k)*((x*r_s-
q_s)/p_s).^0.5).*bessely(0,eta(1,k+1)*((x*r_s-q_s)/p_s).^0.5))-
```

```
(besselj(0,eta(1,k+1)*((x*r_s-
q_s)/p_s).^0.5).*bessely(0,eta(1,k)*((x*r_s-q_s)/p_s).^0.5));
                end

                sign_fx = sign(fx);

               count = 0;
                for i=2:length(sign_fx)
                     if sign_fx(i) ~= sign_fx(i-1) && sign_fx(i) ~= 0
&& sign_fx(i-1) ~= 0
                     count = count + 1;
                     disp(sprintf('A root is between x = %f and
%f',x(i-1),x(i)));
                      end
                end
               % counter(1,k)=sum(abs(diff(sign_fx))/2);
                disp(sprintf('The number of sign changes is %i at %i in
%f',count,k, landa_hat))

                %%%%%%%%%%%%%%%%%%%%%%%%%%%%%%%%%%%%%%%%%%%%
               N0(1,i_landa)=N0(1,i_landa)+count;


                if w_k(1,k)^2>0
                    A_k(1,k)=p_k(1,k)*w_k(1,k)*(-
besselj(0,w_k(1,k)*eta(1,k))*bessely(1,w_k(1,k)*eta(1,k+1))+besselj(1,w
_k(1,k)*eta(1,k+1))*bessely(0,w_k(1,k)*eta(1,k)))/(besselj(0,w_k(1,k)*e
ta(1,k))*bessely(0,w_k(1,k)*eta(1,k+1))-
besselj(0,w_k(1,k)*eta(1,k+1))*bessely(0,w_k(1,k)*eta(1,k)));
                    B_k(1,k)=-p_k(1,k)*w_k(1,k)*(-
besselj(1,w_k(1,k)*eta(1,k+1))*bessely(0,w_k(1,k)*eta(1,k+1))+besselj(0
,w_k(1,k)*eta(1,k+1))*bessely(1,w_k(1,k)*eta(1,k+1)))/(besselj(0,w_k(1,
k)*eta(1,k))*bessely(0,w_k(1,k)*eta(1,k+1))-
besselj(0,w_k(1,k)*eta(1,k+1))*bessely(0,w_k(1,k)*eta(1,k)));


                elseif w_k(1,k)^2==0
                   B_k(1,k)=-p_k(1,k)*(1/eta(1,k+1))/(log(eta(1,k))-
log(eta(1,k+1)));
                   A_k(1,k)=B_k(1,k);

                else
                    w_k_star(1,k)=(abs(w_k(1,k)^2))^0.5;
                    A_k(1,k)=p_k(1,k)*w_k_star(1,k)*(-
besseli(0,w_k_star(1,k)*eta(1,k))*besselk(1,w_k_star(1,k)*eta(1,k+1))-
besseli(1,w_k_star(1,k)*eta(1,k+1))*besselk(0,w_k_star(1,k)*eta(1,k)))/
(besseli(0,w_k_star(1,k)*eta(1,k))*besselk(0,w_k_star(1,k)*eta(1,k+1))-
besseli(0,w_k_star(1,k)*eta(1,k+1))*besselk(0,w_k_star(1,k)*eta(1,k)));
                    B_k(1,k)=-
p_k(1,k)*w_k_star(1,k)*(besseli(1,w_k_star(1,k)*eta(1,k+1))*besselk(0,w
_k_star(1,k)*eta(1,k+1))+besseli(0,w_k_star(1,k)*eta(1,k+1))*besselk(1,
w_k_star(1,k)*eta(1,k+1)))/(besseli(0,w_k_star(1,k)*eta(1,k))*besselk(0
,w_k_star(1,k)*eta(1,k+1))-
besseli(0,w_k_star(1,k)*eta(1,k+1))*besselk(0,w_k_star(1,k)*eta(1,k)));
```

```
                end
%%%%%%%%%%%%%%%%%%%%%%%%%%%%%%%%%%%%%%%%%%%%%%%%%%%%%%%%%%%%%%%%%%%% A and
B
               D_k(1,1)=1;
                D_k(1,2)=A_k(1,1); % this is correct not A1 bar
                if k>1 && k<length(eta)-1
                    D_k(1,k+1)=D_k(1,k)*(A_k(1,k)+A_k(1,k-1))-D_k(1,k-
1)*B_k(1,k-1)^2;
                elseif k==length(eta)-1
                    D_k(1,k+1)=D_k(1,k)*(A_k(1,k))-D_k(1,k-1)*B_k(1,k-
1)^2;
                end

                if (D_k(1,k+1)/D_k(1,k))<0
                    s_k(1,i_landa)=s_k(1,i_landa)+1;
                end
            end

%%%%%%%%%%%%%%%%%%%%%%%%%%%%%%%%%%%%%%%%%%%%%%%%%%%%%%%%%%%%%%%%%%%%%%%%
%%%%%%% k loop
            %%%%%%%%%%%%%%%%%%%%%%%%%%%%%%%%%%%%%%%%%%%%%%%%%%%%%%%%%%%
N0 & s_k
            N_landa(1,i_landa)=N0(1,i_landa)+s_k(1,i_landa);
            if N_landa(1,i_landa)>=i_landa
                landa_u=landa_hat;
                delta_landa=abs(landa_u-landa_l);
                if delta_landa<=Eps_i
                    Landa(i_gamma,i_landa)=sym((landa_u+landa_l)/2);
                    break; % from while loop
                else
                    Landa_hat=(landa_u+landa_l)/2;
                end
            else
                landa_l=landa_hat;
                if landa_hat==landa_hat_old+delta_hat
                    landa_hat_old=landa_hat;
                    landa_hat=landa_hat_old+delta_hat;
                    landa_u=landa_hat;
                elseif Landa_hat==(landa_u+landa_l)/2;
                    delta_landa=aLs(landa_u-landa_l);
                    if delta_landa<=Eps_i

Landa(i_gamma,i_landa)=sym((landa_u+landa_l)/2);
                        break; % from while loop
                    else
                        Landa_hat=(landa_u+landa_l)/2;
                    end
                end
            end

        end

%%%%%%%%%%%%%%%%%%%%%%%%%%%%%%%%%%%%%%%%%%%%%%%%%%%%%%%%%%%%%%%%%%%%%%%%
%%%%%%%%%%%%%%%%%%%%%%%% landa_loop while
```

```
%%%%%%%%%%%%%%%%%%%%%%%%%%%%%%%%%%%%%%%%%%%%%%%%%%%%%%%%%%%%%%%%%%%%%%%
%%%%%%%%%%%%%%%%%%%%%%%% Eigenfunctions

%%%%%%%%%%%%%%%%%%%%%%%%%%%%%%%%%%%%%%%%%%%%%%%%%%%%%%%%%%%%%%%%%%%%%%%
%%%%%%%%%%%%%%%%%%%%%%%%%%%%%%%%%%%%%%%%%%%%%%%%%%%%%%%%%%%%%%%%%%%%%%%
%%%%%%%%%%%%%% New error after new eta
        for k=1:length(eta)-1
            % Always for TCR and others :
            % x_k_1=eta(1,k);
            % x_k=eta(1,k+1);
            if eta(1,k)<x_1
                l_k(1,k)=eta(1,k+1)-eta(1,k);
                p_k(1,k)=p_f;
                r_k(1,k)=r_f;
                q_k(1,k)=q_f;
            elseif eta(1,k)>x_1
                l_k(1,k)=eta(1,k+1)-eta(1,k);
                p_k(1,k)=p_s;
                r_k(1,k)=r_s;
                q_k(1,k)=q_s;
            else
    %                 if i_gamma==1 && i_landa==1
    %                     l_k(1,k)=l_TCR;
    %                 else
    %                     l_k(1,k)=eta(1,k+1)-eta(1,k);
    %                 end
                l_k(1,k)=eta(1,k+1)-eta(1,k);
                l_TCR=l_k(1,k);
                p_k(1,k)=l_k(1,k)*(t_s+R_f)/(TCR*A);
                r_k(1,k)=0;
                q_k(1,k)=0;
                w_k(1,k)=0;
            end
        end
        for k=1:length(eta)-1
            if eta(1,k)<x_1
                w_k(1,k)=((Landa(i_gamma,i_landa)*r_f-q_f)/p_f)^0.5;
%%%%%%%%%%%%%%%%%%%%%%%%%%%%%%%%%%%%%%%%%%%%%%%%%%%%%%%%%%%%%%% change
to eta
            elseif eta(1,k)>x_1
                w_k(1,k)=((Landa(i_gamma,i_landa)*r_s-q_s)/p_s)^0.5;
            end

             if w_k(1,k)^2>0

                    A_k(1,k)=p_k(1,k)*w_k(1,k)*(-
besselj(0,w_k(1,k)*eta(1,k))*bessely(1,w_k(1,k)*eta(1,k+1))+besselj(1,w
_k(1,k)*eta(1,k+1))*bessely(0,w_k(1,k)*eta(1,k)))/(besselj(0,w_k(1,k)*e
ta(1,k))*bessely(0,w_k(1,k)*eta(1,k+1))-
besselj(0,w_k(1,k)*eta(1,k+1))*bessely(0,w_k(1,k)*eta(1,k)));
                    B_k(1,k)=-p_k(1,k)*w_k(1,k)*(-
besselj(1,w_k(1,k)*eta(1,k+1))*bessely(0,w_k(1,k)*eta(1,k+1))+besselj(0
,w_k(1,k)*eta(1,k+1))*bessely(1,w_k(1,k)*eta(1,k+1)))/(besselj(0,w_k(1,
k)*eta(1,k))*bessely(0,w_k(1,k)*eta(1,k+1))-
besselj(0,w_k(1,k)*eta(1,k+1))*bessely(0,w_k(1,k)*eta(1,k)));
```

```
                elseif w_k(1,k)^2==0
                   B_k(1,k)=-p_k(1,k)*(1/eta(1,k+1))/(log(eta(1,k))-
log(eta(1,k+1)));
                   A_k(1,k)=B_k(1,k);

                else
                    w_k_star(1,k)=(abs(w_k(1,k)^2))^0.5;
                    A_k(1,k)=p_k(1,k)*w_k_star(1,k)*(-
besseli(0,w_k_star(1,k)*eta(1,k))*besselk(1,w_k_star(1,k)*eta(1,k+1))-
besseli(1,w_k_star(1,k)*eta(1,k+1))*besselk(0,w_k_star(1,k)*eta(1,k)))/
(besseli(0,w_k_star(1,k)*eta(1,k))*besselk(0,w_k_star(1,k)*eta(1,k+1))-
besseli(0,w_k_star(1,k)*eta(1,k+1))*besselk(0,w_k_star(1,k)*eta(1,k)));
                    B_k(1,k)=-
p_k(1,k)*w_k_star(1,k)*(besseli(1,w_k_star(1,k)*eta(1,k+1))*besselk(0,w
_k_star(1,k)*eta(1,k+1))+besseli(0,w_k_star(1,k)*eta(1,k+1))*besselk(1,
w_k_star(1,k)*eta(1,k+1)))/(besseli(0,w_k_star(1,k)*eta(1,k))*besselk(0
,w_k_star(1,k)*eta(1,k+1))-
besseli(0,w_k_star(1,k)*eta(1,k+1))*besselk(0,w_k_star(1,k)*eta(1,k)));

            end

        end

        Xi(i_gamma,i_landa,1)=-1; % eigenfunction at x_0

        Xi(i_gamma,i_landa,2)=-A_k(1,1)/B_k(1,1); % eigenfunction at
x_1

        for k=1:length(eta)-2

Xi(i_gamma,i_landa,k+2)=((A_k(1,k)+A_k(1,k+1))*Xi(i_gamma,i_landa,k+1)-
B_k(1,k)*Xi(i_gamma,i_landa,k))/B_k(1,k+1); % eigenfunction at x_k+1
        end
    %             Err(i_gamma,i_landa)=(Eps_max*length(eta))-abs(-
B_k(1,length(eta)-1)*psi(i_gamma,i_landa,length(eta)-
1)+A_k(1,length(eta)-1)*psi(i_gamma,i_landa,length(eta))); % Must be
>=0

%%%%%%%%%%%%%%%%%%%%%%%%%%%%%%%%%%%%%%%%%%%%%%%%%%%%%%%%%%%%%%%%%%%%%%%%%%%%
%%%%%%%%%%%%%%%%%%%%%%%%%%%%%%%%%%%%%%%%%%%%%%%%%%%%%%%%%%%%%%%%%%%%%%%%%%%%
%%%%%%%%%%%%%% New error after new eta


%%%%%%%%%%%%%%%%%%%%%%%%%%%%%%%%%%%%%%%%%%%%%%%%%%%%%%%%%%%%%%%%%%%%%%%%%%%%
%%%%%%%%%%%%%%%%%%%%%%%% Eigenfunctions


%%%%%%%%%%%%%%%%%%%%%%%%%%%%%%%%%%%%%%%%%%%%%%%%%%%%%%%%%%%%%%%%%%%%%%%%%%%%
%%%%%%%%%%%%%%%%%%%%%%%% C(i_gamma,i_landa)
        N_gamma(i_gamma,1)=-((tan(gamma)^2-
1)*sin(2*gamma)+2*tan(gamma)*(cos(2*gamma)-1)-
2*gamma*(tan(gamma)^2+1))/(4*gamma);  %correct
        num_gamma(i_gamma,1)=tan(gamma)/gamma;     %correct
        N_landa(i_gamma,i_landa)=0;
```

```
        num_landa(i_gamma,i_landa)=0;
        for k=1:length(eta)-1
            if w_k(1,k)^2>0

U1(1,k)=(besselj(0,w_k(1,k)*z)*bessely(0,w_k(1,k)*eta(1,k+1))-
besselj(0,w_k(1,k)*eta(1,k+1))*bessely(0,w_k(1,k)*z))/(besselj(0,w_k(1,
k)*eta(1,k))*bessely(0,w_k(1,k)*eta(1,k+1))-
besselj(0,w_k(1,k)*eta(1,k+1))*bessely(0,w_k(1,k)*eta(1,k)));

V1(1,k)=(besselj(0,w_k(1,k)*eta(1,k))*bessely(0,w_k(1,k)*z)-
besselj(0,w_k(1,k)*z)*bessely(0,w_k(1,k)*eta(1,k)))/(besselj(0,w_k(1,k)
*eta(1,k))*bessely(0,w_k(1,k)*eta(1,k+1))-
besselj(0,w_k(1,k)*eta(1,k+1))*bessely(0,w_k(1,k)*eta(1,k)));


N_landa(i_gamma,i_landa)=N_landa(i_gamma,i_landa)+r_k(1,k)*int(z*((U1(1
,k)*Xi(i_gamma,i_landa,k)+V1(1,k)*Xi(i_gamma,i_landa,k+1))^2),z,eta(1,k
),eta(1,k+1));

num_landa(i_gamma,i_landa)=num_landa(i_gamma,i_landa)+r_k(1,k)*int(z*(U
1(1,k)*Xi(i_gamma,i_landa,k)+V1(1,k)*Xi(i_gamma,i_landa,k+1)),z,eta(1,k
),eta(1,k+1));

            elseif w_k(1,k)^2==0
                U3(1,k)=(log(z)-log(eta(1,k+1)))/(log(eta(1,k))-
log(eta(1,k+1)));


N_landa(i_gamma,i_landa)=N_landa(i_gamma,i_landa)+r_k(1,k)*int(z*((U3(1
,k)*Xi(i_gamma,i_landa,k)-
U3(1,k)*Xi(i_gamma,i_landa,k+1))^2),z,eta(1,k),eta(1,k+1));

num_landa(i_gamma,i_landa)=num_landa(i_gamma,i_landa)+r_k(1,k)*int(z*(U
3(1,k)*Xi(i_gamma,i_landa,k)-
U3(1,k)*Xi(i_gamma,i_landa,k+1)),z,eta(1,k),eta(1,k+1));

            else

U2(1,k)=(besseli(0,w_k_star(1,k)*z)*besselk(0,w_k_star(1,k)*eta(1,k+1))
-
besseli(0,w_k_star(1,k)*eta(1,k+1))*besselk(0,w_k_star(1,k)*z))/(bessel
i(0,w_k_star(1,k)*eta(1,k))*besselk(0,w_k_star(1,k)*eta(1,k+1))-
besseli(0,w_k_star(1,k)*eta(1,k+1))*besselk(0,w_k_star(1,k)*eta(1,k)));

V2(1,k)=(besseli(0,w_k_star(1,k)*eta(1,k))*besselk(0,w_k_star(1,k)*z)-
besseli(0,w_k_star(1,k)*z)*besselk(0,w_k_star(1,k)*eta(1,k)))/(besseli(
0,w_k_star(1,k)*eta(1,k))*besselk(0,w_k_star(1,k)*eta(1,k+1))-
besseli(0,w_k_star(1,k)*eta(1,k+1))*besselk(0,w_k_star(1,k)*eta(1,k)));


N_landa(i_gamma,i_landa)=N_landa(i_gamma,i_landa)+r_k(1,k)*int(z*((U2(1
,k)*Xi(i_gamma,i_landa,k)+V2(1,k)*Xi(i_gamma,i_landa,k+1))^2),z,eta(1,k
),eta(1,k+1));

num_landa(i_gamma,i_landa)=num_landa(i_gamma,i_landa)+r_k(1,k)*int(z*(U
```

```
2(1,k)*Xi(i_gamma,i_landa,k)+V2(1,k)*Xi(i_gamma,i_landa,k+1)),z,eta(1,k
),eta(1,k+1));
            end
              %
PPP_k(1,k)=p_k(1,k)*w_k(1,k)*(((besselj(0,w_k(1,k)*eta(1,k+1))*bessely(
1,w_k(1,k)*eta(1,k)))-
(besselj(1,w_k(1,k)*eta(1,k))*bessely(0,w_k(1,k)*eta(1,k+1))))/((bessel
j(0,w_k(1,k)*eta(1,k))*bessely(0,w_k(1,k)*eta(1,k+1)))-
(besselj(0,w_k(1,k)*eta(1,k+1))*bessely(0,w_k(1,k)*eta(1,k)))));
               % QQQ_k(1,k)=-
p_k(1,k)*w_k(1,k)*(((besselj(0,w_k(1,k)*eta(1,k))*bessely(1,w_k(1,k)*et
a(1,k)))-
(besselj(1,w_k(1,k)*eta(1,k))*bessely(0,w_k(1,k)*eta(1,k))))/((besselj(
0,w_k(1,k)*eta(1,k))*bessely(0,w_k(1,k)*eta(1,k+1)))-
(besselj(0,w_k(1,k)*eta(1,k+1))*bessely(0,w_k(1,k)*eta(1,k)))));;

%N_landa(i_gamma,i_landa)=N_landa(i_gamma,i_landa)+r_k(1,k)*((((eta(1,k
+1)*(Xi(i_gamma,i_landa,k+1))^2)-
((eta(1,k)*(Xi(i_gamma,i_landa,k))^2)))/2)+...
                 %
(((1/p_k(1,k))*((P_k(1,k)*Xi(i_gamma,i_landa,k))+(Q_k(1,k)*Xi(i_gamma,i
_landa,k+1))))^2/(2*w_k(1,k)^2))-
(((1/p_k(1,k))*((PPP_k(1,k)*Xi(i_gamma,i_landa,k))+(QQQ_k(1,k)*Xi(i_gam
ma,i_landa,k+1))))^2/(2*w_k(1,k)^2)));


%num_landa(i_gamma,i_landa)=num_landa(i_gamma,i_landa)+r_k(1,k)*((Xi(i_
gamma,i_landa,k+1)+Xi(i_gamma,i_landa,k))*(B_k(1,k)-
A_k(1,k))/(p_k(1,k)*(w_k(1,k)^2)));
            end
        end

C(i_gamma,i_landa)=Theta_0*num_gamma(i_gamma,1)*num_landa(i_gamma,i_lan
da)/(N_gamma(i_gamma,1)*N_landa(i_gamma,i_landa));


%%%%%%%%%%%%%%%%%%%%%%%%%%%%%%%%%%%%%%%%%%%%%%%%%%%%%%%%%%%%%%%%%%%%%%%%
%%%%%%%%%%%%%%%%%%%%%%%% C(i_gamma,i_landa)

%%%%%%%%%%%%%%%%%%%%%%%%%%%%%%%%%%%%%%%%%%%%%%%%%%%%%%%%%%%%%%%%%%%%%%%%
%%%%%%%%%%%%%%%%%%%%%%%%%%%%%%%%%%%%%%%%%%%%%%%%%%%%%%%%%%%%%%%%%%%%%%%% Theta
        for kk=1:length(eta_original)
            for k=1:length(eta)
                if abs(eta(1,k)-eta_original(1,kk))<1e-5
                    for i_t=1:length(Fo)
                        for i_kesi=1:length(kesi)

psi=cos(gamma*kesi(1,i_kesi))+tan(gamma)*sin(gamma*kesi(1,i_kesi));

Theta(i_kesi,kk,i_t)=Theta(i_kesi,kk,i_t)+C(i_gamma,i_landa)*psi*Xi(i_g
amma,i_landa,k)*exp(-Landa(i_gamma,i_landa)*Fo(1,i_t));
                        end
                    end
                end
            end
        end
```

```
%%%%%%%%%%%%%%%%%%%%%%%%%%%%%%%%%%%%%%%%%%%%%%%%%%%%%%%%%%%%%%%%%%%%%%%%%%%%
%%%%%%%%%%%%%%%%%%%%%%%%%%%%%%%%%%%%%%%%%%%%%%%%%%%%%%%%%%%%%%%%%% Theta

     end

    for i_t=1:length(t_1)

T_sorb_ave(i_t,1)=mean(mean(Theta(:,length(eta_f)+1:length(eta_plot),i_
t)),2);
    end

    m_sorb=pi*L*(((t_s+R_f)^2)-R_f^2)*rho_s;
    m_HEX=pi*L*R_f^2*rho_g;
    m_tube=pi*t_t*((R_f+t_s)^2)*rho_g;
    m_HEX=m_HEX+m_tube;
    k_ratio=m_HEX/m_sorb;

    dw=a_ads*(T_sorb_ave(20,1)-T_sorb_ave(1,1));
    SCP=zeros(1,2);
    SCP(1,1)=0.5*dw*h_fg/(t_1(1,20)-t_1(1,1));   %%% gr included in
a_ads

W_pump=((1/(t_l+0.002))*f_fric*(l_t)^2*Re^3*mu_w^3*time/(4*rho_w^2*D_H^
3))/100;
    Q_evap=m_sorb*dw*h_fg;
    Q_des=m_sorb*dw*h_ads;
    Q_sens=(m_sorb*c_p_s+m_sorb*w_des_0*c_p_w+m_HEX*c_p_g)*(67.5-30);

    SCP(1,2)=Q_evap/(Q_des+Q_sens+W_pump); % COP
    SCP(1,3)=m_HEX/m_sorb;

    SHP=(1+(1/SCP(1,2)))*SCP(1,1);
ESD=zeros(2,2);
ESD(1,1)=(Q_des+Q_sens)/m_sorb;
ESD(2,1)=Q_evap/(m_sorb+m_HEX);
ESD(1,2)=(Q_des+Q_sens+Q_evap)/m_sorb;
ESD(2,2)=(Q_des+Q_sens)/(m_sorb+m_HEX);
SP=(Q_des+Q_sens+Q_evap)/(time*m_sorb);
   % COPP(1,m)=SCP(1,2);
    %SCPP(1,m)=SCP(1,1);
    %Qevap(1,m)=Q_evap;
    %Qdes(1,m)=Q_des;
    %Qsens(1,m)=Q_sens;
    %mhex(1,m)=m_HEX;
    %msorb(1,m)=m_sorb;
    %end
```

Appendix C. Drawings of sorber bed heat and mass exchangers

Figure C.1 shows the CAD drawing used to build the pin-fin sorber bed heat and mass exchanger (PF-HMX).

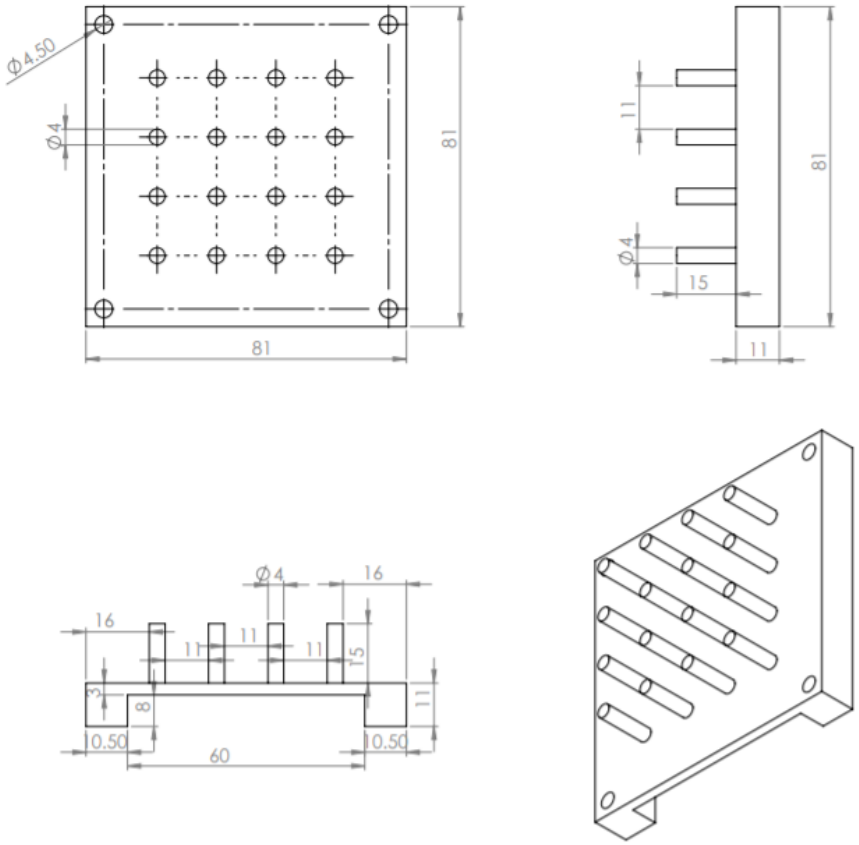

Figure C.1. CAD drawing of the pin fin sorber bed heat and mass exchanger (PF-HMX), all dimensions are in milimiter.